

General Neutralino NLSP with Gravitino Dark Matter vs. Big Bang Nucleosynthesis



II. Institut für Theoretische Physik,
Universität Hamburg



Deutsches Elektronen-Synchrotron DESY,
Theory Group

Diplomarbeit zur Erlangung des akademischen Grades
Diplom-Physiker
(diploma thesis - **with correction**)

Verfasser: Jasper Hasenkamp
Matrikelnummer: 5662889
Studienrichtung: Physik
Eingereicht am: 31.3.2009
Betreuer(in): Dr. Laura Covi, DESY
Zweitgutachter: Prof. Dr. Günter Sigl, Universität Hamburg

Abstract

We study the scenario of gravitino dark matter with a general neutralino being the next-to-lightest supersymmetric particle (NLSP). Therefore, we compute analytically all 2- and 3-body decays of the neutralino NLSP to determine the lifetime and the electromagnetic and hadronic branching ratio of the neutralino decaying into the gravitino and Standard Model particles.

We constrain the gravitino and neutralino NLSP mass via big bang nucleosynthesis and see how those bounds are relaxed for a Higgsino or a wino NLSP in comparison to the bino neutralino case. At neutralino masses $\gtrsim 1$ TeV, a wino NLSP is favoured, since it decays rapidly via a newly found 4-vertex. The Higgsino component becomes important, when resonant annihilation via heavy Higgses can occur.

We provide the full analytic results for the decay widths and the complete set of Feynman rules necessary for these computations. This thesis closes any gap in the study of gravitino dark matter scenarios with neutralino NLSP coming from approximations in the calculation of the neutralino decay rates and its hadronic branching ratio.

Zusammenfassung

Diese Diplomarbeit befasst sich mit dem Gravitino als Dunkler Materie, wobei ein allgemeines Neutralino das nächstleichteste supersymmetrische Teilchen (NLSP) ist. Daher berechnen wir analytisch alle Zwei- und Dreikörperzerfälle des Neutralino-NLSP, um die Lebensdauer sowie das elektromagnetische und hadronische Verzweungsverhältnis des Neutralinos, das in das Gravitino und Teilchen des Standardmodells zerfällt, zu bestimmen.

Die primordiale Nukleosynthese lässt uns Schranken für die Gravitino- sowie für die Neutralinomasse finden. Dabei erkennen wir inwieweit diese Schranken für ein Higgsino- oder Wino-NLSP schwächer im Vergleich zum Bino-NLSP sind. Für Neutralinomassen $\gtrsim 1$ TeV ist ein Wino-NLSP begünstigt, da es schnell über einen neugefundenen 4-vertex zerfällt. Eine Higgsinokomponente wird wichtig, falls resonante Paarvernichtung über schwere Higgsteilchen auftreten kann.

Wir stellen die vollen analytischen Ergebnisse für die Zerfallsbreiten und den vollständigen Satz von Feynmanregeln, die für diese Berechnungen nötig sind, zur Verfügung. Diese Diplomarbeit schließt jede Lücke in der Untersuchung des Gravitinos als Dunkler Materie mit einem Neutralino als NLSP, die rückführbar ist auf Näherungen in der Berechnung der Zerfallsbreiten des Neutralinos oder seines hadronischen Verzweungsverhältnisses.

Contents

1	Introduction	2
2	Nucleosynthesis and Dark Matter in Big Bang Cosmology	5
2.1	Big Bang Cosmology	5
2.2	Nucleosynthesis in Cosmology	10
2.3	Evidence for Dark Matter	15
3	From Supersymmetry to Gravitino Dark Matter	17
3.1	Local Supersymmetry	17
3.2	The Minimal Supersymmetric Standard Model	19
3.3	Symmetry Breaking	22
3.3.1	Supersymmetry Breaking	22
3.3.2	Electroweak Symmetry Breaking	26
3.3.3	Physical Particles	30
3.4	The Gravitino	32
3.4.1	Gravitino Cosmology	34
4	General Neutralino NLSP with Gravitino Dark Matter	37
4.1	Bino NLSP	39
4.2	Wino NLSP	43
4.3	Higgsino NLSP	45
4.4	Varying Gravitino Mass and Intermediate Sparticles	52
4.5	Interference Effects	53

5	Constraints by Big Bang Nucleosynthesis	57
5.1	Bino-Wino	58
5.2	Bino-Higgsino	62
5.3	Wino-Higgsino	62
6	Conclusions	67
A	Notation and Conventions	69
B	Example Calculation	73
C	Kinematics and Parametrisation	75
C.1	2-body decays	76
C.2	3-body decays	76
D	Feynman rules	79
E	Full Analytic Results	86
E.1	2 body decays	87
E.2	3 body decays	89
F	Correction	107
	References	110
	Acknowledgements	115

List of Figures

2.1	BBN predictions and the $\Omega_m - \Omega_\Lambda$ plane	12
2.2	BBN constraints	13
2.3	CMB sky	14
2.4	CMB power spectrum	15
3.1	Schematic structure of SUSY breaking	24
4.1	$\tilde{G} \rightarrow \Psi_\mu \gamma / Z$	39
4.2	$B_{had}^{\tilde{B}}$	41
4.3	$B_{had}^{\tilde{W}}$	44
4.4	$\tilde{W} \rightarrow \Psi_\mu W^+ W^-$	45
4.5	$\tilde{H} \rightarrow \Psi_\mu Z / h$	45
4.6	$\tilde{H} \rightarrow \Psi_\mu Z h$	47
4.7	$B_{had}^{\tilde{H}}$	50
4.8	$B_{had}^{\tilde{H}}$ with 5% bino	51
4.9	B_{had}^X for different $m_{3/2}$	52
4.10	$B_{had}^{\tilde{\gamma}}$	54
4.11	B_{had}	56
5.1	Bino-Wino parameter space	58
5.2	BBN bounds on bino-wino	60
5.3	Bino-Higgsino parameter space	61
5.4	BBN bounds on bino-Higgsino	63

5.5	Wino-Higgsino parameter space	64
5.6	BBN bounds on wino-Higgsino	65
5.7	BBN bounds on wino-Higgsino with $m_{3/2} = 100$ GeV	66
E.1	$\tilde{G} \rightarrow \Psi_\mu \gamma / Z \rightarrow \Psi_\mu q \bar{q}$	93
E.2	$\tilde{H} \rightarrow \Psi_\mu h / Z \rightarrow \Psi_\mu q \bar{q}$	96
E.3	$\chi \rightarrow \Psi_\mu \tilde{q} \rightarrow \Psi_\mu q \bar{q}$	98
F.1	Correction to $\tilde{W} \rightarrow \Psi_\mu W^+ W^-$	107
F.2	Correction to $\tilde{H} \rightarrow \Psi_\mu h Z$	109

List of Tables

- 3.1 SUGRA fields 19
- 3.2 MSSM matter fields 21
- 3.3 MSSM gauge fields 21
- 3.4 Spinor representations 31
- 3.5 Physical particles 36

Chapter 1

Introduction

The nature and identity of the dark matter, that actually makes up more than 80% of the matter in the universe, is one of the major questions in the natural sciences. Even though the Standard Model of particle physics provides an astonishingly good description of the fundamental particles and their interactions, the observational fact that most of the matter of the universe resides in the form of cold non-baryonic dark matter provides impressive evidence for physics beyond the Standard Model [1].

Remarkably, supersymmetry provides a promising candidate for the particle dark matter, since in supersymmetric theories with conserved R -parity the lightest supersymmetric particle (LSP) is stable and thus a compelling candidate for dark matter, if it does not have electromagnetic or strong interactions. The lightest neutralino is one favoured LSP candidate, since it interacts weakly and is naturally one of the lightest supersymmetric particles [2].

Another particularly attractive candidate is the gravitino [3, 4]. The gravitino is a unique and inevitable prediction of any supersymmetric theory containing gravity. As the superpartner of the graviton, it is extremely weakly interacting. Thus, if the gravitino is the LSP, it can be dark matter. But in any case the relic gravitino abundance may not overclose the universe.

Typically, the extremely weak interactions of the gravitino make the gravitino -if it is not the LSP- decay during or after big bang nucleosynthesis (BBN). In this way, the successful prediction of the light element abundances in the universe is spoiled [5, 6, 7, 8].

For gravitino dark matter with conserved R -parity the gravitino is stable and thus does not decay. But then the next-to-lightest supersymmetric particle (NLSP) becomes long-lived and may in turn alter the observed abundances of light elements when it decays [9, 10, 11, 12]. These constraints lead to lower bounds on the NLSP mass $m_{\tilde{\chi}}$, since the

NLSP decays with a lifetime $\propto m_\chi^{-5}$. However, the stabilization of the hierarchy between electroweak and high-energy scales, by cancelling the quadratic divergences in the mass-squared of the Higgs boson, is just one motivation that suggests the NLSP to have a mass in the TeV range [13].

Furthermore, there is a lower bound on the gravitino mass due to the overclosure limit also in scenarios with inflation, at least, if the observed baryon-to-photon ratio stems from baryogenesis via thermal leptogenesis [14, 15, 16]. On the other hand, there is an upper bound on the gravitino mass $m_{3/2}$ by BBN, since the lifetime of the NLSP is also $\propto m_{3/2}^2$. Altogether, both masses m_χ and $m_{3/2}$ are constrained and one of the most severe constraints is to maintain the successful predictions of big bang nucleosynthesis.

We consider gravitino dark matter with neutralino NLSP. Thereby, we compute analytically all 2- and, for the first time, also all 3-body decays of the general neutralino. We find a new vertex from the non-abelian part of the gravitino interaction Lagrangian that becomes leading at masses ≈ 1 TeV but has been neglected so far in the literature. This emphasizes especially a wino-like NLSP, which has up to now not been considered at all.

In the process we regard thresholds by the Breit-Wigner form of propagators and, furthermore, neutralino mixing effects and all possible interferences. That allows us to determine the lifetime and branching ratios of the general neutralino NLSP with gravitino dark matter to a high accuracy. We consider all six quark flavour with their corresponding masses. Thereby, we find that the minimal hadronic branching ratio of the neutralino NLSP has been underestimated more than an order of magnitude in earlier studies [17, 18, 19, 20].

In fact, these results are a crucial input to derive BBN constraints on gravitino dark matter scenarios with neutralino NLSP. Independent from any model at high energy scales, we study the allowed low energy parameter space and search for possibilities to reconcile gravitino dark matter with neutralino NLSP and thermal leptogenesis considering the thermal production of gravitinos after reheating. Thereby, we study the possibilities that a scenario overcomes the BBN bounds either due to favourable decay properties or a low relic density. We also take into account the possibility to produce the gravitino dark matter density in NLSP decays.

This thesis is organized as follows: Chapter 2 reviews briefly the role of nucleosynthesis and dark matter in cosmology. In Chapter 3 we introduce the elementary particle content under consideration, whereas we emphasize the gravitino and the neutralino. In Chapter 4 we investigate all 2- and 3-body decays of a general neutralino NLSP with gravitino dark matter. This allows us to determine the neutralino lifetime and its electromagnetic and hadronic branching ratio considering all effects of interference and

mixing, which we use in Chapter 5 to constrain the scenario via big bang nucleosynthesis. After the conclusions in the last chapter, we list our notation in Appendix A. There is an example calculation in Appendix B, afterwards we discuss the kinematics briefly in Appendix C. We provide the complete set of Feynman rules as derived for the computations of neutralino-to-gravitino decays in Appendix D and we list the full analytic results of all neutralino decay widths in Appendix E.

The results of this work will appear in [21].

Chapter 2

Nucleosynthesis and Dark Matter in Big Bang Cosmology

In this chapter we review briefly the role of nucleosynthesis and dark matter in big bang cosmology. Thereby we are based mainly on [22, 23, 24, 25, 26].

2.1 Big Bang Cosmology

Einstein's equations of general relativity,

$$R_{\mu\nu} - \frac{1}{2}Rg_{\mu\nu} = 8\pi G_N T_{\mu\nu}, \quad (2.1)$$

determine the geometry of space-time by the matter and energy content of the universe. $R_{\mu\nu}$ and R are the Ricci tensor and Ricci scalar respectively, while $g_{\mu\nu}$ is the space-time metric. The right-hand side of Eq. (2.1) consists of the energy-momentum tensor $T_{\mu\nu}$, while G_N denotes Newton's gravitational constant. Eq. (2.1) is a set of ten coupled equations. To solve them analytically, we have to assume symmetries. Fortunately, measurements of the cosmic microwave background (CMB) show that the universe is highly isotropic (see Section 2.2) and galaxy surveys indicate that the universe is also homogeneous on large scales of $O(100 \text{ Mpc})$. The most general expression for a space-time metric, which has a (3D) maximally symmetric subspace of a 4D space-time, is the Friedmann-Robertson-Walker metric,

$$g_{\mu\nu}dx^\mu dx^\nu = ds^2 = dt^2 - a^2(t) \left[\frac{dr^2}{1 - kr^2} + r^2(d\theta^2 + \sin^2\theta d\Phi^2) \right], \quad (2.2)$$

where r , θ and Φ are comoving spatial coordinates. The constant $k = -1, 0, +1$ characterizes the spatial curvature, whereas $k = -1$ corresponds to an open, $k = 0$ to a flat

and $k = +1$ to a closed universe. So the scale factor $a(t)$ describes the evolution with time t completely.

A convenient assumption is to describe the matter and energy of the universe as a perfect fluid, thereby respecting isotropy and homogeneity. The energy-momentum tensor of a perfect fluid in its rest frame is

$$T_{\nu}^{\mu} = \begin{pmatrix} \rho & 0 & 0 & 0 \\ 0 & -p & 0 & 0 \\ 0 & 0 & -p & 0 \\ 0 & 0 & 0 & -p \end{pmatrix}, \quad (2.3)$$

where ρ and p denote as usual energy density and pressure, respectively. These assumptions bring us from Einstein's equations (2.1) to the Friedmann equations,

$$\ddot{a} = -\frac{4\pi G_N}{3} a \sum_i (\rho_i + 3p_i), \quad (2.4)$$

which is also known as acceleration equation, and

$$H^2 \equiv \left(\frac{\dot{a}}{a}\right)^2 = \frac{8\pi G_N}{3} \sum_i \rho_i - \frac{k}{a^2}. \quad (2.5)$$

These equations describe the dynamics of the universe. We introduced the Hubble parameter H that gives the expansion rate \dot{a}/a of the universe. The sum accounts for several forms of energy, which are characterized by their equation of state,

$$p_i = w_i \rho_i. \quad (2.6)$$

There are radiation and relativistic particles with $w_r = 1/3$ and dust or non-relativistic matter with $w_m = 0$. The cosmological constant Λ can be described by an energy component with $w_{\Lambda} = -1$. The energy conservation equation in an isotropic, homogeneous universe reads,

$$\dot{\rho} = -3H(\rho + p). \quad (2.7)$$

This can also be derived from the Friedmann Eq. (2.4) and (2.5). Therefore, the combination of Eq. (2.5) and either energy conservation (2.7) or Eq. (2.4), supplemented by the equation of state (2.6), forms a complete system of equations that determines the two unknown functions $a(t)$ and $\rho(t)$.

The energy of photons and other relativistic particles decreases during their propagation in an expanding universe, i.e. their wavelength λ grows with time. So the redshift parameter

$$z = \frac{\lambda_{obs} - \lambda_{em}}{\lambda_{em}} = \frac{a(t_{obs})}{a(t_{em})} - 1 \quad (2.8)$$

grows with time. λ_{obs} denotes the observed wavelength of a formerly -with wavelength λ_{em} - emitted photon, while $a(t_{obs})$ and $a(t_{em})$ denote the corresponding values of the scale factor. As we can see, there is a one-to-one correspondence between z and the time of emission t_{em} . In this way z is used as a measure of time.

It is convenient to rewrite the Friedmann equations using the density parameter

$$\Omega_i(z) = \frac{\rho_i(z)}{\rho_c(z)}, \quad (2.9)$$

where $\rho_c(z) = 3H^2(z)/(8\pi G_N)$ is the critical density corresponding to a spatially flat universe. The present day critical density is given by [22]

$$\rho_c(0) = \rho_c = \frac{3H_0^2}{8\pi G_N} \simeq 1.05 \times 10^{-5} h^2 \text{ GeV cm}^{-3}, \quad (2.10)$$

where H_0 is the present day Hubble parameter. In the usual parametrization

$$H_0 = 100 h \text{ km s}^2 \text{ Mpc}^{-1} \quad (2.11)$$

with $h \simeq 0.7$. Already the simple extrapolation of this expansion back in time leads to a singularity in the past of the universe. So the history of the universe started in a very dense and hot phase: the ‘‘big bang’’. Since that time the universe expands and due to its expansion cools down. By extrapolating back in time more carefully we get the age of the universe as $\sim 13.7 \times 10^9$ yr [22]. Using the density parameter (2.9) the Friedmann equation (2.5) becomes

$$1 = \sum_i \Omega_i - \frac{k}{a^2 H^2} \equiv \Omega_{tot} - \frac{k}{a^2 H^2}, \quad (2.12)$$

where we have defined the total energy density parameter Ω_{tot} as the sum of the components Ω_i . Evaluated today ($z = 0$) Eq. (2.12) gives a cosmic sum rule

$$1 = \Omega_{tot} - \frac{k}{a_0^2 H_0^2} = \Omega_r + \Omega_m + \Omega_\Lambda - \frac{k}{a_0^2 H_0^2}. \quad (2.13)$$

Neglecting the present day radiation density $\Omega_r = O(10^{-5})$ [22] with $k = 0$, we get

$$1 \simeq \Omega_{tot} = \Omega_m + \Omega_\Lambda. \quad (2.14)$$

The acceleration equation (2.4) using Eq. (2.6) rewritten in Ω_i reads

$$\frac{\ddot{a}}{aH^2} = -\frac{1}{2} \sum_i \Omega_i (1 + 3w_i) \equiv -\frac{1}{2} \Omega_{tot} (1 + 3w_{eff}), \quad (2.15)$$

where we have defined an effective $w = w_{eff} = \sum_i w_i \Omega_i / \Omega_{tot}$.

Inflation Standard big bang theory has two major problems. First, cosmic microwave background observations indicate that the universe was highly isotropic at $z \simeq 1100$. Indeed, the observed CMB sky is many orders of magnitude larger than the causal horizon at that time. If different parts of the CMB sky were causally disconnected, this isotropy could not be achieved by physical interactions. Instead, it must be arranged by fine-tuning of initial conditions. Following the standard theory the observed CMB must have consisted of around 10^5 causally disconnected patches, which would require a tremendous amount of fine-tuning. This issue is known as the *horizon problem*.

Secondly, there is the *flatness problem*. By differentiation of Eq. (2.12) with respect to the time and using Eq. (2.15), we obtain

$$\frac{d(\Omega_{tot} - 1)}{dt} = (1 + 3w_{eff})H\Omega_{tot}(\Omega_{tot} - 1). \quad (2.16)$$

Since Ω_{tot} is positive and the Hubble parameter is always positive in an expanding universe, we see that Ω_{tot} departs from 1 in an universe consisting of matter and radiation unless it is exactly 1 in the beginning. Thus, in order to obtain the present day value of $\Omega_{tot} \simeq 1$ the initial value must be extremely fine-tuned again. Together these are two different problems of fine-tuning that are both resolved by an inflationary phase in the very early universe.

Inflation means exponential expansion driven by $w_{eff} \simeq -1$. If during the inflationary phase the scale factor grows by a factor of $> e^{60}$, this implies that the entire observed universe has been a small causally connected region before the tremendous expansion during inflation. In this way, inflation resolves the horizon problem. From Eq. (2.12) we see that $\Omega_{tot} \rightarrow 1$, if the scale factor grows exponentially with time, i.e. $a \propto e^{Ht}$ with constant H . Therefore, the universe may arrive at $\Omega_{tot} \simeq 1$ regardless of the initial conditions and then stays close to that value until today. In this way, inflation resolves also the flatness problem.

Of course at the end of inflation the density of all particles that have been in the universe is diluted away. The inflationary phase can be realized by a scalar field, the so-called inflaton. Then, the decay of the inflaton at the end of inflation transfers its energy into a hot thermal plasma of elementary particles. This process is known as reheating. After reheating the evolution of the universe is described by standard thermal cosmology.

Baryogenesis via Thermal Leptogenesis The observed baryon-to-photon ratio $\eta := \frac{n_b - n_{\bar{b}}}{n_\gamma} \neq 0$ shows that there has been more matter than antimatter when matter and antimatter particles annihilated in the early universe.

A proposed mechanism to generate the baryon asymmetry is *baryogenesis via thermal*

leptogenesis [15]. While generating a baryon asymmetry it is necessary to satisfy the Sakharov conditions:

- Baryon number B violation,
- C -symmetry and CP -symmetry violation,
- Departure from thermal equilibrium.

In baryogenesis via thermal leptogenesis, first, a lepton asymmetry is generated by CP -violating out-of-equilibrium decays of heavy right-handed Majorana neutrinos. Since heavy right-handed Majorana neutrinos can explain very light neutrinos via the seesaw mechanism, this is closely related to the observation of non-vanishing neutrino masses in the last years. Thus the observation of non-vanishing neutrino masses delivers support for the mechanism of thermal leptogenesis. The lepton asymmetry is then converted into a non-vanishing baryon number through non-perturbative sphaleron processes, that violate the baryon number B .

In order to achieve the observed baryon asymmetry, the model of baryogenesis via thermal leptogenesis requires a high reheating temperature $T_R \gtrsim 10^9$ GeV [16, 27].

Relic Abundances Energies in the early universe are often given according to the characteristic temperature of the thermal plasma. Since the universe expands, the plasma temperature decreases as

$$T = T_0(1 + z), \quad (2.17)$$

where T_0 denotes the present day CMB radiation temperature. At high temperatures ($T \gg m_\chi$) a particle χ in the plasma exists in thermal equilibrium and thus with its equilibrium abundance. The equilibrium abundance is maintained by annihilation of the particle with its antiparticle $\bar{\chi}$ into lighter particles l ($\chi\bar{\chi} \rightarrow l\bar{l}$) and vice versa ($l\bar{l} \rightarrow \chi\bar{\chi}$). As the universe cools to a temperature less than the mass of the particle ($T < m_\chi$), the equilibrium abundance drops exponentially until the rate Γ for the annihilation reaction $\chi\bar{\chi} \rightarrow l\bar{l}$ falls below the expansion rate H , i.e. $\Gamma < H$. At this point, the χ s cease to annihilate, since collisions become unlikely. The interactions which have maintained thermal equilibrium “freeze out” and a relic cosmological abundance remains.

This picture is described quantitatively by the Boltzmann equation, that describes the time evolution of the number density $n_\chi(t)$,

$$\frac{dn_\chi}{dt} + 3Hn_\chi = -\langle\sigma_{Av}\rangle[(n_\chi)^2 - (n_\chi^{eq})^2], \quad (2.18)$$

where $\langle\sigma_A v\rangle$ is the thermally averaged total cross section for annihilation of $\chi\bar{\chi}$ into lighter particles times the relative velocity v . Here, n_χ^{eq} denotes the number density of χ in thermal equilibrium. The second term on the left-hand side accounts for the expansion of the universe, while the right-hand side represents number-changing interactions. The first term in brackets of Eq. (2.18) accounts for depletion due to annihilation, while the second term stems from creation due to the inverse reaction.

There is no closed-form analytic solution to the Boltzmann equation (2.18). However, computer codes like MicrOMEGAs [28] solve it numerically taking into account many different effects. In general, if there are additional particles with a mass within 10% of m_χ that share a quantum number with χ , *coannihilation* will occur. For instance, χ could annihilate readily with such a particle, in which case this reaction could determine the relic abundance. If an annihilation process via a particle A is allowed, it can happen resonantly when the mass of the annihilating particle is $m_\chi \approx m_A/2$. At *resonant annihilation* the particle χ annihilates readily via this channel and thus its relic abundance might be lowered. For instance, MicrOMEGAs includes coannihilation and resonant annihilation, takes proper care of poles, thresholds and many other difficulties that we do not mention here. MicrOMEGAs computes the relic density of the lightest supersymmetric particle in the minimal supersymmetric extension of the Standard Model, see Section 3.2. It is conventional to give the mass density $m_\chi n_\chi$ in units of the present day critical density (2.10) as

$$\Omega_\chi h^2 = m_\chi n_\chi / \rho_c. \quad (2.19)$$

2.2 Nucleosynthesis in Cosmology

The main processes responsible for the chemical equilibrium in the thermal plasma between protons p and neutrons n are the weak reactions:

$$n + \nu_e \rightleftharpoons p + e^-, \quad n + e^+ \rightleftharpoons p + \bar{\nu}_e. \quad (2.20)$$

While the universe cools down, at a temperature below a few MeV, which corresponds to an age of the universe around 0.5 s , the neutron-to-proton ratio n_n/n_p “freezes out”. At these comparable low temperatures, the universe obeys well understood Standard Model physics. The weak interactions become inefficient to maintain the equilibrium, which leads to a neutron-to-proton ratio of

$$\frac{n_n}{n_p} = e^{-\frac{m_n - m_p}{T_{fo}}} \approx \frac{1}{6}, \quad (2.21)$$

where T_{fo} is the freeze-out temperature. Due to neutron decay,

$$n \rightarrow pe^{-}\bar{\nu}_e, \quad (2.22)$$

this ratio further decreases to about 1/7 before neutrons are stabilized in bound states, e.g. deuterium. Regardless of the exact process, nearly all neutrons fuse to helium ${}^4\text{He}$. Therefore, we can estimate the relative abundance by weight $Y_p = \rho_{4\text{He}}/(\rho_n + \rho_p)$ of ${}^4\text{He}$. With n_N denoting the total number of nucleons, it is

$$Y_p \approx X_{4\text{He}} := \frac{4n_{4\text{He}}}{n_N} = \frac{2n_n}{n_p + n_n} = \frac{2n_n/n_p}{1 + n_n/n_p} \approx 25\%. \quad (2.23)$$

This and other processes have a strong sensitivity to the baryon-to-photon ratio [22]

$$\eta := \frac{n_b}{n_\gamma} \simeq 6 \times 10^{-10}. \quad (2.24)$$

For instance, deuterium is destroyed by photons with an energy larger than the binding energy of deuterium, i.e. $\gamma + D \rightarrow n + p$. Anyway, a few minutes after standard big bang, nuclear interactions become effective in building light elements. This procedure is known as big bang nucleosynthesis (BBN). The computation of light element abundances like deuterium D, helium ${}^3\text{He}$ or ${}^4\text{He}$ and lithium ${}^7\text{Li}$ involves all the details of nuclear interactions. There are computer codes [11] predicting the abundances in good agreement with data from astrophysical observations, see Figure 2.1. In doing so, BBN predicts a present day baryon abundance,

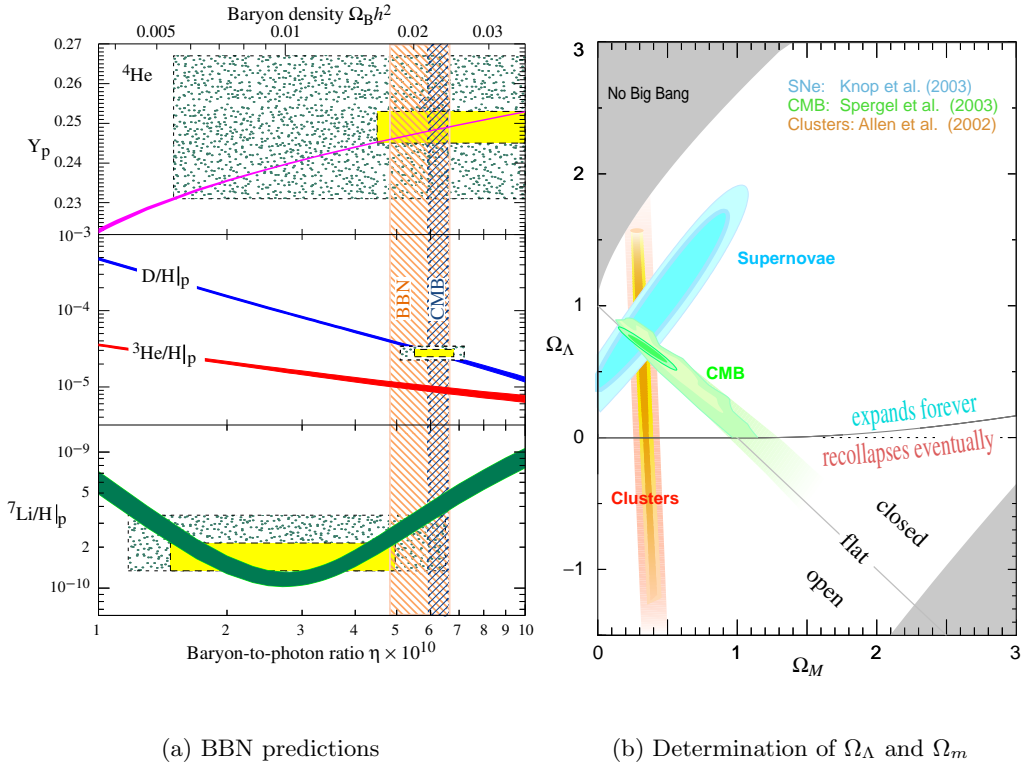
$$0.018 < \Omega_b h^2 < 0.023. \quad (2.25)$$

We point out that BBN gives us the deepest insight into the early universe. We gain testable informations about physics just happening a second after the big bang. If we want to maintain the success of BBN, we get constraints on physics beyond the Standard Model.

Big bang nucleosynthesis constraints especially the relic abundance $\Omega_\chi h^2$ (2.19) of late-decaying massive particles χ . If the lifetime of χ is longer than ~ 0.1 s, its decay may cause non-thermal nuclear reactions during or after BBN, altering the predictions of the standard BBN scenario.

The constraints by BBN differ for radiative and hadronic decays, since these decay processes cause different types of reactions. One simple example is the destruction of a previous build light element by an energetic photon. Examples for this photo dissociation are

$$\gamma + D \rightarrow n + p, \quad \gamma + {}^3\text{He} \rightarrow p + D \quad \text{or} \quad \gamma + {}^4\text{He} \rightarrow n + {}^3\text{He}. \quad (2.26)$$



(a) BBN predictions

 (b) Determination of Ω_Λ and Ω_m

Figure 2.1: (a): The abundances of ${}^4\text{He}$, D, ${}^3\text{He}$, and ${}^7\text{Li}$ as predicted by the standard model of big-bang nucleosynthesis - the bands show the 95% CL range. Boxes indicate the observed light element abundances (smaller boxes: $\pm 2\sigma$ statistical errors; larger boxes: $\pm 2\sigma$ statistical and systematic errors). The narrow vertical band indicates the CMB measure of the cosmic baryon density, while the wider band indicates the BBN Λ CDM range (both at 95% CL). (b): Shown is the preferred region in the $\Omega_m - \Omega_\Lambda$ plane from the compilation of different data. Figures are taken from [22].

For sure, also hadronic decays lead to distortions. For instance, emitted hadrons could lose energy during scattering processes by the emission of photons and thus induce photo dissociation as well. But there are also many other processes. To name another example, antinucleons released in hadronic decays tend to increase the neutron-to-proton ratio n_n/n_p as they are more likely to annihilate with protons. A BBN calculation with decaying particles requires the detailed study of the thermalization of the decay products in the plasma. Actual calculations include this and consider many processes of photo dissociation and the impact of hadronic decay products [9, 10, 11, 12]. Maintaining the predictions of standard big bang nucleosynthesis, they offer constraints on the relic abundance of decaying relic particles $\Omega_\chi h^2$ as a function of their lifetime τ (4.1). Such constraints are shown in Figure 2.2. As we can see, the physics of BBN varies with time

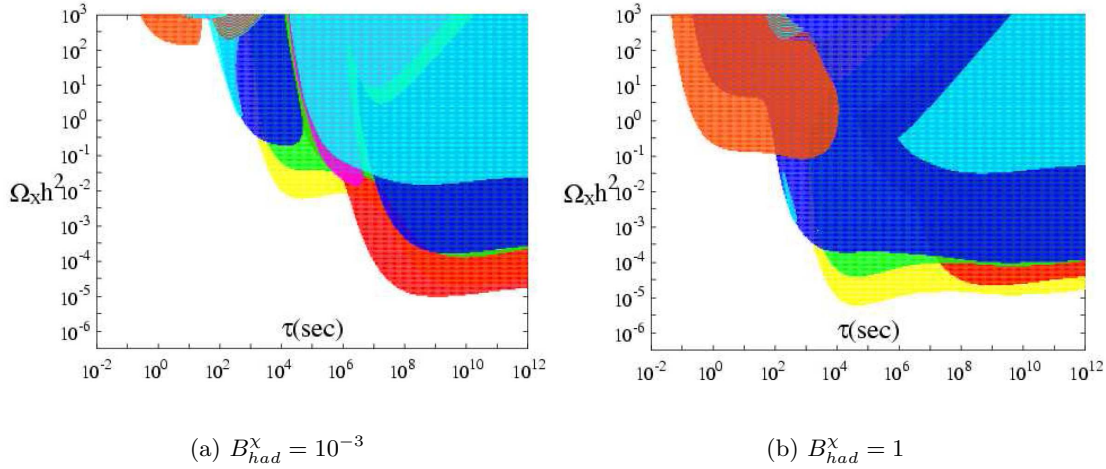


Figure 2.2: (b): BBN constraints on the abundance of relic decaying neutral particles $\Omega_\chi h^2$ (if they would have not decayed) as a function of their lifetime for a $M_\chi = 1$ TeV particle with hadronic branching ratio $B_{had} = 1$. The colored regions are excluded and correspond to the constraints imposed by the observationally inferred upper limit on ${}^4\text{He}$ - orange -, upper limit on ${}^2\text{H}$ - blue -, upper limit on ${}^3\text{He}/{}^2\text{H}$ - red -, and lower limit on ${}^7\text{Li}$ - light blue -. Constraints derived from ${}^6\text{Li}/{}^7\text{Li}$ are shown by the green region. The region indicated by yellow violates the less conservative ${}^6\text{Li}/{}^7\text{Li}$ constraint but should not be considered ruled out. (a): The same as (b) but for hadronic branching ratio $B_{had} = 10^{-3}$. The region excluded by the lower limit on ${}^2\text{H}/\text{H}$ is indicated by the color magenta. Figures are taken from [11].

and different abundances and relative abundances lead to constraints at different times. Therefore, the upper bounds on $\Omega_\chi h^2$ in Figure 2.2 are given as a function of the lifetime of χ .

Cosmic Microwave Background As the universe cools down at $z \simeq 1100$, which corresponds to a time of $\sim 10^{12}$ s after big bang, the temperature of the photons drops below the energy to ionize hydrogen, i.e. $T \lesssim 0.25$ eV. Around this time nearly all free electrons and protons recombine and form neutral hydrogen H . At the time of *recombination*, the universe becomes transparent to the photon background radiation. The present-day cosmic microwave background is the redshifted relic of this radiation. The Cosmic Background Explorer (COBE) satellite mission found that the CMB spectrum corresponds to an almost perfect black body with a temperature of $T_0 \simeq 2.7$ K $\simeq 2.3 \times 10^{-4}$ eV [22]. This is what we expect, since a black body by definition emits the spectrum that would be present in an environment in thermal equilibrium. Furthermore, COBE found the CMB highly isotropic, i.e. temperature anisotropies are of $O(10^{-5})$.

Temperature fluctuations are induced by the slightly inhomogeneous matter distribution at recombination. Figure 2.3 shows the microwave sky as observed by the Wilkinson Microwave Anisotropy Probe (WMAP) [1]. WMAP investigates the temperature anisotropies found by COBE in detail. Expansion of the temperature anisotropies $\delta T/T$

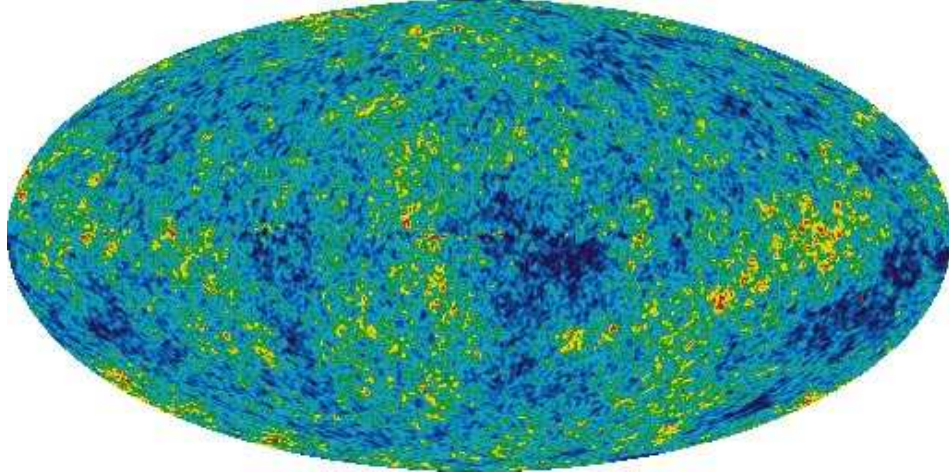


Figure 2.3: CMB temperature fluctuations from the 5-year WMAP data seen over the full sky. The colors (red/blue) represent temperature fluctuations of about $\pm 0.0002^\circ$. Image from <http://map.gsfc.nasa.gov/>.

of Figure 2.3 in spherical harmonics Y_{lm} ,

$$\frac{\delta T}{T}(\Theta, \Phi) = \sum_{l=2}^{\infty} Y_{lm}(\Theta, \Phi), \quad (2.27)$$

gives the CMB power spectrum (see Figure 2.4) in terms of the multipole moment l , where the variance C_l of a_{lm} is given by

$$C_l \equiv \langle |a_{lm}|^2 \rangle = \frac{1}{2l+1} \sum_{m=-l}^l |a_{lm}|^2. \quad (2.28)$$

The analysis of the power spectrum gives us particular information on the universe at the time of recombination. For instance, the position of the first peak implies that the universe is spatially flat, i.e. $\Omega_{tot} \simeq 1$. As one can see in Figure 2.1 the analysis of the CMB power spectrum implies also $\Omega_\Lambda \simeq 0.75$ and $\Omega_m \simeq 0.25$. The amount of baryonic matter can be inferred from the difference in magnitude between the first and second peak, whereas the difference in magnitude between the second and third peak gives the amount of dark matter. These informations are extracted by fits of cosmological models. As can be seen in Figure 2.1, the Λ CDM model, which assumes a cosmological constant

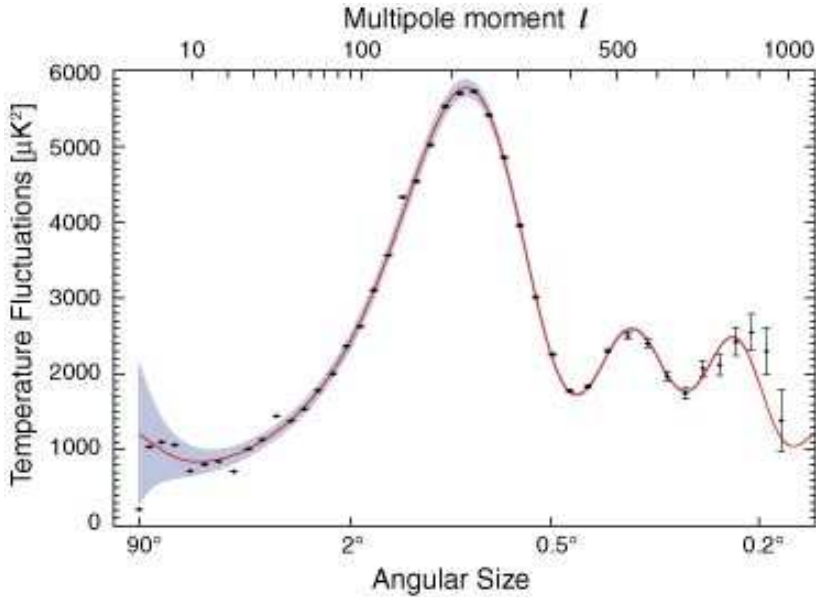


Figure 2.4: CMB power spectrum. Image from <http://map.gfsc.nasa.gov/>

Λ and cold dark matter (CDM := particles that are non-relativistic before structure formation), fits successfully.

Gravitino dark matter scenarios are also constrained by the CMB. Late NLSP decays can lead to unacceptable spectral distortions. However, for gravitino dark matter with neutralino NLSP these constraints have been found to be less constraining than the bounds by big bang nucleosynthesis [29, 30, 31].

2.3 Evidence for Dark Matter

Observations on different scales give striking evidence for the existence of non-baryonic particle dark matter in the universe, where 'dark' means unseen at least up to now. Here, it is a component Ω_{DM} in the cosmic sum rule (2.14), so that

$$1 \simeq \Omega_{tot} = \Omega_m + \Omega_\Lambda = \Omega_b + \Omega_{DM} + \Omega_\Lambda, \quad (2.29)$$

where Ω_m is split into a baryonic component Ω_b and a dark component Ω_{DM} . On cosmological scales from the analysis of WMAP data [1] as sketched above

$$\Omega_b h^2 = 0.02273 \pm 0.00062 \quad \text{and} \quad \Omega_m h^2 = 0.1326 \pm 0.0063 \quad (2.30)$$

are found for the abundance of baryons and matter in the universe. The $1-\sigma$ error is indicated. This is consistent with the predictions of BBN (2.25). Since $\Omega_b < \Omega_m$, this

necessitates a non-baryonic component of matter to be consistent. This is one example of observations that rule out baryonic candidates like unseen astrophysical objects at least to make up all the dark matter. In contrast to others, cosmological observations allow us to determine directly the total amount of dark matter in the universe. There is also evidence from other disconnected observations, but we just name some of them.

On the scale of galaxy cluster, evidence for dark matter is found via several methods based on its gravitational interaction. Astrophysicists determine the mass-to-light ratio M/L , i.e. the ratio of the mass inferred from gravitation M and the observable “shining” mass L , thereby considering all known forms of matter. A convenient calibration is $\Omega_m = (M/L)/1000$. For instance, the mass of a galaxy cluster M can be determined by the application of the virial theorem to the observed distribution of radial velocities within the cluster. Galaxy cluster are bound states of gravity. In short, the radial velocities are too large to be bound by L which indicates a substantial amount of dark matter. Most dynamical estimates are consistent with a value

$$\Omega_m = (M/L)/1000 \sim 0.2 - 0.3. \quad (2.31)$$

These conclusions can be checked against estimates from gravitational lensing data. Following general relativity, light propagates along geodesics which deviate from straight lines when passing near intense gravitational fields. From the distortion of the images of background objects due to the galaxy cluster, one can infer its mass M and even its mass distribution.

There is also evidence on galactic and subgalactic scale. Again, it is gathered by different measurements of velocities of stars and dust not only in other galaxies but also in the Milky Way. These are compared to the gravitational potential due to the known matter. Indeed, also the Milky Way seems to have a particle dark matter halo. The study of microlensing events in the direction of the galactic center shows the lack of compact dark matter in the galactic disk, thus favouring particle dark matter. Gravitational lensing around individual massive elliptical galaxies provides evidence for substructure on scales of $\sim 10^6$ solar masses.

The present day value of the dark matter density as given by the particle data group [22] is

$$\Omega_{DM} = \Omega_m - \Omega_b = 0.105(8) h^{-2} \approx 0.20, \quad (2.32)$$

where the figure in parentheses gives the $1\text{-}\sigma$ uncertainty in the last place.

Chapter 3

From Supersymmetry to Gravitino Dark Matter

In this chapter we introduce briefly the elementary particle content under consideration in this thesis. We will mainly follow the reviews on supersymmetry and supergravity provided in [32, 33, 34]. For more detailed discussions of the gravitino field we refer to [35, 36, 37].

3.1 Local Supersymmetry

Supersymmetry (SUSY) is a space-time symmetry, i.e. an extension of the symmetries of translations, rotations and boosts. SUSY turns bosonic states into fermionic states, and vice versa. The operator Q_α that generates such transformations is an anticommuting spinor with

$$Q_\alpha|\text{Boson}\rangle \simeq |\text{Fermion}\rangle, \quad Q_\alpha|\text{Fermion}\rangle \simeq |\text{Boson}\rangle. \quad (3.1)$$

Translations, rotations and boosts together form Poincaré symmetry. Under general assumptions Poincaré symmetry is the maximal space-time symmetry of identical particles [38], i.e. leaving the particle spin unchanged. SUSY, in turn, is the maximal possible extension of Poincaré symmetry [39]. Particles are transformed into particles with spin differing by 1/2. If SUSY is discovered, all mathematically consistent space-time symmetries will have been realized in nature.

There are many theoretical motivations for supersymmetry [13]. Here, we want to name two of them. The first is SUSY's contribution to the solution of the *hierarchy problem*. The squared mass m_h^2 of the Standard Model Higgs boson h receives quadratically di-

vergent contributions by loop corrections. The one-loop corrections at leading order due to fermions

$$\Delta m_h^2 = -\frac{|\lambda_f|^2}{8\pi^2}\Lambda_{UV}^2 + \dots \quad (3.2)$$

and scalars

$$\Delta m_h^2 = \frac{\lambda_s}{16\pi^2}\Lambda_{UV}^2 + \dots \quad (3.3)$$

are proportional to the corresponding couplings $|\lambda_f|^2$ and λ_s respectively. They are quadratically divergent with Λ_{UV} , which should be interpreted as at least the energy scale at which new physics enters to alter the high-energy behaviour of the theory. At the Planck scale,

$$M_p = \frac{1}{\sqrt{8\pi G_N}} = 2.435 \times 10^{18} \text{ GeV}, \quad (3.4)$$

where G_N is Newton's gravitational constant [22], quantum gravitational effects become important. Therefore, a new framework will certainly be required at M_p . If $\Lambda_{UV} = M_p$ the ‘‘natural’’ scale of m_h^2 , including quantum corrections, seems to be like M_p^2 rather than something near to the electroweak scale $m_Z^2 \sim (100 \text{ GeV})^2$. So the hierarchy problem stems from the fact that the ratio $M_p/m_Z \sim 10^{16}$ is so huge. In connection with the Higgs mechanism (see Section 3.3.2) this is a problem for the entire mass spectrum of the Standard Model (SM). Regarding Eq. (3.2) and Eq. (3.3), the cancellation of all such contributions to scalar masses is achieved, if each fermion is accompanied by two complex scalars with $\lambda_s = |\lambda_f|$. This is actually unavoidable, once we assume the existence of supersymmetry. So SUSY does not resolve the hierarchy itself, but it stabilizes particles against quantum corrections. We will see in Section 3.2 how SUSY alters the particle content of the Standard Model.

Secondly, SUSY provides a promising candidate for the particle dark matter of Chapter 2. In supersymmetric theories with R -parity (3.9) being preserved the lightest supersymmetric particle (LSP) is stable. If the LSP is also neutral, it is a viable candidate with distinct properties. In this thesis, we consider gravitino dark matter.

The parameter ξ_α of global SUSY transformations¹ is space-time independent. By defining ξ_α to be space-time dependent, $\xi_\alpha \rightarrow \xi_\alpha(x)$, SUSY becomes a *local symmetry*. This corresponds to gauging supersymmetry. Since the gravitino is the gauge field of local supersymmetry transformations, it is an unique and inevitable prediction of local supersymmetry. Local supersymmetry combines the principles of supersymmetry and general relativity, which is the current theory of gravity. Therefore, it is referred to as supergravity (SUGRA).

¹We consider unextended $N = 1$ supersymmetry in four spacetime dimensions $D = 4$.

In the next section we define the field content under consideration in this thesis. Independently, supergravity, i.e. local supersymmetry, extends this field content unambiguously by the gravity supermultiplet (Table 3.1). In some sense it is the minimal field content

Table 3.1: Gravity supermultiplet

Name	Bosons	Fermions	$(\text{SU}(3)_C, \text{SU}(2)_L)_Y$
Graviton, gravitino	$g_{\mu\nu}$	Ψ_μ	$(\mathbf{1}, \mathbf{1})_0$

of any SUGRA model. It consists of the spin-2 graviton, that mediates gravity, and the spin-3/2 gravitino. Both are neutral with respect to the SM gauge group (3.5).

SUGRA is non-renormalizable. Shortened, quantum corrections diverge and for SUGRA it is not known how to deal with them. To this day there is no consistent quantum theory of gravity. We assume that SUGRA is an appropriate low-energy approximation of a more general theory. As effective theory the request of renormalizability disappears (cf. Fermi theory of weak interaction).

3.2 The Minimal Supersymmetric Standard Model

The Minimal Supersymmetric Standard Model (MSSM) is the minimal phenomenologically viable supersymmetric extension of the Standard Model of particle physics (SM). Due to supersymmetry there is a supersymmetric partner particle to each SM fermion and SM gauge boson. Global SUSY is assumed. So to begin with, the MSSM does not contain gravity. The spin-1/2 fermions, i.e. three families of quarks and leptons, reside in chiral supermultiplets with their spin-0 scalar boson partners. The spin-1 gauge bosons, i.e. gluons, W and B bosons, reside in gauge supermultiplets with their spin-1/2 fermionic partners. There are two chiral Higgs supermultiplets. Each consists of one spin-0 Higgs SU(2)-doublet and its spin-1/2 fermionic superpartner. The chiral supermultiplets in Table 3.2 and the gauge supermultiplets in Table 3.3 make up the field content of the MSSM. They are summarized according to their transformation properties under the Standard Model gauge group,

$$G_{SM} = G_{MSSM} = \prod_{\alpha=1}^3 G_\alpha = \text{U}(1)_Y \times \text{SU}(2)_L \times \text{SU}(3)_C. \quad (3.5)$$

Here, α labels the SM gauge groups.

Particles in the same supermultiplet transform in identical gauge group representations. Superpartners are denoted by a tilde. See, for instance, the gauginos $\lambda^{(\alpha)a}$ in Table 3.3. They are the fermionic partners of the SM gauge bosons $A_\mu^{(\alpha)a}$, where a labels the gauge group generators.

All matter fields of Table 3.2 are written in terms of left-handed Weyl spinors χ_L since they stem from left-chiral supermultiplets. Therefore, we enter the left-handed hermitian conjugate $(\cdot)^\dagger$ of a right-handed field instead of the field itself. In four component spinor representation the matter fermions can be given as

$$\chi_L = \begin{pmatrix} (\chi_\alpha)_{W/B} \\ 0 \end{pmatrix}, \quad (3.6)$$

where W/B indicates quantities used in the book by Wess and Bagger [40]. Strongly interacting particles reside in color triplets $\mathbf{3}$, i.e. quarks and squarks. Since we do not encounter any strong interaction process in this thesis, colour indices are not written out. In contrast, $SU(2)_L$ doublets $\mathbf{2}$ ($\mathbf{2} = \bar{\mathbf{2}}$) are explicitly given in Table 3.2. Gauge singlets are denoted by $\mathbf{1}$ or in the case of $U(1)_Y$ carry hypercharge $Y = 0$. Note that the normalization of the hypercharges is such that the electric charge Q is given by $Q = T_3 + Y/2$, where T_3 denotes the weak isospin eigenvalue $\pm 1/2$ for upper/lower entries in the $SU(2)_L$ doublets and accordingly $T_3 = 0$ for $SU(2)_L$ singlets. The SM contains three families of quarks and leptons, so the family index I in Table 3.2 counts $I = 1, 2, 3$. It is clear, that there is an antiparticle for each particle of Table 3.2.

The Lagrangian of the MSSM is determined by the superpotential,

$$W_{\text{MSSM}} = \tilde{U}^* \mathbf{y}_u \tilde{Q} \cdot H_u - \tilde{D}^* \mathbf{y}_d \tilde{Q} \cdot H_d - \tilde{E}^* \mathbf{y}_e \tilde{L} \cdot H_d + \mu H_u \cdot H_d. \quad (3.7)$$

which is a holomorphic function of the scalars of the supermultiplets. The doublet structure is tied together as $\tilde{Q} \cdot H_u = \varepsilon^{ij} \tilde{Q}_i H_{uj}$, with ε^{ij} given in Appendix A. Furthermore, $\tilde{U}^* \mathbf{y}_u \tilde{Q}$ is meant to be a matrix multiplication in family space, $\tilde{U}^* \mathbf{y}_u \tilde{Q} = \tilde{U}^{*I} y_u^{IJ} \tilde{Q}^J$.

R-parity Accidentally, the Standard Model conserves baryon number B and lepton number L . So the proton as lightest baryon with $B = 1$ is absolutely stable, since there is no baryon to decay into and decays into something else would violate baryon number conservation. W_{MSSM} is the most general superpotential that does respect gauge invariance and all SM conservation laws. The MSSM contains by definition only renormalizable interactions and only terms that respect baryon and lepton number conservation. But the most general renormalizable superpotential which does respect gauge invariance contains also B and L violating terms,

$$W_{\text{PR}} = \mu_i H_u \cdot \tilde{L} + \frac{1}{2} \lambda_{ijk} \tilde{L}_i \cdot \tilde{L}_j \tilde{E}_k^* + \lambda'_{ijk} \tilde{L}_i \cdot \tilde{Q}_j \tilde{D}_k^* + \frac{1}{2} \lambda''_{ijk} \epsilon^{abc} \tilde{U}_i^* \tilde{D}_j^* \tilde{D}_{kc}^*, \quad (3.8)$$

Table 3.2: Matter fields of the MSSM

Name	Scalar Bosons ϕ^i	Fermions χ_L^i	$(\text{SU}(3)_C, \text{SU}(2)_L)_Y$
Sleptons, leptons $I = 1, 2, 3$	$\tilde{L}^I = \begin{pmatrix} \tilde{\nu}_L^I \\ \tilde{e}_L^{-I} \end{pmatrix}$	$L^I = \begin{pmatrix} \nu_L^I \\ e_L^{-I} \end{pmatrix}$	$(\mathbf{1}, \mathbf{2})_{-1}$
	$\tilde{E}^{*I} = \tilde{e}_R^{-*I}$	$E^{\dagger I} = e_R^{-\dagger I}$	$(\mathbf{1}, \mathbf{1})_{+2}$
Squarks, quarks $I = 1, 2, 3$ ($\times 3$ colors)	$\tilde{Q}^I = \begin{pmatrix} \tilde{u}_L^I \\ \tilde{d}_L^I \end{pmatrix}$	$Q^I = \begin{pmatrix} u_L^I \\ d_L^I \end{pmatrix}$	$(\mathbf{3}, \mathbf{2})_{+\frac{1}{3}}$
	$\tilde{U}^{*I} = \tilde{u}_R^{*I}$	$U^{\dagger I} = u_R^{\dagger I}$	$(\bar{\mathbf{3}}, \mathbf{1})_{-\frac{4}{3}}$
	$\tilde{D}^{*I} = \tilde{d}_R^{*I}$	$D^{\dagger I} = d_R^{\dagger I}$	$(\bar{\mathbf{3}}, \mathbf{1})_{+\frac{2}{3}}$
Higgs, Higgsinos	$H_d = \begin{pmatrix} H_d^0 \\ H_d^- \end{pmatrix}$	$\tilde{H}_d = \begin{pmatrix} \tilde{H}_d^0 \\ \tilde{H}_d^- \end{pmatrix}$	$(\mathbf{1}, \mathbf{2})_{-1}$
	$H_u = \begin{pmatrix} H_u^+ \\ H_u^0 \end{pmatrix}$	$\tilde{H}_u = \begin{pmatrix} \tilde{H}_u^+ \\ \tilde{H}_u^0 \end{pmatrix}$	$(\mathbf{1}, \mathbf{2})_{+1}$

where in the last summand $a, b, c = 1, 2, 3$ are $\text{SU}(3)_C$ indices. Some of these terms lead to proton decay, whereas no proton decay has been observed.

Usually, the presence of all baryon and lepton number violating terms is forbidden by requiring the conservation of an additional global symmetry, so called R -parity, defined for each particle as

$$P_R = (-1)^{3(B-L)+2s}, \quad (3.9)$$

where s denotes the spin of the particle. In the MSSM with only renormalizable interactions and conserved R -parity the proton is absolutely stable.

Table 3.3: Gauge fields of the MSSM

Name	Gauge bosons $A_\mu^{(\alpha)a}$	Gauginos $\lambda^{(\alpha)a}$	$(\text{SU}(3)_C, \text{SU}(2)_L)_Y$
B-boson, bino	$A_\mu^{(1)a} = B_\mu \delta^{a1}$	$\lambda^{(1)a} = \tilde{B} \delta^{a1}$	$(\mathbf{1}, \mathbf{1})_0$
W-bosons, winos	$A_\mu^{(2)a} = W_\mu^a$	$\lambda^{(2)a} = \tilde{W}^a$	$(\mathbf{1}, \mathbf{3})_0$
gluon, gluino	$A_\mu^{(3)a} = G_\mu^a$	$\lambda^{(3)a} = \tilde{g}^a$	$(\mathbf{8}, \mathbf{1})_0$

From Eq. (3.9) it is easy to check that Standard Model particles and the Higgs bosons have even R -parity ($P_R = +1$), while all supersymmetric partners have odd R -parity ($P_R = -1$). This implies, that sparticles must be produced in pairs, that heavier sparticles must decay into lighter ones and that the LSP must be absolutely stable, since it has no allowed decay mode. Thus the LSP becomes a “natural” candidate for particle dark matter.

Again, the gauge group (3.5), the field content summarized in Tables 3.2, 3.3 and the superpotential (3.7) define the Minimal Supersymmetric Standard Model. In this thesis exact R -parity (3.9) conservation is assumed. The whole MSSM Lagrangian can, for instance, be found in [41].

3.3 Symmetry Breaking

In the previous sections we defined the field content under consideration. Tables 3.3, 3.2 and 3.1 list gauge eigenstates. In general, gauge eigenstates differ from physical mass eigenstates. Gauge eigenstates can mix, so that the mass eigenstates become linear combinations of gauge eigenstates. Equally, one can give the gauge eigenstates as linear combinations of mass eigenstates. In the MSSM there are different possible sources of mixing that are due to the *spontaneous breakdown of symmetries*.

Furthermore, the field content is given in two-component Weyl spinors. These are combined to form four spinors. In this section we give the physical particle spectrum as used for computations in this thesis.

3.3.1 Supersymmetry Breaking

The mass operator P^2 commutes with the SUSY operators,

$$[P^2, Q_\alpha] = [P^2, \bar{Q}_{\dot{\alpha}}] = 0. \quad (3.10)$$

Therefore, particles within the same supermultiplet are degenerate in mass. Since no sparticles have been observed yet, supersymmetry has to be a broken symmetry, if realized in nature.

In the MSSM, supersymmetry breaking is parameterized by additional terms in the

Lagrangian,

$$\begin{aligned}
 \mathcal{L}_{soft}^{MSSM} = & -\frac{1}{2}(M_3\tilde{g}^a\tilde{g}^a + M_2\tilde{W}^a\tilde{W}^a + M_1\tilde{B}\tilde{B} + h.c.) \\
 & -(\tilde{U}^* \mathbf{a}_u \tilde{Q} \cdot H_u - \tilde{D}^* \mathbf{a}_d \tilde{Q} \cdot H_d - \tilde{E}^* \mathbf{a}_e \tilde{L} \cdot H_d + h.c.) \\
 & -\tilde{Q}^\dagger \mathbf{m}_Q^2 \tilde{Q} - \tilde{L}^\dagger \mathbf{m}_L^2 \tilde{L} - \tilde{U}^\dagger \mathbf{m}_U^2 \tilde{U} - \tilde{D}^\dagger \mathbf{m}_D^2 \tilde{D} - \tilde{E}^\dagger \mathbf{m}_E^2 \tilde{E} \\
 & -m_{H_u}^2 H_u^* H_u - m_{H_d}^2 H_d^* H_d - (bH_u H_d + h.c.). \tag{3.11}
 \end{aligned}$$

In Eq. (3.11), M_3 , M_2 and M_1 are gluino, wino and bino mass terms. Here, we suppress all gauge indices. In the second line each of \mathbf{a}_u , \mathbf{a}_d , \mathbf{a}_e is a complex 3×3 matrix in family space. They are in direct correspondence with the Yukawa couplings of W_{MSSM} (3.7). The third line of Eq. (3.11) consists of squark and slepton mass terms. Each of \mathbf{m}_Q^2 , \mathbf{m}_L^2 , \mathbf{m}_U^2 , \mathbf{m}_D^2 , \mathbf{m}_E^2 is a hermitian 3×3 matrix in family space. In the last line we have SUSY breaking contributions to the Higgs potential.

The supersymmetry-breaking couplings in $\mathcal{L}_{soft}^{MSSM}$ are soft (of positive mass dimension) in order to naturally maintain a hierarchy between the electroweak scale and the Planck scale, i.e. in order not to reintroduce quadratically divergent contributions to scalar masses (3.3). Eq. (3.11) is the most general renormalizable soft SUSY breaking Lagrangian that respects gauge invariance and R -parity in the MSSM.

In a viable model soft mass terms make sparticles heavy enough to be in accord with experiment. In principle, due to off-diagonal entries $*$ in the family matrices of $\mathcal{L}_{soft}^{MSSM}$,

$$\mathbf{a}_u, \dots, \mathbf{m}_E^2 \sim \begin{pmatrix} \cdot & * & * \\ * & \cdot & * \\ * & * & \cdot \end{pmatrix}, \tag{3.12}$$

any scalars with the same charges and R -parity can mix with each other. For the squarks and sleptons of the MSSM the general hypothesis of *flavour-blind soft parameters* predicts that most of these mixings are very small. Since these would have even smaller impact on our results, as an appropriate simplification, we take these mixings to be zero. So all family matrices of $\mathcal{L}_{soft}^{MSSM}$ are assumed to be diagonal, i.e.

$$\mathbf{a}_u = \dots = \mathbf{m}_E^2 = \begin{pmatrix} 1 & 0 & 0 \\ 0 & 1 & 0 \\ 0 & 0 & 1 \end{pmatrix}. \tag{3.13}$$

However, the soft parameters can not be arbitrary.

In order to understand how patterns like Eq. (3.13) can emerge, it is necessary to consider models in which SUSY is spontaneously broken. The condition for the spontaneous breakdown of a symmetry is a ground state that (in contrast to the underlying

Lagrangian) does not respect this symmetry. Since the ground state ought to be Lorentz invariant, it may not carry spin. Typically, scalars, i.e. the auxiliary fields of some chiral supermultiplets (*F-term breaking*), acquire non-zero vacuum expectation values $\langle F \rangle$ and thus break SUSY. In order not to break conserved gauge symmetries, these scalars are neutral under those. Although SUSY breaking is strongly constrained, it is not known how it should be done and there are many different SUSY breaking scenarios. We mention two of them below. However, models of SUSY breaking lead to particular soft parameters in Eq. (3.11). Then we can compute physical quantities like mass spectra and lifetimes, so that experiments and cosmology can lead to constraints or even rule out scenarios. We will see in Chapter 5 how big bang nucleosynthesis constrains SUGRA models.

In supergravity, an analogon to the Higgs mechanism of electroweak-symmetry breaking exists, i.e. the *super Higgs mechanism*. Spontaneous breaking always implies a Goldstone particle with the same quantum numbers as the broken symmetry generator. Since Q_α is fermionic, in the case of SUSY breaking the Goldstone particle ought to be a fermion. This goldstino is absorbed by the gravitino, which acquires thereby its $\pm 1/2$ spin components and a mass

$$m_{3/2} \sim \langle F \rangle / M_p, \quad (3.14)$$

where $\langle F \rangle$ is the vacuum expectation value (VEV) that breaks SUSY.

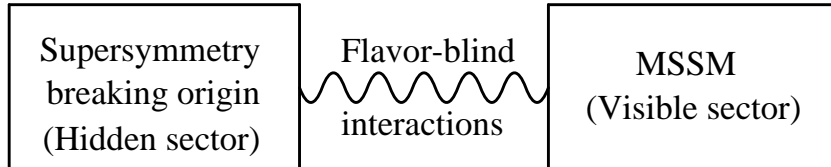


Figure 3.1: The presumed schematic structure for supersymmetry breaking. Figure taken from [32].

SUSY Breaking Mechanisms Spontaneous supersymmetry breaking requires an extension of the MSSM, because in the MSSM there is no candidate gauge singlet to acquire a VEV². Electroweak symmetry breaking is discussed in Section 3.3.2. On the search for a natural explanation of Eq. (3.13), SUSY breaking is expected to occur in a “hidden sector” of particles without direct couplings to the “visible sector”, consisting of the supermultiplets of the MSSM. However, the two sectors have some common in-

²A Fayet-Iliopoulos term for $U(1)_Y$ must be subdominant compared to other sources of supersymmetry breaking in the MSSM, if not absent altogether, because some squarks or sleptons would get non-zero VEVs breaking color and/or electromagnetism.

teractions that mediate SUSY breaking from the hidden sector to the visible sector, see Figure 3.1, which results in the MSSM soft terms (3.11).

In *Planck-scale-mediated supersymmetry breaking* (PMSB) scenarios the mediating interaction is gravitational. If in PMSB supersymmetry is broken in the hidden sector by a VEV $\langle F \rangle$, then the order of the soft terms m_{soft} should be by dimensional analysis

$$m_{soft} \sim \langle F \rangle / M_p. \quad (3.15)$$

The *minimal supergravity* (mSUGRA) model implies convenient assumptions leading to

$$\begin{aligned} M_3 = M_2 = M_1 = m_{1/2} &= f \frac{\langle F \rangle}{M_p}, \\ \mathbf{m}_Q^2 = \mathbf{m}_L^2 = \mathbf{m}_U^2 = \mathbf{m}_D^2 = \mathbf{m}_E^2 &= m_0^2 \mathbb{1}, \quad m_{H_u}^2 = m_{H_d}^2 = m_0^2 = k \frac{|\langle F \rangle|^2}{M_p^2}, \\ \mathbf{a}_u = A_0 \mathbf{y}_u, \quad \mathbf{a}_d = A_0 \mathbf{y}_d, \quad \mathbf{a}_e &= A_0 \mathbf{y}_e = \alpha \frac{\langle F \rangle}{M_p} \mathbf{y}_e, \\ b = B_0 \mu &= \beta \frac{\langle F \rangle}{M_p} m, \end{aligned} \quad (3.16)$$

at a renormalization scale $Q \approx M_p$. Here, f, k, α, β , are undetermined parameters. But then the soft terms in $\mathcal{L}_{soft}^{MSSM}$ (3.11) are all determined by just four parameters, i.e. $m_{1/2}, m_0^2, A_0$ and B_0 . As we can see from Eq. (3.14) and (3.15), in PMSB the gravitino mass $m_{3/2}$ is comparable to the masses of the MSSM sparticles

$$m_{3/2} \sim m_{soft} \sim \langle F \rangle / M_p \sim O(100 \text{ GeV}), \quad (3.17)$$

so that the gravitino can be the LSP with $m_{3/2}$ expected to be at least of order 100 GeV. The low energy SUSY spectrum can be obtained by solving renormalization group equations which can be done in the MSSM by computer codes like, for instance, SOFT-SUSY [42]. In a given theory renormalization group equations describe the evolution of physical quantities like masses and couplings with the scale Q . Therefore, with a given input like (3.3.1) SOFTSUSY can compute the SUSY spectrum at scales below the scale of electroweak symmetry breaking.

In *gauge-mediated supersymmetry breaking* (GMSB) models, the ordinary gauge interactions, rather than gravity, mediate SUSY breaking from the hidden sector to the visible sector. The basic idea is to introduce new chiral supermultiplets that couple to the scalar, which acquires a VEV $\langle F \rangle$, and also couple indirectly to the sparticles of the MSSM through the ordinary $U(1)_Y \times SU(2)_L \times SU(3)_C$ (3.5) gauge boson and gaugino interactions. The new fields appear in loop diagrams only, but thereby they generate

particular soft terms. Using dimensional analysis, one estimates for the order of the MSSM soft terms

$$m_{soft} \sim \frac{\alpha}{4\pi} \frac{\langle F \rangle}{M_{mess}}, \quad (3.18)$$

where $\alpha/4\pi$ is a loop factor for Feynman diagrams involving the gauge interactions (3.5) and M_{mess} is the characteristic mass scale of the new-introduced supermultiplets. The gauge interactions (3.5) are flavour blind, which in turn leads to flavour-blind soft terms (3.13). By comparison of Eq. (3.18) with (3.14) we see that, in contrast to PMSB, gauge-mediated supersymmetry breaking models predict a gravitino that is much lighter than the MSSM sparticles $m_{3/2} \ll m_{soft}$ as long as $M_{mess} \ll M_p$. The gravitino is almost certainly the LSP.

The fact, that the gravitino is a possible LSP candidate in Planck-scale mediated supersymmetry breaking models and even almost certainly the LSP in gauge-mediated supersymmetry breaking models [43, 44], is one motivation for the investigation of gravitino dark matter scenarios. In both mechanisms the lightest neutralino (cf. Section 3.3.2) is one of the lightest sparticles [2, 45] and thus it is a candidate to be the next-to-lightest supersymmetric particle (NLSP) with gravitino dark matter. Typically, the lightest neutralino has a dominant bino component. Therefore, studies are made with a bino NLSP, e.g. [17, 18, 19, 46]. However, for instance, in [47] an extended gauge mediation model is proposed that can naturally have a Higgsino NLSP. In order to be independent of a particular SUSY breaking model, we investigate gravitino dark matter with general neutralino NLSP.

As mentioned above there are many SUSY breaking mechanisms. For instance, we do not mention anomaly-mediated SUSY breaking, since it does not have the gravitino as LSP.

3.3.2 Electroweak Symmetry Breaking

It is clear that the electroweak symmetry is broken down to electromagnetism,

$$SU(2)_L \times U(1)_Y \rightarrow U(1)_{em}. \quad (3.19)$$

In the MSSM this can be achieved dynamically after supersymmetry breaking by radiative corrections to the soft Higgs masses m_{H_u} , m_{H_d} . One of the Higgs masses evolves to a negative value at the electroweak scale and thus breaks electroweak symmetry, since thereby the neutral Higgs fields H_u^0 and H_d^0 acquire non-zero vacuum expectation values

$$\langle H_u^0 \rangle = v_u/\sqrt{2} \quad \text{and} \quad \langle H_d^0 \rangle = v_d/\sqrt{2}, \quad (3.20)$$

that break the electroweak symmetry. The ratio of the vacuum expectation values (VEVs) is traditionally written as

$$\tan \beta \equiv v_u/v_d. \quad (3.21)$$

Since this is compatible with the SM Higgs mechanism the VEVs are related to the SM Higgs VEV v ,

$$v_u^2 + v_d^2 = v^2 = 4m_Z^2/(g^2 + g'^2) \approx (246 \text{ GeV})^2. \quad (3.22)$$

From (3.21) and (3.22) we see,

$$\begin{aligned} v_u &= v \sin \beta, \\ v_d &= v \cos \beta. \end{aligned} \quad (3.23)$$

H_d and H_u together consist of eight real scalar degrees of freedom. They are two complex $SU(2)_L$ doublets, giving $2 \cdot 2 \cdot 2 = 8$. When the electroweak symmetry is broken, three of them G^0 , G^\pm , become the longitudinal modes of the Z^0 and W^\pm massive vector bosons. The gauge boson mass eigenstates are given by [48]

$$\begin{pmatrix} A_\mu \\ Z_\mu^0 \end{pmatrix} = \begin{pmatrix} \cos \Theta_W & \sin \Theta_W \\ -\sin \Theta_W & \cos \Theta_W \end{pmatrix} \begin{pmatrix} B_\mu \\ W_\mu^0 \end{pmatrix}, \quad (3.24)$$

$$W_\mu^\pm = \frac{1}{\sqrt{2}}(W_\mu^1 \mp iW_\mu^2), \quad (3.25)$$

where Θ_W is the known weak mixing angle.

The remaining five ($8 - 3 = 5$) Higgs scalar mass eigenstates consist of two CP-even neutral scalars h^0 and H^0 , one CP-odd neutral scalar A^0 and a charged (+1) scalar H^+ and its conjugate charged (-1) scalar H^- . By convention, h^0 is lighter than H^0 . Here, the superscripts indicate as usual the electric charge. We will omit them sometimes at neutral particles, e.g. $h \equiv h^0$. The neutral gauge-eigenstate fields can be expressed in terms of the mass eigenstate fields as:

$$\begin{pmatrix} H_u^0 \\ H_d^0 \end{pmatrix} = \frac{1}{\sqrt{2}} \left\{ \begin{pmatrix} v_u \\ v_d \end{pmatrix} + \begin{pmatrix} \cos \alpha & \sin \alpha \\ -\sin \alpha & \cos \alpha \end{pmatrix} \begin{pmatrix} h^0 \\ H^0 \end{pmatrix} + i \begin{pmatrix} \sin \beta_0 & \cos \beta_0 \\ -\cos \beta_0 & \sin \beta_0 \end{pmatrix} \begin{pmatrix} G^0 \\ A^0 \end{pmatrix} \right\} \quad (3.26)$$

α and β_0 are mixing angles. We take v_u, v_d to minimize the tree-level potential in this analysis, so that $\beta_0 = \beta$. If one might to minimize the loop-corrected effective potential instead, it is more useful to expand around VEVs that do not minimize the tree-level potential. However, we have the tree-level Higgs masses,

$$m_{h,H}^2 = \frac{1}{2}(m_A^2 + m_Z^2 \mp \sqrt{(m_A^2 - m_Z^2)^2 + 4m_Z^2 m_A^2 \sin^2 2\beta}), \quad (3.27)$$

$$m_A^2 = 2b/\sin 2\beta = 2|\mu|^2 + m_{H_u}^2 + m_{H_d}^2. \quad (3.28)$$

The mixing angle α is traditionally chosen to be negative. At tree-level, α is determined by

$$\frac{\sin 2\alpha}{\sin 2\beta} = - \left(\frac{m_H^2 + m_h^2}{m_H^2 - m_h^2} \right), \quad \frac{\tan 2\alpha}{\tan 2\beta} = \left(\frac{m_A^2 + m_Z^2}{m_A^2 - m_Z^2} \right). \quad (3.29)$$

It follows that $-\pi/2 < \alpha < 0$ (provided $m_A > m_Z$). The limit $m_A \gg m_Z$ is referred to as the decoupling limit. Then, the particles A^0 , H^0 and H^\pm are much heavier than h^0 and h^0 has the same couplings as the Standard Model Higgs. The angle α becomes very nearly $\beta - \frac{\pi}{2}$. As we see from Eq. (3.28), $m_A \gg m_Z$ is typically achieved by a large μ parameter. In any case, one light Higgs boson h , whereas the other Higgses H , A , H^\pm , decouple as heavy particles, represents a minimal Higgs configuration. We will use the decoupling limit later in this analysis.

Already in the SM the quark gauge eigenstates are mixed. The quark mixing matrix (CKM matrix) is known by experiment, see [22]. Mixing with the third generation is small ($O(10^{-3})$). First and second generation mixing is larger ($O(10^{-1})$). However, since the consideration of quark mixing would give a negligible correction ($O(10^{-3})$) only, we take the quark mixing matrix diagonal (3.13). This means we identify their gauge and mass eigenstates.

Neutralinos and Charginos Due to electroweak symmetry breaking, Higgsinos and electroweak gauginos mix with each other. The neutral Higgsinos ($\tilde{H}_u^0, \tilde{H}_d^0$) and the neutral gauginos (\tilde{B}, \tilde{W}^0) combine to form four mass eigenstates called *neutralinos*. The charged Higgsinos and winos combine to form two mass eigenstates with electric charge ± 1 called *charginos*. We present the neutralinos, since we analyze neutralino-to-gravitino decays. We denote the neutralino mass eigenstates by χ_i^0 ($i = 1, 2, 3, 4$). By convention, these are labeled in ascending order, so that $m_{\chi_1^0} < m_{\chi_2^0} < m_{\chi_3^0} < m_{\chi_4^0}$.

In the gauge-eigenstate basis $\Psi^0 = (\tilde{B}, \tilde{W}^0, \tilde{H}_d^0, \tilde{H}_u^0)^T$, the neutralino mass part of the Lagrangian is

$$\mathcal{L}_{\text{neutralino mass}} = -\frac{1}{2}(\Psi^0)^T \mathbf{M}_{\tilde{\chi}} \Psi^0 + h.c., \quad (3.30)$$

where

$$\mathbf{M}_{\tilde{\chi}} = \begin{pmatrix} M_1 & 0 & -c_\beta s_W m_Z & s_\beta s_W m_Z \\ 0 & M_2 & c_\beta c_W m_Z & -s_\beta c_W m_Z \\ -c_\beta s_W m_Z & c_\beta c_W m_Z & 0 & -\mu \\ s_\beta s_W m_Z & -s_\beta c_W m_Z & -\mu & 0 \end{pmatrix}. \quad (3.31)$$

Here we have introduced abbreviations $s_\beta = \sin \beta$, $c_\beta = \cos \beta$, $s_W = \sin \Theta_W$, $c_W = \cos \Theta_W$. The entries M_1 and M_2 are the soft masses from Eq. (3.11) of bino \tilde{B} and wino \tilde{W}^a , while the entries $-\mu$ are the supersymmetric Higgsino mass terms of Eq. (3.7). So

these terms have different sources, which might lead to phenomenological consequences. The terms proportional to m_Z stem from electroweak symmetry breaking. Since Θ_W is also known, they are fixed by $\tan\beta$. The mass matrix $\mathbf{M}_{\tilde{\chi}}$ can be diagonalized by a unitary matrix \mathbf{N} to obtain mass eigenstates:

$$\tilde{\chi}_i^0 = \mathbf{N}_{ij} \Psi_j^0, \quad (3.32)$$

so that

$$\mathbf{N}^* \mathbf{M}_{\tilde{\chi}} \mathbf{N}^{-1} = \begin{pmatrix} m_{\chi_1^0} & 0 & 0 & 0 \\ 0 & m_{\chi_2^0} & 0 & 0 \\ 0 & 0 & m_{\chi_3^0} & 0 \\ 0 & 0 & 0 & m_{\chi_4^0} \end{pmatrix} \quad (3.33)$$

has real positive entries on the diagonal. The indices (i, j) on \mathbf{N}_{ij} are (mass, gauge) eigenstate labels. The mass eigenvalues and the mixing matrix \mathbf{N}_{ij} can be given in closed form in terms of the parameters M_1 , M_2 , μ and $\tan\beta$ [49].

We take M_1 and M_2 real and positive by convention. The off-diagonal terms proportional to m_Z in Eq. (3.31) are also defined to be real. The phase of μ within that convention is then really a physical parameter and can not be rotated away. Thus there can be CP-violating effects in low-energy physics that are not observed. Therefore, we assume μ is real in the same set of conventions, so that \mathbf{N}_{ij} becomes an orthogonal matrix. This is usual although not strictly mandatory.

An analog discussion holds for the charged Higgsinos and winos forming charginos. In the gauge eigenstate basis $\Psi^\pm = (\tilde{W}^+, \tilde{H}_u^+, \tilde{W}^-, \tilde{H}_d^-)^T$ we have the chargino mass term

$$\mathcal{L}_{\text{chargino mass}} = -\frac{1}{2} (\Psi^\pm)^T \mathbf{M}_{\tilde{\chi}^\pm} \Psi^\pm + h.c., \quad (3.34)$$

where the chargino mass matrix $\mathbf{M}_{\tilde{\chi}^\pm}$ can be written in 2×2 block form

$$\mathbf{M}_{\tilde{\chi}^\pm} = \begin{pmatrix} 0 & \mathbf{X}^T \\ \mathbf{X} & 0 \end{pmatrix}, \quad (3.35)$$

with

$$\mathbf{X} = \begin{pmatrix} M_2 & gv_u/\sqrt{2} \\ gv_d/\sqrt{2} & \mu \end{pmatrix} = \begin{pmatrix} M_2 & \sqrt{2}s_\beta m_W \\ \sqrt{2}c_\beta m_W & \mu \end{pmatrix}. \quad (3.36)$$

The mass eigenstates are related to the gauge eigenstates by two unitary 2×2 matrices \mathbf{U} and \mathbf{V} according to

$$\begin{pmatrix} \tilde{\chi}_1^+ \\ \tilde{\chi}_2^+ \end{pmatrix} = \mathbf{V} \begin{pmatrix} \tilde{W}^+ \\ \tilde{H}_u^+ \end{pmatrix}, \quad \begin{pmatrix} \tilde{\chi}_1^- \\ \tilde{\chi}_2^- \end{pmatrix} = \mathbf{U} \begin{pmatrix} \tilde{W}^- \\ \tilde{H}_d^- \end{pmatrix}. \quad (3.37)$$

The matrices \mathbf{U} and \mathbf{V} are chosen so that

$$\mathbf{U}^* \mathbf{X} \mathbf{V}^{-1} = \begin{pmatrix} m_{\tilde{\chi}_1^\pm} & 0 \\ 0 & m_{\tilde{\chi}_2^\pm} \end{pmatrix} \quad (3.38)$$

with positive real entries $m_{\tilde{\chi}_i^\pm}$ that are explicitly given by

$$m_{\tilde{\chi}_1^\pm}, m_{\tilde{\chi}_2^\pm} = \frac{1}{2} (|M_2|^2 + |\mu|^2 + 2m_W^2 \mp \sqrt{(|M_2|^2 + |\mu|^2 + 2m_W^2)^2 - 4|\mu M_2 - m_W^2 \sin \beta|^2}). \quad (3.39)$$

Here, we see that the chargino mass eigenvalues are determined by the soft wino mass M_2 , the Higgsino mass term μ and $\tan \beta$. Except M_1 , these are the same parameters as in the neutralino case. If the lightest neutralino should be the NLSP with gravitino dark matter, we have to make sure that no chargino becomes lighter than the lightest neutralino. We will see in Chapter 5 that this excludes large regions in the parameter space. Note that charginos are mixed states of wino and Higgsino. There is no bino component, i.e. the mass matrix is independent of the soft bino mass M_1 .

3.3.3 Physical Particles

Table 3.5 comprises the physical particles as used in this thesis. We also list charginos, gluinos and gluons. Spin and R -parity values are provided. Thus it is easy to identify scalars (spin= 0), fermions (spin= 1/2, 3/2) and gauge bosons (spin= 1). And it is easy to see whether a particle is a Standard Model field or Higgs boson, since they have $P_R = +1$, in contrast to the sparticles with $P_R = -1$. We list explicitly gauge and mass eigenstates. In the case of squarks, sleptons, quarks and leptons, the identification of gauge and mass eigenstates is an assumption and approximation respectively (cp. Section 3.3). This assumption gives minor errors and is appropriate for our purpose.

Table 3.4 lists the corresponding four spinor representation for each fermion of Table 3.5. There are no Majorana spinors (A.23) in the Standard Model whereas SUSY introduces some Majorana fermions. Especially, neutralinos, the goldstino and the gravitino are Majorana. Since we investigate neutralino-to-gravitino decays, this is of special importance. Because Majorana fields are self-conjugate, they yield different Wick contractions from those of Dirac fields (A.15). This leads to ambiguities in the determination of the relative sign of interfering Feynman diagrams. Therefore we use the method proposed in [50] and introduce a continuous fermion flow, i.e. an arbitrary orientation of each fermion line. Proceeding in opposite direction to the fermion flow then allows one to form chains of Dirac matrices so that the relative sign of interfering diagrams is obtained

Name	Spinor representation
quarks	Dirac
charged leptons	Dirac
neutrinos	left-handed ³
neutralinos	Majorana
charginos	Dirac
gluinos	Majorana
gravitino	Vector-Majorana

Table 3.4: Spinor Representations

in the same manner as in the case of Dirac fermions. The fermionic vertices are read off from the Lagrangian as usual.

In Appendix D we provide the complete set of Feynman rules derived for computations in this thesis. If they are standard vertices of Glashow-Weinberg-Salam (GWS) theory of weak interaction, they are derived/taken from [48] and checked against [41]. Otherwise they are derived from the Lagrangian as given in Eq. (25.24) and Eq. (G.2) in the book of Wess and Bagger [40]. Especially gravitino vertices are checked in the high-energy limit against the Feynman rules as they are provided in [35].

For Majorana spinors λ^a we use the notation

$$\lambda^a = \begin{pmatrix} -i(\lambda_\alpha^a)_{W/B} \\ i(\bar{\lambda}^{a\dot{\alpha}})_{W/B} \end{pmatrix}, \quad (3.40)$$

where $(\lambda_\alpha^a)_{W/B}$ is a two-component Weyl spinor. W/B indicates again quantities used in the book by Wess and Bagger [40]. Even if we use the gauginos λ^a to present our notation, since they are Majorana fields after electroweak symmetry breaking and at high energies, we point out that also neutral Higgsinos become Majorana after electroweak symmetry breaking. Together with the gauginos they form Majorana neutralinos with the same notation.

The gravitino is a Majorana vector-spinor,

$$\Psi_\mu = \begin{pmatrix} -i(\Psi_{\mu\alpha})_{W/B} \\ i(\bar{\Psi}_\mu^{\dot{\alpha}})_{W/B} \end{pmatrix}. \quad (3.41)$$

³In the Standard Model neutrinos have no right-handed component and thus are chiral left-handed fermions and exactly massless. However, non-vanishing neutrino masses have been observed in the last years. Actually, one possible explanation of small neutrino masses is the introduction of heavy right-handed neutrinos.

Note that we include factors of i and a relative sign between $P_L\Psi_\mu$ and $P_R\Psi_\mu$ in the definition of the gravitino as well as for the gauginos (3.40). The projection operators P_L and P_R are defined in Appendix A.

The gravitino is the only vector-Majorana particle. It is a fermion and carries a vector index μ , cf. Section 3.4. Therefore we denote it in text often as Ψ_μ . Alternatives are Ψ or $\Psi_{3/2}$. We refer to these notations in equations to prevent confusion concerning the vector index. For instance, a mass m with subscript $\rightarrow m_\mu$ could be mixed up with an vector m_μ that carries an vector index μ .

The Dirac traces occurring in the evaluation of squared matrix elements are performed using the Mathematica package FEYN CALC [51]. Whenever this is performed by hand or checked in a limit, we are in agreement with the results of FEYN CALC.

3.4 The Gravitino

The Lagrangian of the free massive gravitino can be written as

$$\mathcal{L}_\psi^{\text{free}} = -\frac{1}{2}\varepsilon^{\mu\nu\rho\sigma}\bar{\psi}_\mu\gamma_5\gamma_\nu\partial_\rho\psi_\sigma - \frac{1}{4}m_{3/2}\bar{\psi}_\mu[\gamma^\mu, \gamma^\nu]\psi_\nu. \quad (3.42)$$

The variation of the Lagrangian gives the equation of motion. For the free massive gravitino this is the Rarita-Schwinger equation

$$-\frac{1}{2}\varepsilon^{\mu\nu\rho\sigma}\gamma_5\gamma_\nu\partial_\rho\psi_\sigma - \frac{1}{4}m_{3/2}[\gamma^\mu, \gamma^\nu]\psi_\nu = 0. \quad (3.43)$$

Since the gravitino satisfies the constraints

$$\gamma^\mu\psi_\mu = 0, \quad (3.44a)$$

$$\partial^\mu\psi_\mu = 0, \quad (3.44b)$$

it can be shown that the Rarita-Schwinger equation (3.43) reduces for each vector component μ of the gravitino to the Dirac equation

$$(i\not{\partial} - m_{3/2})\psi_\mu = 0. \quad (3.45)$$

The gravitino is, furthermore, self conjugate and thus represented by a vector-Majorana spinor as listed in Table 3.4. The polarization tensor for a gravitino with four-momentum P is given by [37]

$$\begin{aligned} \Pi_{\mu\nu}^+(P) &= \sum_s \psi_\mu^{+(s)}(P)\bar{\psi}_\nu^{+(s)}(P) \\ &= -(\not{P} + m_{3/2})\left\{g_{\mu\nu} - \frac{P_\mu P_\nu}{m_{3/2}^2} - \frac{1}{3}\left(g_{\mu\rho}g_{\nu\sigma} - g_{\mu\rho}\frac{P_\nu P_\sigma}{m_{3/2}^2} - \frac{P_\mu P_\rho}{m_{3/2}^2}g_{\nu\sigma} + \frac{P_\mu P_\rho P_\nu P_\sigma}{m_{3/2}^4}\right)\gamma^\rho\gamma^s\right\}, \end{aligned} \quad (3.46)$$

where the sum accounts the four gravitino helicities $s = \pm 3/2, \pm 1/2$. Following [36], $\Pi_{\mu\nu}^+$ is the polarization tensor for the positive frequency mode functions, whereby

$$\begin{aligned} \Pi_{\mu\nu}^-(P) &= \sum_s \psi_\mu^{-s}(P) \bar{\psi}_\nu^{-s}(P) \\ &= -(\not{P} - m_{3/2}) \left\{ g_{\mu\nu} - \frac{P_\mu P_\nu}{m_{3/2}^2} - \frac{1}{3} \left(g_{\mu\rho} g_{\nu\sigma} - g_{\mu\rho} \frac{P_\nu P_\sigma}{m_{3/2}^2} - \frac{P_\mu P_\rho}{m_{3/2}^2} g_{\nu\sigma} + \frac{P_\mu P_\rho P_\nu P_\sigma}{m_{3/2}^4} \right) \gamma^\rho \gamma^s \right\}, \end{aligned} \quad (3.47)$$

is the one for the negative frequency mode functions.

The polarization tensor obeys

$$\gamma^\mu \Pi_{\mu\nu}^\pm(P) = 0, \quad \Pi_{\mu\nu}^\pm(P) \gamma^\nu = 0, \quad (3.48a)$$

$$P^\mu \Pi_{\mu\nu}^\pm(P) = 0, \quad \Pi_{\mu\nu}^\pm(P) P^\nu = 0, \quad (3.48b)$$

$$(\not{P} \mp m_{3/2}) \Pi_{\mu\nu}^\pm(P) = 0, \quad \Pi_{\mu\nu}^\pm(P) (\not{P} \mp m_{3/2}) = 0. \quad (3.48c)$$

To consider gravitino interactions we add the interaction Lagrangian

$$\begin{aligned} \mathcal{L}_{\Psi, \text{int}}^{(\alpha)} &= -\frac{i}{\sqrt{2}M_p} [\mathcal{D}_\mu^\alpha \phi^{*i} \bar{\Psi}_\nu \gamma^\mu \gamma^\nu \chi_L^i - \mathcal{D}_\mu^\alpha \phi^i \bar{\chi}_L^i \gamma^\nu \gamma^\mu \Psi_\nu] \\ &\quad - \frac{i}{8M_p} \bar{\psi}_\mu [\gamma^\rho, \gamma^\sigma] \gamma^\mu \lambda^{(\alpha)a} F_{\rho\sigma}^a + O(M_p^{-2}) \end{aligned} \quad (3.49)$$

to Eq. (3.42). We see immediately that each operator in (3.49) is suppressed by the Planck scale, since the natural scale of supergravity is the Planck scale. Therefore, gravitino interactions are 'super weak', which makes the gravitino a viable dark matter candidate. Terms that are suppressed by higher orders of M_p are surely negligible. Eq. (3.49) refers to the notation in Eq. (3.6) and (3.41). The covariant derivative of the scalar fields in the MSSM is

$$\mathcal{D}_\mu^{(\alpha)} \phi^i = \partial_\mu \phi^i + i g_\alpha A_\mu^{(\alpha)a} T_{a,ij}^{(\alpha)} \phi^j. \quad (3.50)$$

Here, $T_{a,ij}^{(\alpha)}$ are the generators of the Standard Model gauge group (3.5),

$$\begin{aligned} T_{a,ij}^{(1)} &= \frac{1}{2} Y_i \delta_{ij} \delta_{a1}, \\ T_{a,ij}^{(2)} &= \sigma_{a,ij}, \\ T_{a,ij}^{(3)} &= \lambda_{a,ij}, \end{aligned} \quad (3.51)$$

where Y_i denotes the $U(1)_Y$ hypercharge of the corresponding particle, σ_a are the Pauli sigma matrices as defined in (A.8) and λ_a denote the Gell-Mann matrices of strong

interactions that we do not give explicitly, since we do not consider processes of strong interactions. The field strength tensor $F_{\rho\sigma}^{(\alpha)a}$ in Eq. (3.49) is given by

$$F_{\mu\nu}^{(\alpha)a} = \partial_\mu A_\nu^{(\alpha)a} - \partial_\nu A_\mu^{(\alpha)a} - g_\alpha f^{(\alpha)abc} A_\mu^{(\alpha)b} A_\nu^{(\alpha)c}. \quad (3.52)$$

As usual $f^{(\alpha)abc}$ denote the totally antisymmetric structure constants of the corresponding gauge group α given via

$$[T_a, T_b] = i f^{abc} T_c. \quad (3.53)$$

Since $U(1)_Y$ is abelian, the left hand side of Eq. (3.53) vanishes and thus

$$f^{(1)abc} = 0 \quad \text{for } U(1)_Y. \quad (3.54)$$

We consider gravitino tree-level interactions suppressed by M_p^{-1} . Feynman rules can be extracted from the Lagrangian in the usual way, while we use -as mentioned above- the method proposed in [50]. In Appendix D we list all gravitino tree-level vertices as derived from Eq. (25.24) and (G.2) in the book of Wess and Bagger [40] using also the form (3.49) of the interaction Lagrangian.

3.4.1 Gravitino Cosmology

In the early universe also gravitinos are in thermal equilibrium. But the relic density of those gravitinos overcloses the universe, i.e. $\Omega_{3/2} = \rho_{3/2}/\rho_c > 1$. Then the universe would have re-collapsed. This problem is resolved by inflation, see Section 2.1, since the initial abundance of gravitinos is diluted away. As described in Section 2.1, the gravitino density can be reproduced in the thermal plasma after reheating. The thermally produced gravitino relic density [52],

$$\Omega_{3/2}^{TP} h^2 \simeq 0.3 \left(\frac{100 \text{ GeV}}{m_{3/2}} \right) \left(\frac{T_R}{10^{10} \text{ GeV}} \right) \left(\frac{m_{\tilde{g}}}{1 \text{ TeV}} \right), \quad (3.55)$$

is mainly determined by the gravitino mass $m_{3/2}$, the gluino mass $m_{\tilde{g}}$ and the reheating temperature T_R after inflation. The electroweak contributions are provided in [14]. Especially for non-universal scenarios, the electroweak contributions become more important, i.e. up to 40%. The restored gravitino density may not overclose the universe again, which constrains the possible values of the gravitino mass $m_{3/2}$, the reheating temperature T_R and the gluino mass $m_{\tilde{g}}$.

If the gravitino is not the LSP it decays with a lifetime roughly given by [53]

$$\tau_{3/2} \approx \frac{1}{\alpha_{3/2}} \frac{M_p^2}{m_{3/2}^3}, \quad (3.56)$$

where $\alpha_{3/2}$ is a dimensionless number of at most $O(1)$. Thus we have an estimate of the gravitino lifetime

$$\tau_{3/2} \gtrsim 3.2 \text{ years} \left(\frac{100 \text{ GeV}}{m_{3/2}} \right)^3, \quad (3.57)$$

that is surely in conflict with nucleosynthesis happening seconds after the big bang, see Section 2.2. This can be circumvented in two ways. First, as can be seen from Eq. (3.57), an extremely heavy gravitino at least of $O(100 \text{ TeV})$ could decay early enough. Via Eq. (3.14) this would, in turn, imply a high scale $\langle F \rangle$ of spontaneous supersymmetry breaking [5, 7, 53].

The second possibility is that the gravitino is the LSP. As presented in Chapter 4 and 5, the decays of the next-to-lightest supersymmetric particle happen much faster, but are also strongly constrained by big bang nucleosynthesis. In Chapter 4 we determine the lifetime of the general neutralino NLSP. If the gravitino is the LSP, the gravitino density (3.55) may not exceed the dark matter density (2.32), i.e. $\Omega_{3/2} < \Omega_{DM}$.

There is a possible conflict with baryogenesis via thermal leptogenesis, because for reasonable values of the gluino mass $m_{\tilde{g}} \sim 0.7 - 1 \text{ TeV}$ [2] the gravitino mass may not be much smaller than 100 GeV when the reheating temperature T_R is of $O(10^{10} \text{ GeV})$ or must at least be $> 10 \text{ GeV}$ if the reheating temperature is of $O(10^9 \text{ GeV})$.

We will see how the upper bound on the gravitino mass by BBN constraints is reconcilable with the lower bound from thermal gravitino production and baryogenesis.

After decoupling from the thermal plasma, each NLSP χ decays into one gravitino LSP and Standard Model particles. The resulting density of these non-thermally produced gravitinos is [54]

$$\Omega_{3/2}^{NTP} h^2 = \frac{m_{3/2}}{m_\chi} \Omega_\chi h^2 \quad (3.58)$$

where m_χ is the mass of the NLSP and $\Omega_\chi h^2$ is the relic density of the NLSP, if they would have not decayed. Thus the total gravitino density $\Omega_{3/2} h^2$ is given by the sum of thermally produced and via decays produced gravitinos, i.e.

$$\Omega_{3/2} h^2 = \Omega_{3/2}^{TP} h^2 + \Omega_{3/2}^{NTP} h^2. \quad (3.59)$$

Table 3.5: Physical Particles

Name	Spin	P_R	Gauge Eigenstates	Mass Eigenstates
Higgs bosons	0	+1	$H_u^0 H_d^0 H_u^+ H_d^-$	$h^0 H^0 A^0 H^\pm$
squarks \tilde{q}	0	-1	$\tilde{u}_L \tilde{u}_R \tilde{d}_L \tilde{d}_R$ $\tilde{s}_L \tilde{s}_R \tilde{c}_L \tilde{c}_R$ $\tilde{t}_L \tilde{t}_R \tilde{b}_L \tilde{b}_R$	(same)
sleptons \tilde{l}	0	-1	$\tilde{e}_L \tilde{e}_R \tilde{\nu}_e$ $\tilde{\mu}_L \tilde{\mu}_R \tilde{\nu}_\mu$ $\tilde{\tau}_L \tilde{\tau}_R \tilde{\nu}_\tau$	(same)
quarks q	1/2	+1	$u_L u_R d_L d_R$ $s_L s_R c_L c_R$ $t_L t_R b_L b_R$	(same)
leptons l	1/2	+1	$e_L e_R \nu_e$ $\mu_L \mu_R \nu_\mu$ $\tau_L \tau_R \nu_\tau$	(same)
neutralinos	1/2	-1	$\tilde{B}^0 \tilde{W}^0 \tilde{H}_u^0 \tilde{H}_d^0$	$\chi_1^0 \chi_2^0 \chi_3^0 \chi_4^0$
charginos	1/2	-1	$\tilde{W}^\pm \tilde{H}_u^\pm \tilde{H}_d^\mp$	$\chi_1^\pm \chi_2^\pm$
gluinos	1/2	-1	\tilde{g}^a	(same)
gauge bosons (γ, Z, W^\pm)	1	+1	$B_\mu W_\mu^a$	$A_\mu Z_\mu^0 W_\mu^\pm$
gluons	1	+1	g_μ^a	(same)
gravitino (with goldstino)	3/2 (1/2)	-1	Ψ_μ	(same)

Chapter 4

General Neutralino NLSP with Gravitino Dark Matter

As mentioned in Section 2.2, big bang nucleosynthesis (BBN) constraints the decay of long-lived massive particles. Since we investigate gravitino dark matter with neutralino NLSP that freezes out with its relic abundance, we investigate the decay of the neutralino NLSP χ . Since BBN happens at a certain time and its constraints depend on time, we are interested in the neutralino lifetime

$$\tau = \frac{1}{\Gamma}, \quad (4.1)$$

where Γ is the total decay width (C.1) of the neutralino.

Since BBN constraints differ for electromagnetic (em) and hadronic (had) energy release (cp. Section 2.2), we are interested in the electromagnetic branching ratio and hadronic branching ratio respectively. The branching ratio B of a particle χ into something X is defined as the ratio of the partial decay width $\Gamma(\chi \rightarrow X)$ and the total decay width Γ_{tot} of the decaying particle,

$$B(X) := \frac{\Gamma(\chi \rightarrow X)}{\Gamma_{tot}}, \quad (4.2)$$

where the total decay width is the sum of all partial decay widths,

$$\Gamma_{tot} := \sum_X \Gamma(\chi \rightarrow X). \quad (4.3)$$

Due to R -parity conservation the neutralino NLSP with gravitino dark matter must decay into a gravitino and Standard Model particles. To comply the SM conservation laws, these are produced in pairs of particle and antiparticle. Thus the hadronic branching

ratio is given by

$$B_{had} = \frac{\sum_q \Gamma(\chi \rightarrow \dots q\bar{q}\Psi_\mu)}{\Gamma_{tot}}, \quad (4.4)$$

where \dots denotes anything allowed. A decay releases hadronic energy, when at least one pair of quarks is produced. The sum runs over all quark flavor $q = \{u, d, c, s, b, t\}$. One expects that 3-body decays $\chi \rightarrow q\bar{q}\Psi_\mu$ are the leading contribution to B_{had} . Other hadronic channels require at least two intermediate gauge bosons. Thus those are naturally suppressed. They lead at least to 5-body decays, i.e. $\chi \rightarrow l^+l^-q\bar{q}\Psi_\mu$ or $\chi \rightarrow q\bar{q}q\bar{q}\Psi_\mu$. Furthermore, we found the radiative corrections $\chi \rightarrow \gamma q\bar{q}\Psi_\mu$ to be negligible. Thus one expects the hadronic ratio to be given by

$$B_{had} = \frac{\sum_q \Gamma(\chi \rightarrow q\bar{q}\Psi_\mu)}{\Gamma_{tot}}. \quad (4.5)$$

However, if a 3-body decay into heavy unstable particles can proceed directly via a 4-vertex, its contribution can become large at large masses of the decaying particle when the decay is no longer suppressed due to the phase space. Since the heavy unstable particles decay, these neutralino decays lead in the end at least to 5-body decays. Thus they are not considered by Eq. (4.5). We consider the hadronic branching ratio to be given by

$$B_{had} = B_{had}^\chi = \left\{ \sum_q \Gamma(\chi \rightarrow q\bar{q}\Psi_\mu) + \sum_{all4v.} B_{had}^{\chi4v.} \times \Gamma(\chi\text{-4-vertex}) \right\} / \Gamma_{tot}, \quad (4.6)$$

where the sum runs over all neutralino 4-vertices multiplied by the corresponding hadronic branching ratio. We consider all six quark flavour including top, cp. Section 3.3.3.

The electromagnetic branching ratio B_{em} is defined as the branching ratio into particles that can interact electromagnetically, i.e. carry electromagnetic charge. From all SM particles only neutrinos are not electromagnetically charged. So all other decays, including quark pair production, account for the electromagnetic branching ratio. It is

$$B_{em} = B_{em}^\chi = \frac{1}{\Gamma_{tot}} \left\{ \sum_q [\Gamma(\chi \rightarrow \Psi_\mu h \rightarrow \Psi_\mu q\bar{q}) + \Gamma(\chi \rightarrow \Psi_\mu Z \rightarrow \Psi_\mu q\bar{q})] + \sum_l [\Gamma(\chi \rightarrow \Psi_\mu h \rightarrow \Psi_\mu l^+l^-) + \Gamma(\chi \rightarrow \Psi_\mu Z \rightarrow \Psi_\mu l^+l^-)] \right\}, \quad (4.7)$$

where we have made the same approximations as in Eq. (4.5). From Eq. (4.7) we see

$$B_{em} = 1 - B_{inv}, \quad (4.8)$$

where B_{inv} denotes the branching ratio into Ψ_μ and solely neutrinos. The leading contribution to B_{inv} stems from $\chi \rightarrow \nu\bar{\nu}\Psi_\mu$.

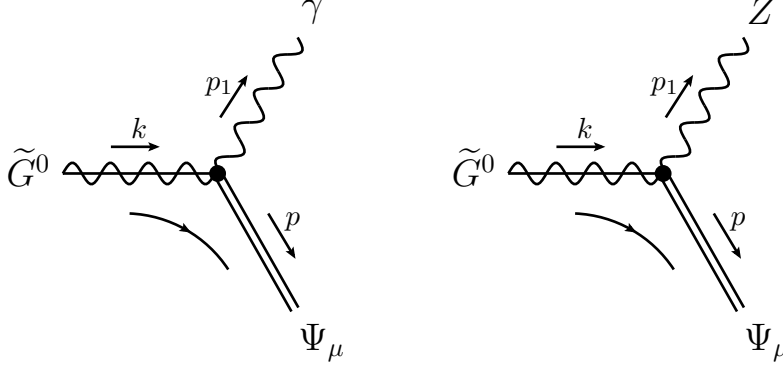


Figure 4.1: Tree-level Feynman diagrams of the gaugino 2-body decays.

The lightest neutralino

$$\chi_1^0 \equiv \chi = \mathbf{N}_{11}\tilde{B} + \mathbf{N}_{12}\tilde{W}^0 + \mathbf{N}_{13}\tilde{H}_d^0 + \mathbf{N}_{14}\tilde{H}_u^0 \quad (4.9)$$

is a linear combination of Bino, neutral Wino and both neutral Higgsinos, see Section 3.3.2. Note that it is $\mathbf{N}_{11}^2 + \mathbf{N}_{12}^2 + \mathbf{N}_{13}^2 + \mathbf{N}_{14}^2 = 1$. Firstly, we consider the pure gauge eigenstates and then investigate interference effects. Sometimes we refer to gaugino neutralino $\tilde{G} = \mathbf{N}_{11}\tilde{B} + \mathbf{N}_{12}\tilde{W}^0$, whereas $\mathbf{N}_{13} = \mathbf{N}_{14} = 0$, or to Higgsino neutralino \tilde{H} , which is a mixed state of the neutral Higgsinos only. Analytic results of 2- and 3-body decay widths used in this chapter are explicitly listed in Appendix E. There you can also find Feynman diagrams of all processes referred to in this chapter.

4.1 Bino NLSP

The bino can decay into photon and gravitino and the decay rate is given by

$$\Gamma(\tilde{B} \rightarrow \Psi_\mu \gamma) = \frac{\cos^2 \Theta_W}{48\pi M_p^2} \frac{m_{\tilde{B}}^5}{m_{3/2}^2} (1 - x_{3/2}^2)^3 (1 + 3x_{3/2}^2), \quad (4.10)$$

where $x_{3/2} = \frac{m_{3/2}}{m_{\tilde{B}}}$ is the gravitino to neutralino mass ratio. This decay channel contributes only to electromagnetic energy and is always open, since the photon is massless.

If it is kinematically allowed, the bino can also decay into Z boson and gravitino. The Feynman diagrams for both 2-body decays are shown in Figure 4.1. As in any other Feynman diagram, the gravitino Ψ_μ is represented as a double solid line, gauge bosons are shown as wiggled lines while the neutralino is always depicted as its corresponding gauge eigenstate. Bino \tilde{B} and wino \tilde{W}^0 are gauginos that are depicted as wiggled lines with additional straight solid lines. For the kinematics of 2-body decays see Appendix C.

The decay rate of the Z channel is given by

$$\begin{aligned} \Gamma(\tilde{B} \rightarrow \Psi_\mu Z) &= \frac{\sin^2 \Theta_W}{48\pi M_p^2} \frac{m_\chi^5}{m_{3/2}^2} \beta_{\tilde{B} \rightarrow \Psi_\mu Z} \\ &\times [(1 - x_{3/2}^2)^2 (1 + 3x_{3/2}^2) - x_Z^2 \{3 + x_{3/2}^3 (x_{3/2} - 12) \\ &- x_Z^2 (3 - x_{3/2}^2 - x_Z^2)\}], \end{aligned} \quad (4.11)$$

where $x_Z = \frac{m_Z}{m_{\tilde{B}}}$ is the Z boson to neutralino mass ratio. $\beta_{A \rightarrow BC}$ is a kinematic function, i.e. for $m_A > m_B + m_C$

$$\beta_{A \rightarrow BC} \equiv [1 - 2(x_B^2 + x_C^2) + (x_B^2 - x_C^2)^2]^{1/2} \quad (4.12)$$

and $\beta_{A \rightarrow BC} = 0$ otherwise. Here and in the following parts we use $x_i = \frac{m_i}{m_A}$ is the mass ratio between particle i and A. $\tilde{B} \rightarrow \Psi_\mu Z$ produces em energy for all possible Z decay modes with the exception $Z \rightarrow \nu\bar{\nu}$. But it may also produce hadronic energy if followed by $Z \rightarrow q\bar{q}$.

The total decay rate Γ_{tot} of bino neutralino is in good approximation given by

$$\Gamma_{tot}^{\tilde{B}} = \Gamma(\tilde{B} \rightarrow \Psi_\mu \gamma) + \Gamma(\tilde{B} \rightarrow \Psi_\mu Z). \quad (4.13)$$

There is an off-shell contribution by the Z boson, but off-shell contributions are of order Γ/m compared to the on-shell case. Since $\Gamma_Z/m_Z \approx 1/45$ and the Z channel is not leading, this contribution is even smaller than $1/45$ and thus negligible at the determination of Γ_{tot} .

The electromagnetic branching ratio $B_{em} \simeq 1$, because the only contribution to B_{inv} stems from the processes $Z \rightarrow \nu\bar{\nu}$. Thereby, the Z channel with $B_{inv}^Z = 0.2$ is always subleading. However, $B = 1$ is the upper bound anyway.

The hadronic branching ratio is given in Figure 4.2 as a function of the bino mass at a fixed gravitino mass $m_{3/2} = 1$ GeV. At low masses we see that the branching ratio is in the percentage level. It increases after the kinematic threshold of the Z boson. As we can also see from Eq. (4.18) and Eq. (4.19), $\tilde{B} \rightarrow \Psi_\mu \gamma$ is always the dominant decay channel. Clearly, the relative contribution of $\tilde{B} \rightarrow \Psi_\mu Z$ increases, when real Z production is allowed. Since Z decays stronger in quarks than the photon produces a quark pair, this leads to an increase of the hadronic branching ratio. Since the lightest neutralino is by construction the NLSP, there are no further kinematic thresholds. Thus the asymptotic value $B_{had} \simeq 0.18$ stays valid for any higher neutralino mass. It is computed from

$$\begin{aligned} B_{had}^{\tilde{B}} &= \frac{1}{\Gamma_{tot}^{\tilde{B}}} \sum_q [\Gamma(\chi \rightarrow \Psi_\mu \gamma \rightarrow \Psi_\mu q\bar{q}) + \Gamma(\chi \rightarrow \Psi_\mu Z \rightarrow \Psi_\mu q\bar{q}) \\ &+ \Gamma(\chi \rightarrow \Psi_\mu (\gamma^*/Z^*) \rightarrow \Psi_\mu q\bar{q})], \end{aligned} \quad (4.14)$$

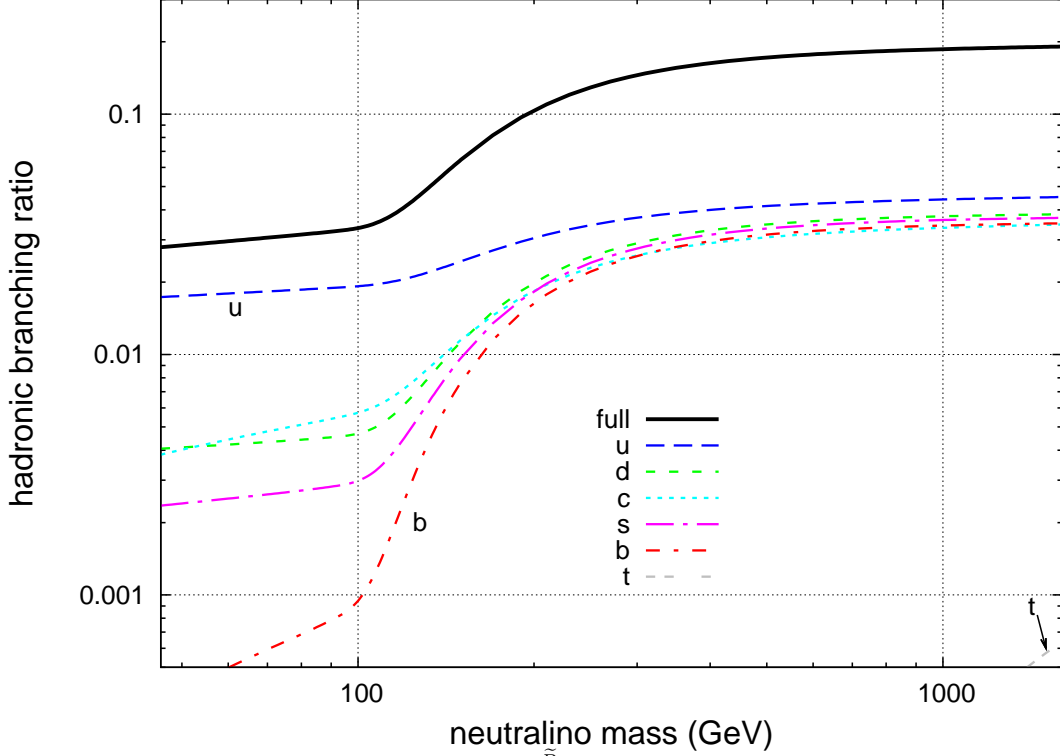


Figure 4.2: Hadronic branching ratio $B_{had}^{\tilde{B}}$ of a pure bino NLSP. Depicted are also the particular contributions of the six quark flavour $q = u, d, c, s, b, t$ that add up to the full branching ratio.

where $\Gamma_{tot}^{\tilde{B}}$ is given by Eq. (4.13).

In principle, there is an off-shell contribution by virtual squarks. It is the process $\chi \rightarrow q\tilde{q}^* \rightarrow \Psi_\mu q\tilde{q}$ with an virtual squark \tilde{q} . Off-shell contributions of much heavier particles are in good approximation negligible for our purpose. Since squarks are mostly much heavier than the lightest neutralino, we neglect these processes here. We investigate the effect of a light squark and a light slepton in Section 4.4

In Figure 4.2 we depict separately the contribution of each quark flavour. Following Eq. (4.5) we see that the sum of all contributions gives the full hadronic branching ratio. Especially at low masses, the leading contribution is the decay into a pair of up quarks. This is understood by consideration of the 3-body decay via intermediate photon, i.e. $\chi \rightarrow \Psi_\mu \gamma^* \rightarrow \Psi_\mu q\bar{q}$. In the limit of near massless quarks with $m_{3/2} \ll m_\chi$ the leading contribution of Eq. (E.26) reads

$$\Gamma(\tilde{G} \rightarrow \Psi_\mu \gamma^* \rightarrow \Psi_\mu q\bar{q}) = \alpha_{QED} \frac{|\mathbf{N}_{11} \cos \Theta_W + \mathbf{N}_{12} \sin \Theta_W|^2 Q^2 m_\chi^5}{6(2\pi)^2 M_p^2} \frac{m_\chi^5}{m_{3/2}^2} \ln \left(\frac{m_{\tilde{G}}}{2m_q} \right), \quad (4.15)$$

where Q denotes the electric quark charge and α_{QED} is the QED coupling constant. Here, the general gaugino \tilde{G} is used to make clear that this stays valid for a wino NLSP. We see that the contribution is enhanced by a logarithmic IR divergence. Obviously, Eq. (4.15) becomes maximal for the lightest quark, i.e. the up quark. Because of the IR divergence, B_{had} does not vanish at low masses. Evaluation of

$$B_{had}^{\tilde{G}}(\text{via } \gamma^*) = \frac{\sum_q \Gamma(\tilde{G} \rightarrow \Psi_\mu \gamma^* \rightarrow \Psi_\mu q \bar{q})}{\Gamma(\tilde{G} \rightarrow \Psi_\mu \gamma)} \gtrsim 0.03 \quad (4.16)$$

tells us in contrast that it always stays greater than $\simeq 0.03$ in the mass range under consideration. In the case of intermediate Z boson the IR divergence is not present. $\Gamma(\tilde{G} \rightarrow \Psi_\mu Z \rightarrow \Psi_\mu q \bar{q})$ (E.27) becomes large when the Z boson can be produced on shell. Since we work with the Breit-Wigner form of propagators (E.14), we include the behaviour around thresholds exactly. After the Z threshold charm, down, strange and even bottom catch up and their contributions are more or less indistinguishable at high masses. There the hadronic decay rate via intermediate Z boson is properly approximated by the decay into Z boson weighted by the respective hadronic branching ration (cp. [18]), i.e.

$$\sum_q \Gamma(\tilde{G} \rightarrow \Psi_\mu Z \rightarrow \Psi_\mu q \bar{q}) \approx \Gamma(\tilde{G} \rightarrow \Psi_\mu Z) \times B_{had}^Z. \quad (4.17)$$

Due to the high top quark mass $m_t = 171.2$ GeV, the contribution of the decay into a pair of top quarks is kinematically suppressed. In the mass range under consideration it is negligible and it does not become $O(10^{-1})$ up to neutralino masses $m_\chi = O(10$ TeV).

As in any other plot of hadronic branching ratios in this thesis, a shift of the gravitino mass leads in good approximation to a shift of kinematic thresholds only. Thus the change due to a smaller gravitino mass would not be resolvable, while heavier gravitinos lead to even longer lived neutralinos, see Eq. (4.18), (4.19). However, we comment on this issue in Section 4.4.

The actual experimental lower bound as given by the particle data group of the neutralino mass is $m_\chi = 46$ GeV (95%CL) [22]. This determines the lowest mass of the neutralino mass range used in branching ratio plots in this thesis. We set the upper bound $m_\chi = 1600$ GeV by consideration of the BBN bounds (see Chapter 5).

To see the order of magnitude of the decay rates, we provide the approximate formulas

$$\Gamma(\tilde{B} \rightarrow \Psi_\mu \gamma) \simeq (7.7 * 10^4 s)^{-1} \left(\frac{m_{\tilde{B}}}{100 \text{ GeV}} \right)^5 \left(\frac{m_{3/2}}{1 \text{ GeV}} \right)^{-2} \quad (4.18)$$

and

$$\Gamma(\tilde{B} \rightarrow \Psi_\mu Z) \approx (2.0 * 10^4 s)^{-1} \left(\frac{m_{\tilde{B}}}{200 \text{ GeV}} \right)^5 \left(\frac{m_{3/2}}{1 \text{ GeV}} \right)^{-2}. \quad (4.19)$$

The decay into photon and an appropriate light gravitino has no kinematic suppression, so that the given prefactor in Eq. (4.18) is nearly phase space independent. Already at the chosen values of $m_{\tilde{B}}$ and $m_{3/2}$ the phase space factor is practically one. In the case of decay into Z boson, there is kinematic suppression. At $m_{\tilde{B}} = 200$ GeV and $m_{3/2} = 1$ GeV the decay is no more strongly suppressed. The phase space factor evaluates to an order one factor, i.e. $\simeq 0.394$.

Since gravitino couplings are suppressed by the Planck mass, the NLSP is naturally long-lived. This we see immediately from Eq. (4.18) and Eq. (4.19). The neutralino NLSP with gravitino dark matter is long-lived at moderate mass ratios $m_{3/2}/m_\chi$. To shorten the lifetime $\tau = 1/\Gamma$ we need to decrease the mass ratio by making the neutralino heavier and/or the gravitino lighter.

4.2 Wino NLSP

At low masses the decay channels of bino and wino are the same, i.e. two body decay into gravitino and photon or Z boson. And the discussion of bino applies also to wino. The decay rates expressed by the bino decay rates are

$$\Gamma(\tilde{W} \rightarrow \Psi_\mu \gamma) = \frac{\sin^2 \Theta_W}{\cos^2 \Theta_W} \Gamma(\tilde{B} \rightarrow \Psi_\mu \gamma) \quad (4.20)$$

and

$$\Gamma(\tilde{W} \rightarrow \Psi_\mu Z) = \frac{\cos^2 \Theta_W}{\sin^2 \Theta_W} \Gamma(\tilde{B} \rightarrow \Psi_\mu Z). \quad (4.21)$$

The factor $\frac{\cos^2 \Theta_W}{\sin^2 \Theta_W} \simeq 3.3$ explains the larger hadronic branching ratio of about 50% in Figure 4.3 at neutralino masses around 300 GeV compared to the bino case. The stronger coupling to Z leads to more hadronic decays. Below the Z threshold the photon channel dominates anyway. Therefore, the branching ratios do not differ in this region.

If it is kinematically allowed, the wino can decay directly into a pair of W bosons via the 4-vertex shown in Figure 4.4. Whether this decay gives a contribution to electromagnetic or hadronic energy depends on the further decays of the W bosons.

Since W^\pm does not decay into $\nu\bar{\nu}$ at tree level, the electromagnetic branching ratio of this decay $B_{em} \simeq 1$. $\tilde{W} \rightarrow \Psi_\mu W^+ W^-$ already produce hadronic energy if only one W decays into a pair of quarks, $W^\pm \rightarrow q\bar{q}$. So the hadronic branching ratio of this channel is roughly given by

$$B_{had}^{\tilde{W}4v} = 1 - (1 - B_{had}^{W^+})^2 \simeq 0.89. \quad (4.22)$$

This is the counter-probability of both Ws not decaying into hadrons, in which the branching ratio of W into hadrons $B_{had}^{W^+} = 0.676$ [22]. So this process produces with

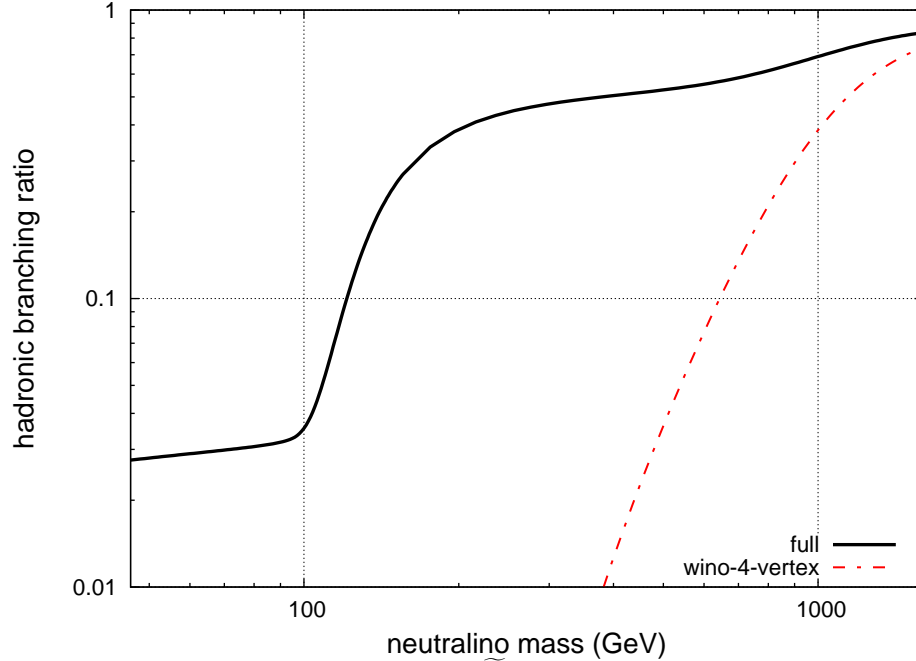


Figure 4.3: Hadronic branching ratio $B_{had}^{\widetilde{W}}$ of a wino NLSP. Depicted is also the particular contribution of the wino 4-vertex to the full branching ratio.

a high probability of 89% hadronic energy. Since these are 5-body decays, it is an additional contribution, that is not considered in Eq. (4.5). In the limit $m_{3/2}, m_W \ll m_\chi$ the decay rate of this channel (Eq. (E.21)) becomes

$$\lim_{m_{3/2}, m_W \ll m_\chi} \Gamma(\widetilde{W} \rightarrow \Psi_\mu W^+ W^-) = \frac{1}{128(2\pi)^3 M_p^2} \frac{g^2}{270} \frac{m_\chi^9}{m_W^4 m_{3/2}^2}, \quad (4.23)$$

where $g \equiv g_2$ denotes the gauge coupling of weak interaction. This limit shows the leading order of neutralino mass. In contrast to Eq. (4.10) and Eq. (4.11), it is m_χ^9 rather than m_χ^5 . Therefore, it becomes the leading decay channel at neutralino masses $m_\chi \approx 1 \text{ TeV} \gg m_W$, whereas it is absent for pure bino. In Figure 4.3 we depict the contribution of the wino 4-vertex to the full hadronic branching ratio and see that it leads to a further increase of B_{had} at higher neutralino masses. The asymptotic value of $B_{had} = 0.89$ is given by Eq. (4.22).

This channel exists only for non-abelian interactions. Since $U(1)_Y$ is abelian, it does not exist for the bino.

Together, the total decay rate of gaugino neutralino is in good approximation given by

$$\Gamma_{tot}^{\widetilde{G}} = \Gamma(\widetilde{G} \rightarrow \Psi_\mu \gamma) + \Gamma(\widetilde{G} \rightarrow \Psi_\mu Z) + \Gamma(\widetilde{W}\text{-4-vertex}). \quad (4.24)$$

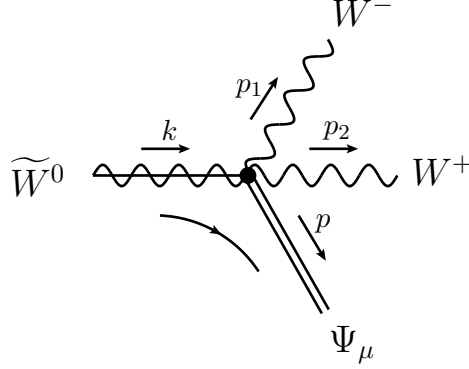


Figure 4.4: Feynman diagram of the direct decay $\tilde{W} \rightarrow \Psi_\mu W^+ W^-$ via the wino 4-vertex.

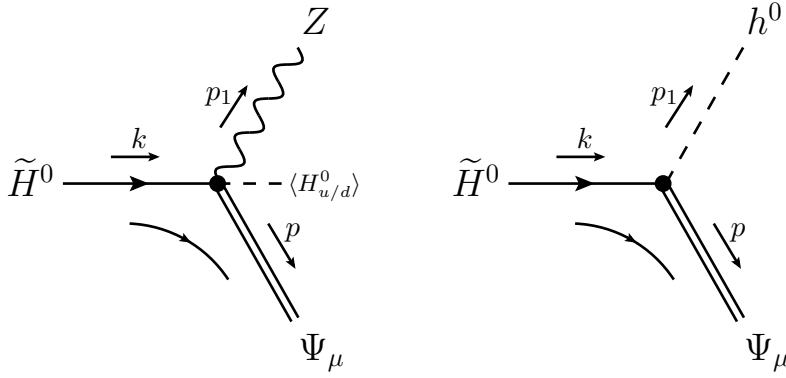


Figure 4.5: Tree-level Feynman diagrams of the Higgsino 2-body decays into Z, h.

4.3 Higgsino NLSP

If kinematically allowed, the Higgsino $\tilde{H} = \mathbf{N}_{13}\tilde{H}_d^0 + \mathbf{N}_{14}\tilde{H}_u^0$ can decay into a gravitino and a Z or any neutral Higgs boson. In the Feynman diagrams of Figure 4.5 the neutralino is drawn as solid line, since it corresponds to a Higgsino that is a chiral fermion which are drawn as solid lines. At tree level there is no photon channel for a pure Higgsino. The Higgsino decay rate into gravitino and Z boson is

$$\begin{aligned}
 \Gamma(\tilde{H} \rightarrow \Psi_\mu Z) &= \frac{[-\mathbf{N}_{13} \cos \beta + \mathbf{N}_{14} \sin \beta]^2}{96\pi M_p^2} \frac{m_\chi^5}{m_{3/2}^2} \beta_{\chi \rightarrow \Psi_\mu Z} \\
 &\times [(1 + x_{3/2})^2 (1 - x_{3/2})^4 \\
 &- x_Z^2 \{(1 - x_{3/2})^2 (3 + 2x_{3/2} - 9x_{3/2}^2) \\
 &- x_Z^2 (3 - 2x_{3/2} - 9x_{3/2}^2 - x_Z^2)\}] \quad (4.25)
 \end{aligned}$$

and into gravitino and the light Higgs boson it is

$$\begin{aligned}
 \Gamma(\tilde{H} \rightarrow \Psi_\mu h) &= \frac{|-\mathbf{N}_{13} \sin \alpha + \mathbf{N}_{14} \cos \alpha|^2}{96\pi M_p^2} \frac{m_\chi^5}{m_{3/2}^2} \beta_{\chi \rightarrow \Psi_\mu h} \\
 &\times [(1 - x_{3/2})^2 (1 + x_{3/2})^4 \\
 &- x_h^2 \{(1 + x_{3/2})^2 (3 - 2x_{3/2} + 3x_{3/2}^2) \\
 &- x_h^2 (3 + 2x_{3/2} + 3x_{3/2}^2 - x_h^2)\}] \quad (4.26)
 \end{aligned}$$

The phase space factors are just slightly more complicated compared to the gaugino Z channel (Eq. (E.27)). There is no interference between the gaugino and Higgsino Z channels. So the decay rate into gravitino and Z boson of a mixed neutralino is simply given by the sum of both channels, i.e.

$$\Gamma(\chi \rightarrow \Psi_\mu Z) = \Gamma(\tilde{G} \rightarrow \Psi_\mu Z) + \Gamma(\tilde{H} \rightarrow \Psi_\mu Z). \quad (4.27)$$

In Appendix E we list explicitly the rates into heavy scalar Higgs H and pseudoscalar Higgs A . We give the full expression with \mathbf{N}_{1j} , because a priori α and β are also unknown. So at this point it makes no sense to investigate $\tilde{H}_d^0, \tilde{H}_u^0$ separately.

Nevertheless, Higgsino neutralino tends to have $\mathbf{N}_{13} = \mathbf{N}_{14} = 1/\sqrt{2}$ (cf. [33]). This can be expected by the structure of the mass matrix (3.31). $\tilde{H}_d^0, \tilde{H}_u^0$ have the same mass parameter μ . Mixing happens only due to the off-diagonal terms determined by m_Z , $\tan \beta$ and α . We use $\mathbf{N}_{13} = \mathbf{N}_{14} = 1/\sqrt{2}$ to find the estimate formulas

$$\Gamma(\tilde{H} \rightarrow \Psi_\mu Z) \approx (2.4 * 10^4 s)^{-1} \left(\frac{m_\chi}{200\text{GeV}}\right)^5 \left(\frac{m_{3/2}}{1\text{GeV}}\right)^{-2} \quad (4.28)$$

and

$$\Gamma(\tilde{H} \rightarrow \Psi_\mu h) \approx (3.0 * 10^4 s)^{-1} \left(\frac{m_\chi}{200\text{GeV}}\right)^5 \left(\frac{m_{3/2}}{1\text{GeV}}\right)^{-2}, \quad (4.29)$$

where we assume a Higgs mass $m_h = 115$ GeV and the decoupling limit with moderate $\tan \beta = 10$. At $m_{\tilde{H}} = 200$ GeV with $m_{3/2} = 1$ GeV the decay into h is no more strongly suppressed. The phase space factor evaluates to an order one factor $\simeq 0.204$. Comparison to Eq. (4.18) and Eq. (4.19) shows that the partial decay widths of the Higgsino channels are of the same order of magnitude as the partial decay width of the gaugino Z channel. Of course the gaugino photon channel stays dominant. It is clear, that $\chi \rightarrow \Psi_\mu h$ depends strongly on the unknown Higgs mass. So Eq. (4.29) is understood as a benchmark.

If it is kinematically allowed, the Higgsino can decay directly into gravitino, Z and Higgs boson via the 4-vertex shown in Figure 4.6. Whether this decay gives a contribution to

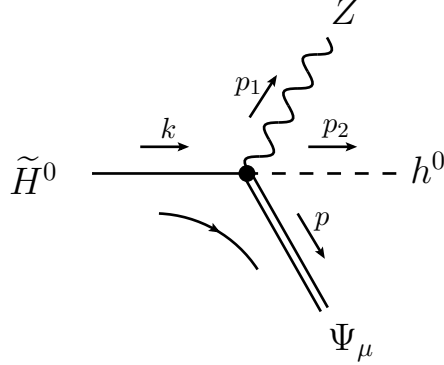


Figure 4.6: Feynman diagram of the direct decay $\tilde{H} \rightarrow \Psi_\mu Zh$ via the Higgsino 4-vertex.

electromagnetic or hadronic energy depends on the further decays of the primary decay products. As we will see, Higgs bosons decay in large part hadronically. In addition, there is the Z boson decay. Thus the hadronic branching ratio of $\tilde{H} \rightarrow \Psi_\mu Zh$ is well approximated by $B_{had}^{\tilde{H}4v.} = 1$, since it is at each point in parameter space > 0.97 .

In the decoupling limit with $\tan\beta = 10$ and $\mathbf{N}_{13} = \mathbf{N}_{14} = 1/\sqrt{2}$, the decay rate of $\tilde{H} \rightarrow \Psi_\mu Zh$ (E.23) becomes at large neutralino masses $m_{3/2}, m_Z, m_h \ll m_\chi$

$$\lim_{m_{3/2}, m_Z, m_h \ll m_\chi} \Gamma(\tilde{H} \rightarrow \Psi_\mu Zh) = \frac{1}{320(2\pi)^2 M_p^2} \frac{\alpha_{QED}}{s_W^2 c_W^2} \frac{1}{45} \frac{m_\chi^7}{m_Z^2 m_{3/2}^2}, \quad (4.30)$$

where α_{QED} is the coupling constant of quantum electrodynamics. This limit shows the leading order of neutralino mass. In contrast to Eq. (4.25) and Eq. (4.26), it is m_χ^7 rather than m_χ^5 . Therefore, the decay via the 4-vertex becomes the leading decay channel at large Higgsino masses, but we found that this happens not until Higgsino masses $\gtrsim 5$ TeV. Thus up to $m_\chi = 2$ TeV, Higgsino decays happen more than a magnitude faster via the 2-body decays than via this 5-body decay.

There are also Higgsino 4-vertices for the heavy Higgs bosons H, A , but since those are mostly heavy, their contribution is even smaller.

We point out that even a neutralino with a mass of $m_\chi = 1$ TeV decays stronger via the wino 4-vertex (4.23) than via the Higgsino 4-vertex (4.30) even if the wino component is just $\sim 1\%$.

The total decay rate of a pure Higgsino neutralino with $m_\chi > m_h, m_Z$ can be approxi-

mated by the sum of the 2-body decays and the Higgsino 4-vertices

$$\begin{aligned}\Gamma_{tot} \approx & \Gamma(\tilde{H} \rightarrow \Psi_\mu Z) + \Gamma(\tilde{H} \rightarrow \Psi_\mu h) \\ & + \Gamma(\tilde{H} \rightarrow \Psi_\mu H) + \Gamma(\tilde{H} \rightarrow \Psi_\mu A) \\ & + \Gamma(\tilde{H}\text{-4-vertices})\end{aligned}\quad (4.31)$$

where

$$\Gamma(\tilde{H}\text{-4-vertices}) = \Gamma(\tilde{H} \rightarrow \Psi_\mu Z h) + \Gamma(\tilde{H} \rightarrow \Psi_\mu Z H) + \Gamma(\tilde{H} \rightarrow \Psi_\mu Z A) \quad (4.32)$$

accounts for the sum of the widths of the three possible direct decays $\tilde{H} \rightarrow \Psi_\mu Z h$, $\tilde{H} \rightarrow \Psi_\mu Z H$ and $\tilde{H} \rightarrow \Psi_\mu Z A$ via the corresponding 4-vertices.

In principle, there are also off-shell contributions. But those are negligible when the real production of Z or h is allowed. $\Gamma_Z/m_Z \approx 1/45$ and naturally $\Gamma_h/m_h \ll 1/45$, so that the error in the total decay rate due to this approximation at large Higgsino masses $m_\chi \gg m_h, m_Z$ is at maximum of order $1/45$. As in the bino case, all further off-shell contributions are surely negligible. At low masses the situation is different. If the 2-body decays are kinematically forbidden, Higgsino decays into pairs of quarks or leptons via off-shell processes only. Since off-shell processes are suppressed by the square of the squared mass of the virtual particle (cp. (E.15)), it depends mainly on the particle masses which process is leading. Typically, all squarks, sleptons and the other Higgs bosons (H,A) are much heavier than Z and the light Higgs boson h. Then their off-shell contributions to the total decay rate are negligible at any Higgsino mass. We choose a Higgs mass $m_h = 115 \text{ GeV} > 91 \text{ GeV} \simeq m_Z$. Therefore, at low masses $m_\chi < m_Z$ the Higgsino decays mainly via off-shell Z, i.e. $\chi \rightarrow \Psi_\mu Z^* \rightarrow \Psi_\mu q\bar{q}$, $\chi \rightarrow \Psi_\mu Z^* \rightarrow \Psi_\mu l^+ l^-$ and $\chi \rightarrow \Psi_\mu Z^* \rightarrow \Psi_\mu \nu\bar{\nu}$. To determine the hadronic branching ratio of a pure Higgsino, that is shown in Figure 4.7, we need the full results of Appendix E to compute

$$\begin{aligned}\Gamma_{tot}^{\tilde{H}} = & \sum_q \left[\Gamma(\tilde{H} \rightarrow \Psi_\mu h \rightarrow \Psi_\mu q\bar{q}) + \Gamma(\tilde{H} \rightarrow \Psi_\mu Z \rightarrow \Psi_\mu q\bar{q}) \right] \\ & + \sum_l \left[\Gamma(\tilde{H} \rightarrow \Psi_\mu h \rightarrow \Psi_\mu l^+ l^-) + \Gamma(\tilde{H} \rightarrow \Psi_\mu Z \rightarrow \Psi_\mu l^+ l^-) \right] \\ & + \sum_\nu \Gamma(\tilde{H} \rightarrow \Psi_\mu Z \rightarrow \Psi_\mu \nu\bar{\nu}) + \Gamma(\tilde{H} \rightarrow \Psi_\mu Z h).\end{aligned}\quad (4.33)$$

Here, we are in the decoupling limit, so that we do not consider the other Higgs bosons. The sums consider all quark flavour, charged leptons and all neutrinos. It is clear, that the Higgs coupling to neutrinos is negligible due to the very small neutrino masses.

In some scenarios there is a stau $\tilde{\tau}$ with a mass $m_{\tilde{\tau}} \simeq m_\chi$ nearly degenerate to the neutralino mass. It is clear, that this would change the situation at masses below the Z

mass. The Higgsino would decay via off-shell stau rather than off-shell Z. However, there are good reasons not to consider these special situations in detail. Firstly, a neutralino NLSP decaying only via off-shell processes becomes even longer-lived and thus runs for sure into problems with big bang nucleosynthesis, see Chapter 2. And secondly, a bino fraction of one percent $\mathbf{N}_{11} = 1/\sqrt{100}$ is already enough to make the photon channel the leading decay channel at low masses again. Then we can approximate the total decay rate as the sum of all 2-bodies like at any other neutralino mass. The error due to this becomes maximal around the threshold of real Z production, since the off-shell contribution becomes relatively large while the 2-body decay is kinematically suppressed. We found that a mixed gaugino fraction of a few percent brings the error down to the percentage level, see below. But, for sure, it depends also on the chosen parameter values. However, this affects only a small mass region. So for all other mixed cases the total decay rate is in good approximation (error smaller than $O(10^{-3})$) given by the sum of all 2-body decays and the 4-vertices,

$$\begin{aligned} \Gamma_{tot} \simeq & \Gamma(\chi \rightarrow \Psi_\mu \gamma) + \Gamma(\chi \rightarrow \Psi_\mu Z) + \Gamma(\chi \rightarrow \Psi_\mu h) \\ & + \Gamma(\chi \rightarrow \Psi_\mu H) + \Gamma(\chi \rightarrow \Psi_\mu A) + \Gamma(\tilde{H}\text{-4-vertices}) \\ & + \Gamma(\tilde{W}\text{-4-vertex}). \end{aligned} \quad (4.34)$$

Since by construction the neutralino is the NLSP with gravitino dark matter, there are no other tree-level decay processes. All sparticles are heavier than the lightest neutralino. So they can not be produced in decays of it.

Higgs couplings to fermions are proportional to the mass of the corresponding fermion and Higgs couplings to electroweak gauge bosons are proportional to the squared mass of the corresponding gauge boson [48]. Therefore, Higgses decay mainly into heavy quarks, $h \rightarrow b\bar{b}$, or into pairs of gauge bosons, $h \rightarrow W^+W^-$ and $h \rightarrow ZZ$, if kinematically allowed. As we have seen in Section 4.2 decays into pairs of gauge bosons give negligible contributions to B_{inv} . So the electromagnetic branching ratio of a Higgsino neutralino is $B_{em} \simeq 1$ again, since the leading contribution to B_{inv} , $ZZ \rightarrow \nu\bar{\nu}\nu\bar{\nu}$, is small.

Furthermore, we have seen that decays into pairs of gauge bosons give in large part hadronic energy. So the hadronic branching ratio of Higgses is near to one. The hadronic branching ratio of a pure Higgsino neutralino is given in the decoupling limit by

$$B_{had}^{\tilde{H}} = \frac{\sum_q [\Gamma(\tilde{H} \rightarrow \Psi_\mu h \rightarrow \Psi_\mu q\bar{q}) + \Gamma(\tilde{H} \rightarrow \Psi_\mu Z \rightarrow \Psi_\mu q\bar{q})] + \Gamma(\tilde{H}\text{-4-vertices})}{\Gamma_{tot}}, \quad (4.35)$$

where Γ_{tot} is the total decay rate of a pure Higgsino as given in Eq. (4.33). Again, the Higgs mass $m_h = 115$ GeV. The other Higgses are too heavy to be produced and the light one is too light to decay into gauge bosons. The effect of light Higgses H, A is a further

increase of B_{had} , since as mentioned above Higgs decays produce in large part, i.e. $> 90\%$, hadronic energy. Moreover, there is a strong dependence on the Higgsino composition, $\tan\beta$ and α . Therefore, we are in the decoupling limit with moderate $\tan\beta = 10$ just to have a benchmark. With these parameters we show the hadronic branching ratio of a

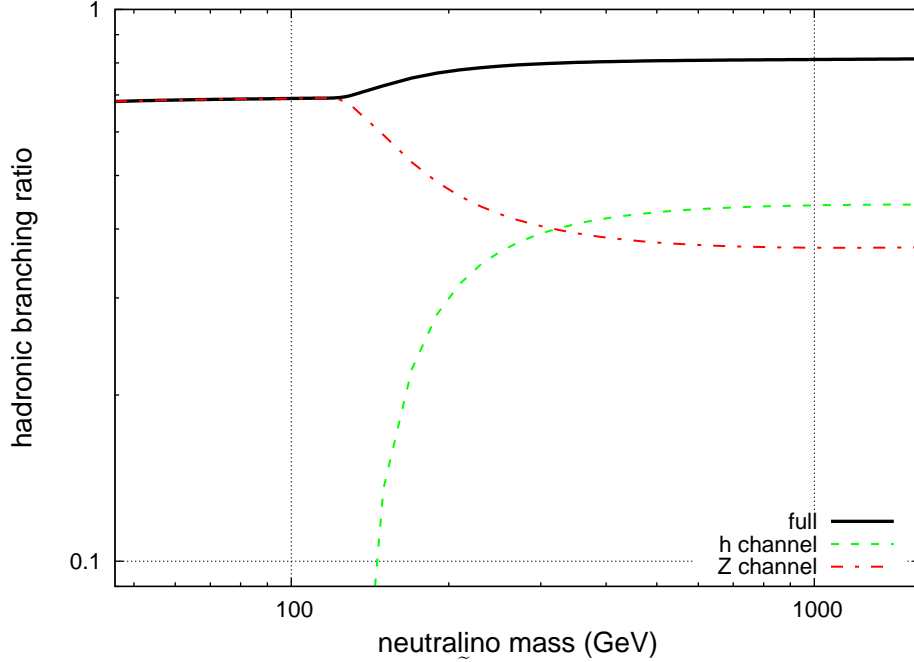


Figure 4.7: Hadronic branching ratio $B_{had}^{\tilde{H}}$ of a Higgsino NLSP. Depicted are also the particular contributions to the full branching ratio due to the processes via h and Z.

pure Higgsino neutralino ($\mathbf{N}_{13} = \mathbf{N}_{14} = 1/\sqrt{2}$) in Figure 4.7. Additionally, we show the separate contributions of the processes via h and Z. They add up to the full branching ratio following Eq. (4.35). At masses below the Higgs mass, decays happen via Z. The off-shell Higgs contribution is small, because $m_h > m_Z$. So the hadronic branching ratio is roughly that of a Z boson. After the Higgs mass threshold its relative contribution catches up and at high masses it is a little bit larger than the Z contribution. For sure, the details of this are parameter dependent. Nevertheless, we see that in general Higgsino neutralino has a large hadronic branching ratio, especially compared to the gaugino case with moderate neutralino masses. It is $B_{had}^{\tilde{H}} > B_{had}^Z$.

As mentioned above a small bino fraction is sufficient to make the photon channel leading below the Z mass threshold. This is shown in Figure 4.8, where a fraction of 5% bino ($\mathbf{N}_{11} = \sqrt{0.05}$, $\mathbf{N}_{12} = 0$, $\mathbf{N}_{13} = \mathbf{N}_{14} = \sqrt{0.475}$) makes the photon channel leading below the Z mass threshold. $B_{had} \simeq 0.03$ is due to the photon channel. Compared to the pure Higgsino case, we see that the asymptotic value at large neutralino masses is lowered, i.e. roughly from 0.8 to 0.58. Due to the small bino fraction the photon channel

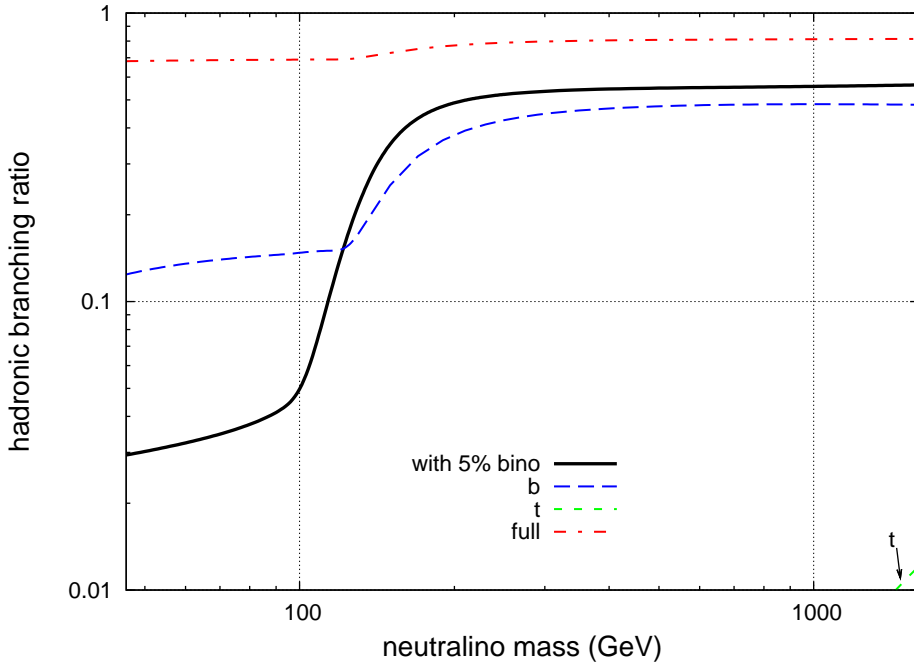


Figure 4.8: Hadronic branching ratio of a mainly Higgsino NLSP with a fraction of 5% bino. As reference the pure case is replotted from Figure 4.7. Depicted are also the particular contributions to the full hadronic branching ratio of Figure 4.7 due to the decays into a pair of bottom (b) or top (t) quarks.

is suppressed. Nevertheless it leads to a significant decrease of B_{had} even though the other channels are open at large neutralino masses. This shows that a mixed neutralino tends to decay via its strong photon channel.

Furthermore, we show the bottom and top quark contributions to the full hadronic branching ratio of a pure Higgsino neutralino in Figure 4.8. Firstly, the top quark contribution is again negligible and it does not become $O(10^{-1})$ up to neutralino masses $m_\chi = O(10 \text{ TeV})$. The bottom quark contribution shows a difference to the gaugino case. In the gaugino case at large m_χ all quarks (except top) give roughly the same relative contribution. This is in contrast to the Higgsino case, because then the decay into a pair of bottom quarks makes up more than half of the hadronic decays. This is due to the fact, that the light Higgs decays into $b\bar{b}$ with a branching ratio near to one. Even though the branching ratio of $Z \rightarrow b\bar{b}$ is smaller, together they make $b\bar{b}$ the leading hadronic decay channel.

4.4 Varying Gravitino Mass and Intermediate Sparticles

The effect of a heavy gravitino on the hadronic branching ratio B_{had} as given in this thesis is mainly a shift of kinematic thresholds. This can be seen in Figure 4.9, where we leave any parameter unchanged but the gravitino mass $m_{3/2}$. We see that the threshold of real Z production is shifted to larger neutralino masses for larger gravitino masses. It is clear that neutralino masses $m_\chi < m_{3/2}$ are excluded to keep the gravitino as the

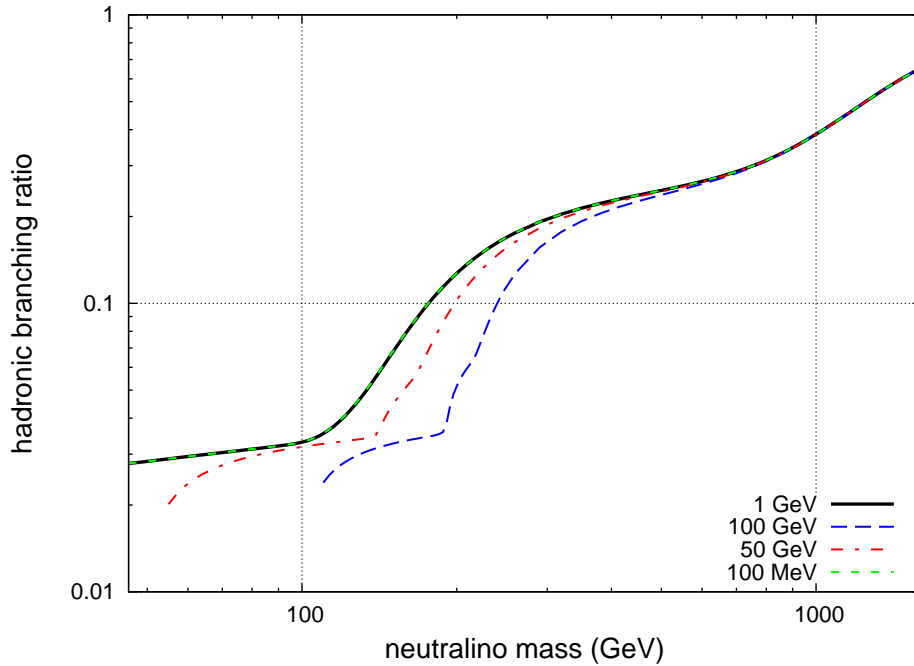


Figure 4.9: Hadronic branching ratio of a maximally mixed neutralino NLSP for different values of the gravitino mass, i.e. $m_{3/2} = 100$ MeV, 1 GeV, 50 GeV and 100 GeV. The graphs with $m_{3/2} = 100$ MeV and 1 GeV overlap completely.

LSP. Therefore, we start the data lines at some low neutralino masses.

In most scenarios with a neutralino NLSP the squarks are much heavier than the NLSP and even the sleptons are manifestly heavier. Then all processes with intermediate sparticles, $\chi \rightarrow q\tilde{q} \rightarrow \Psi_\mu q\bar{q}$, $\chi \rightarrow \tilde{q}\tilde{q} \rightarrow \Psi_\mu q\bar{q}$, $\chi \rightarrow \tilde{l}\tilde{l} \rightarrow \Psi_\mu l\bar{l}, \dots$, are negligible for the lifetime and the hadronic branching ratio, because they are suppressed by the fourth power of their mass, for an example see (E.52). The full analytic results for these processes are provided in Appendix E. By construction the lightest neutralino is the lightest supersymmetric partner particle, so that sparticles can not be produced on shell in decays of it. Nevertheless, there are scenarios with a light stop \tilde{t} or a light stau $\tilde{\tau}$ degenerate in mass with the lightest neutralino, i.e. $m_{\tilde{t}} \text{ or } m_{\tilde{\tau}} \simeq m_\chi$. Since an intermediate stop leads to decays into a pair of top quarks, $\chi \rightarrow t\tilde{t} \rightarrow \Psi_\mu t\bar{t}$, the

contribution of this process is negligible for lifetime and hadronic branching ratio.

For a pure Higgsino the decay via a mass degenerate stau is leading at low masses until a particle can be produced on shell. Then this decay becomes rapidly leading. In nearly all other cases the intermediate stau channel, $\chi \rightarrow \tau\tilde{\tau} \rightarrow \Psi_\mu\tau\bar{\tau}$, is negligible in the determination of lifetime and hadronic branching ratio. In the determination of the lifetime a mass degenerate stau, $m_{\tilde{\tau}} = 1.01 \times m_\chi$, leads under in some sense optimized conditions at maximum to a correction on the percentage level. We conclude that in the determination of lifetime and branching ratio all intermediate sparticle contributions are negligible, except the mentioned artificial cases of pure and nearly pure (bino fraction $< 1\%$) Higgsino.

The same is valid for gaugino-Higgsino interferences in between the intermediate sparticle channels $\tilde{G}/\tilde{H} \rightarrow q(\tilde{q}/\tilde{\bar{q}}) \rightarrow \Psi_\mu q\bar{q}$, since interferences can maximally be of the same order as the channels themselves. Interferences between the intermediate squark channel and the other channels are discussed in the next section.

4.5 Interference Effects

The results for the branching ratios discussed above are not directly transferable to the case of a general neutralino NLSP χ . In the case of general neutralino, interference effects appear and can alter the decay rate and/or the hadronic branching ratio.

This happens for mixed gaugino neutralino. The supersymmetric partner of the photon, the photino $\tilde{\gamma}$, is a special gaugino with the same mixture of bino and wino as the photon is a mixed state of B boson and W^0 boson. Following, Eq. (3.24) the photino corresponds to $\tilde{\gamma} = \cos\Theta_W\tilde{B} + \sin\Theta_W\tilde{W}^0$. In the photino case the gaugino Z channel (E.27) drops out. The photino couples maximally to the photon leading to an $B_{had}^{\tilde{\gamma}}$ at low masses approximately given by Eq. (4.15) summed over the light quarks. In this way the hadronic branching ratio of the mixed case is lower than both pure cases, which is shown in Figure 4.10. This effect is noticeable at low masses until the decay $\chi \rightarrow \Psi_\mu W^+W^-$ via the wino component (E.21) of the photino takes over. For sure, this depends strongly on the composition. To illustrate this, as an additional example, we add the maximally mixed case ($\mathbf{N}_{11} = \mathbf{N}_{12} = 1/\sqrt{2}$, $\mathbf{N}_{13} = \mathbf{N}_{14} = 0$) to Figure 4.10.

For the Higgsino neutralino we considered already the maximally mixed case in Section 4.3, since it is at the same time the most likely mixture. In general, the interferences as in Eq. (4.26) are not negligible, since they are of the same size as the pure contributions. On the other hand, an effect like in the gaugino case that really lowers the hadronic branching ratio does not exist. One can tune out either the Z channel or

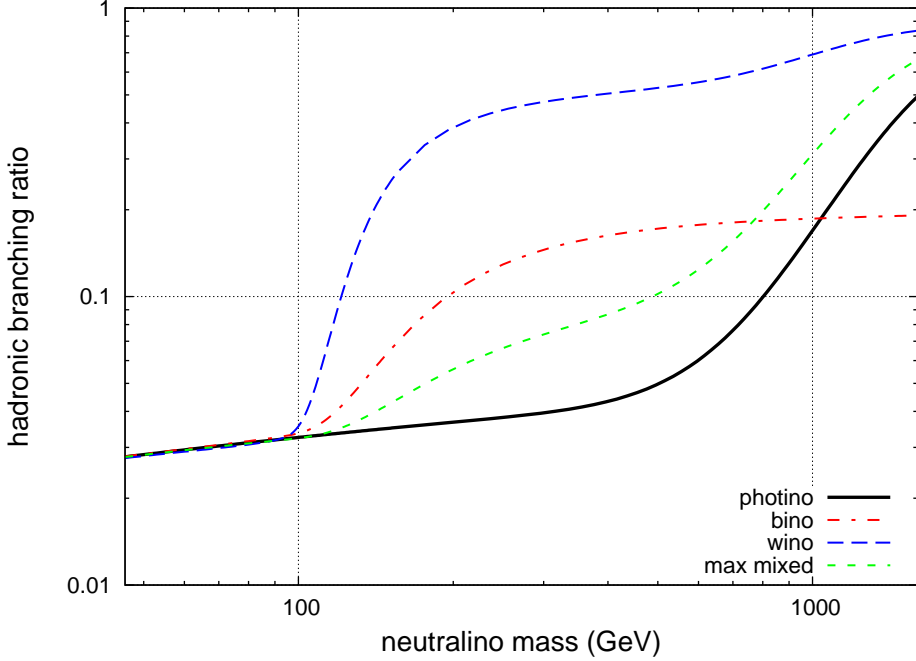


Figure 4.10: Hadronic branching ratio of a photino NLSP. As reference the pure bino and wino cases are replotted. Depicted is also the maximally mixed gaugino case.

the h channel, because the mixing angles α in Eq. (4.26) and β in Eq. (4.25) are not independent of each other, but related at tree level via Eq. (3.29). However, this can not lead to a decrease of $B_{had}^{\tilde{H}}$ below B_{had}^Z , because B_{had}^h is even bigger than B_{had}^Z .

We compute the interferences between different 3-body decay channels into gravitino and a pair of quarks. We comment on their relative contributions, for instance,

$$\frac{\sum_q \Gamma(\tilde{G} \rightarrow \Psi_\mu(\gamma^*/Z^*) \rightarrow \Psi_\mu q\bar{q})}{\sum_q \left[\Gamma(\tilde{G} \rightarrow \Psi_\mu \gamma \rightarrow \Psi_\mu q\bar{q}) + \Gamma(\tilde{G} \rightarrow \Psi_\mu Z \rightarrow \Psi_\mu q\bar{q}) \right]}. \quad (4.36)$$

Here, the denominator would be given by Eq. (E.28), while the nominator is the sum of Eq. (E.26) and Eq. (E.27). For a gaugino there are 3-bodies producing quark pairs via photon and Z boson. We find the relative contribution of the interference between γ and Z , $\tilde{G} \rightarrow \Psi_\mu(\gamma^*/Z^*) \rightarrow \Psi_\mu q\bar{q}$ (E.28), in the mass range under consideration to be mainly a correction on the percentage level. For the Higgsino there are interferences between light h and heavy CP-even neutral Higgs H and between Z boson and CP-odd Higgs A . For a pure Higgsino the relative contribution of the interference $\tilde{H} \rightarrow \Psi_\mu(h^*/H^*) \rightarrow \Psi_\mu q\bar{q}$ (E.32) is of order one at masses $m_\chi < m_h$. When the light h can be produced on shell, the relative contribution becomes negligible ($O(10^{-4})$). The relative contribution of $\tilde{H} \rightarrow \Psi_\mu(Z^*/A^*) \rightarrow \Psi_\mu q\bar{q}$ (E.36) is at maximum $O(10^{-4})$.

For a general neutralino χ there are also gaugino-Higgsino interferences. Firstly, there

are no gaugino-Higgsino interferences at the 2-body decays, see Eq. (4.27). At the 3-body decays many interferences between gaugino and Higgsino components occur only with at least one off shell sparticle. There are decay channels via intermediate squarks for gaugino $\tilde{G} \rightarrow q\tilde{q} \rightarrow \Psi_\mu q\bar{q}$ and Higgsino $\tilde{H} \rightarrow q\tilde{q} \rightarrow \Psi_\mu q\bar{q}$. Interferences in between these two channels can maximally be of the same order as the channels themselves. We comment on the contribution due to the processes with intermediate squarks only in Section 4.4.

There are scenarios with a light squark (stop) in the spectrum. If its mass is close to the neutralino NLSP mass, $m_{\tilde{q}} \simeq m_\chi$, it could have significant influence on the hadronic branching ratio via interferences with the photon or Z channels, $\chi \rightarrow \Psi_\mu(\gamma^*, Z^*/\tilde{q}^*) \rightarrow \Psi_\mu q\bar{q}$ (E.58)(E.61). Since stop mediates decays into a pair of top quarks, its contribution stays negligible anyway. But even for other squarks the relative contributions of these interference terms are negligible. If interferences between squarks and the photon are possible, the photon channel dominates the interferences anyway. The same applies for Z , while there the photon channel is in the most cases open at the same time.

Interferences between channels with intermediate Higgs and squark $\chi \rightarrow \Psi_\mu(h^*, H^*, A^*/\tilde{q}^*) \rightarrow \Psi_\mu q\bar{q}$ are also found to be negligible, since there even the leading terms are suppressed by $(m_q/m_\chi)^3$. Altogether, for a general neutralino the gaugino-Higgsino interferences are subleading and in the very most cases they are in good approximation negligible for our purpose.

More important is the gaugino-Higgsino mixture. Properties of the pure gauge eigenstates are discussed in the previous sections. From there we take that the total decay rate of a general neutralino is -for the most part- well approximated by

$$\begin{aligned} \Gamma_{tot} \simeq & \Gamma(\chi \rightarrow \Psi_\mu \gamma) + \Gamma(\chi \rightarrow \Psi_\mu Z) + \Gamma(\chi \rightarrow \Psi_\mu h) \\ & + \Gamma(\chi \rightarrow \Psi_\mu H) + \Gamma(\chi \rightarrow \Psi_\mu A) + \Gamma(\tilde{H}\text{-4-vertices}) \\ & + \Gamma(\tilde{W}\text{-4-vertex}). \end{aligned} \quad (4.37)$$

From the discussion in this chapter we conclude that the electromagnetic branching ratio of a general neutralino NLSP with gravitino dark matter is near to one at any parameter point, i.e.

$$B_{em} \simeq 1. \quad (4.38)$$

Furthermore, we can conclude that the hadronic branching ratio of a general neutralino is actually given by the sum of Eq. (4.35) with additional summands for A and H bosons and Eq. (4.14) and by consideration of some off-shell interferences, thereby achieving a

high accuracy,

$$\begin{aligned}
 B_{had} = & \left\{ \sum_q [\Gamma(\chi \rightarrow \Psi_\mu \gamma \rightarrow \Psi_\mu q \bar{q}) + \Gamma(\chi \rightarrow \Psi_\mu Z \rightarrow \Psi_\mu q \bar{q}) \right. \\
 & + \Gamma(\chi \rightarrow \Psi_\mu h \rightarrow \Psi_\mu q \bar{q}) + \Gamma(\chi \rightarrow \Psi_\mu H \rightarrow \Psi_\mu q \bar{q}) + \Gamma(\chi \rightarrow \Psi_\mu A \rightarrow \Psi_\mu q \bar{q}) \\
 & + \Gamma(\chi \rightarrow \Psi_\mu (\gamma^*/Z^*) \rightarrow \Psi_\mu q \bar{q}) + \Gamma(\chi \rightarrow \Psi_\mu (h^*/H^*) \rightarrow \Psi_\mu q \bar{q}) \\
 & \left. + \Gamma(\tilde{H}\text{-4-vertices}) + 0.89 \Gamma(\tilde{W}\text{-4-vertex}) \right\} / \Gamma_{tot}, \tag{4.39}
 \end{aligned}$$

where Γ_{tot} is given by Eq. (4.37). With this we are able to compute the lifetime and the hadronic branching ratio of a general neutralino NLSP with gravitino dark matter by numerical evaluation of the non-negligible contributions of Appendix E in a convenient amount of computing time and by far more accurate than in any reference. In Figure 4.11 we show together the formerly found hadronic branching ratios of pure gauge eigenstates (bino, wino, Higgsino). These are overplotted by the hadronic branching ratio of a maximally mixed neutralino ($\mathbf{N}_{11} = \mathbf{N}_{12} = \mathbf{N}_{13} = \mathbf{N}_{14} = 1/\sqrt{4}$). Here we are again in the decoupling limit. The ability to compute the lifetime $\tau = 1/\Gamma_{tot}$ from Eq. (4.37)

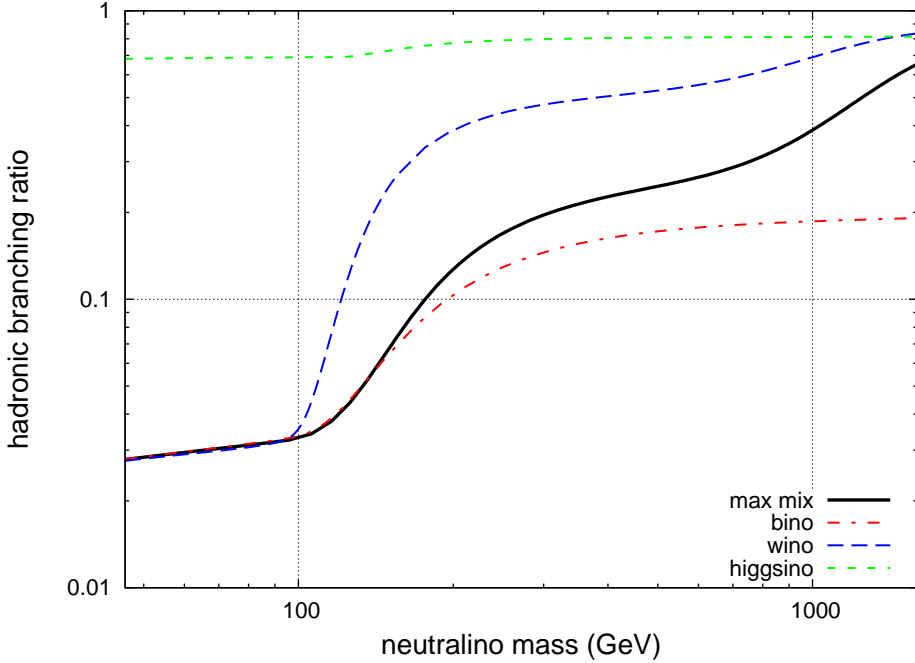


Figure 4.11: Hadronic branching ratios of the pure gauge eigenstates and the maximally mixed neutralino NLSP.

and hadronic branching ratio (4.39) for any given set of parameters will be used for the computations of Chapter 5.

Chapter 5

Constraints by Big Bang Nucleosynthesis

As discussed in Section 3.4.1 late decays of the gravitino, that spoil the success of big bang nucleosynthesis, do not occur if the gravitino is the LSP. In this case the NLSP decays much faster, but is also long lived and decays at relatively late times into gravitino and Standard Model particles. As mentioned in Section 2.2 these late decays are constrained via big bang nucleosynthesis. In Chapter 4 we investigate all decay channels of the general neutralino NLSP with gravitino dark matter. In doing so we determine the neutralino lifetime, the electromagnetic and the hadronic branching ratio.

Now, we determine constraints on the neutralino and gravitino mass by big bang nucleosynthesis. As noted in Chapter 2 the neutralino NLSP “freezes out” with its relic density $\Omega_\chi h^2$, that is computed here with MicrOMEGAs [28]. To determine the hadronically decaying part of Ω_χ we multiply the relic density by the hadronic branching ratio

$$\Omega_\chi h^2 \times B_{had}, \quad (5.1)$$

where B_{had} is given by Eq. (4.39). Since the electromagnetic branching ratio of the neutralino $B_{em} \simeq 1$, this is trivial for the electromagnetic constraints. The neutralino lifetime $\tau_\chi = 1/\Gamma_{tot}$ is at any point computed using Eq. (4.37).

As discussed in Section 3.3.2 the mass and composition of the lightest neutralino is determined by four parameters, i.e. the soft masses of bino M_1 and wino M_2 , the ratio of the Higgs VEVs $\tan\beta$ and the supersymmetric Higgsino mass term μ . Since moderate values of $\tan\beta$ are favoured [45], we fix $\tan\beta = 10$ as a benchmark. Then three parameters are left. We investigate these parameters by varying two of them while we keep the third fixed. So we get a bino-wino plane, a bino-higgsino plane and a wino-

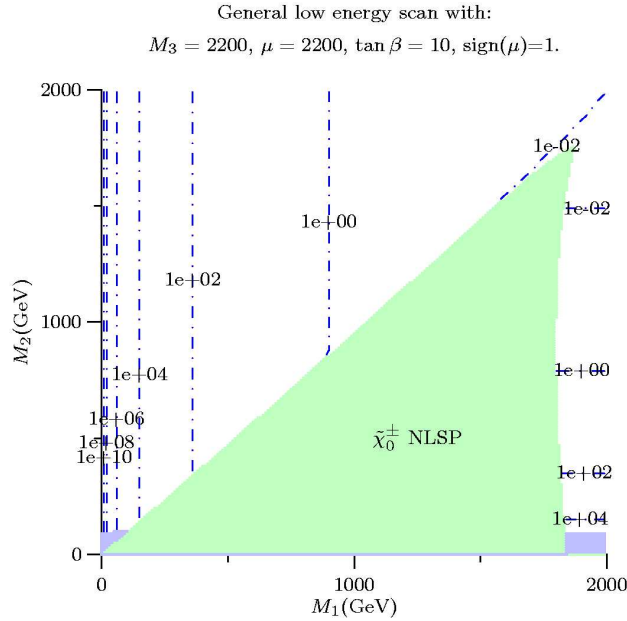


Figure 5.1: Parameter space of a bino-wino neutralino in the M_1 - M_2 plane. The blue (dark grey) region is excluded by the LEP searches and in the green (light grey) region the light chargino is the NLSP. There are depicted also neutralino lifetime contours for a gravitino mass $m_{3/2} = 1$ GeV.

higgsino plane scan. These are presented in Section 5.1, Section 5.2 and Section 5.3, respectively. During scans in these parameters we have to make sure that the lightest neutralino is always the NLSP. Because the chargino masses are also determined by M_2 , $\tan \beta$ and μ , we are especially in danger to get a chargino χ^\pm NLSP. We choose other SUSY parameters such that the sleptons and squarks are essentially decoupled with a mass around 2.2 TeV. SOFTSUSY [42] computes the physical mass spectrum, especially the mixing and mass of the lightest neutralino, dependent on our input, while MicrOMEGAs [28] computes also the needed Higgs widths. We point out that our treatment does not depend on any specific model at high energies.

5.1 Bino-Wino

We discuss the case of a mixed bino-wino NLSP in the decoupling limit, so that the parameter $\mu = 2200$ GeV is surely larger than M_1 and M_2 . We show the parameter space in these last two variables in Figure 5.1 including the mass bounds from the Large Electron-Positron Collider (LEP) [22]. The composition changes continuously from approximately pure bino in the upper left corner along the diagonal with $M_1 = M_2$

to approximately pure wino in the lower right corner. Since we consider a finite value of μ , a small Higgsino component is always present. We see that at light masses many mixed states, that would have a large wino component, lead to a chargino NLSP instead. Furthermore, the LEP searches put a lower limit on the soft wino mass $M_2 \gtrsim 100$ GeV. So at low masses the neutralino is either nearly pure wino or has a dominant bino component. This can also be seen in Figure 5.2, where the neutralino is in the most points mainly bino. Especially, since we do not assume gaugino mass unification, there is no lower bound on the soft bino mass, which allows a very light bino neutralino.

Figure 5.2 shows how BBN constraints the gravitino dark matter scenario with neutralino NLSP in the $\Omega_\chi h^2$ -vs.- τ_χ plane. The thin lines from upper left to lower right are BBN bounds extracted from [11]. They can also be inferred from Figure 2.2. Either they are for a decaying particle with $B_{had} = 0$ giving the electromagnetic bounds (EM BBN bounds) or they are for a particle with $B_{had} = 1$ giving the hadronic bounds (Hadronic BBN bounds). Even though it is stated, that the shape of hadronic constraints differ with the hadronic branching ratio [11], the effect is appropriately approximated by an overall shift of the bounds. However, the hadronic bounds are most severe at any point for $B_{had} = 1$. We denote all points on the right of the thin red line ruled out, since they would spoil the predictions of BBN. Thereby, the dashed line of the hadronic BBN bounds stems from a less conservative relative abundance of ${}^6\text{Li}/{}^7\text{Li}$. Thus points between the dashed and the solid red line should not be considered as ruled out, but there the NLSP decays increase the relative abundance of ${}^6\text{Li}$.

While the gravitino mass is fixed in a plot, the neutralino mass runs from left to right from 2 TeV to the minimal value not excluded yet. What is excluded depends on the composition. We come back to this in Section 5.3. In any plot we see as expected that the lifetime increases with decreasing neutralino mass (cf. Eq. (4.18)).

In Figure 5.2 we see electromagnetic and hadronic BBN bounds on a given scenario with gravitino masses of $m_{3/2} = 1$ GeV and $m_{3/2} = 10$ GeV and fixed parameters μ , $\tan\beta$, $\text{sign}(\mu)$ and soft gluino mass M_3 . The deformation between the left and the right curves is due to the mass dependence of the hadronic branching ratio, whereas the electromagnetic branching ratio is always near to one.

On the first sight, the electromagnetic bounds are less constraining than the hadronic ones. Nevertheless, a light wino with a $m_{3/2} = 10$ GeV gravitino seems to overcome the hadronic bounds due to the low relic density and low hadronic branching ratio, but, however, it does not overcome the electromagnetic bounds. This stays valid for higher gravitino masses.

Due to the lower relic density, the wino is less constrained than the bino. With $m_{3/2} = 1$

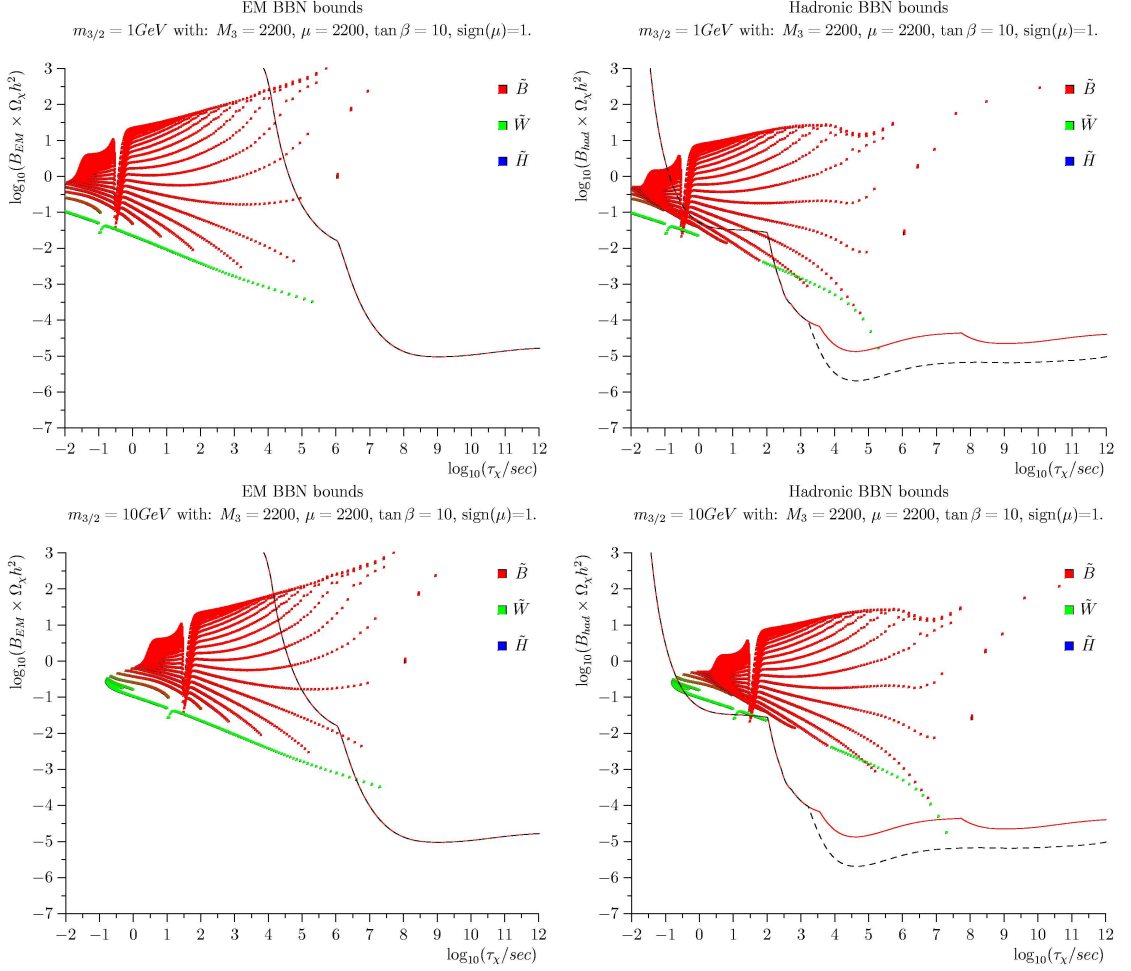


Figure 5.2: Bino-wino neutralino in the $B_i \times \Omega_{\chi} h^2$ -vs- τ plane compared with electromagnetic (left) and hadronic (right) BBN constraints for the case of 1 (upper) and 10 (lower) GeV gravitino mass. The neutralino mass decreases from left to right from 2 TeV to a few GeV for bino neutralino. The composition is chroma coded, whereby red (dark grey) indicates bino and green (light grey) indicates wino. The deformation between the left and right plots is due to the different branching ratios. Bounds are taken from [11], thereby the dashed line corresponds to less conservative bounds from ${}^6\text{Li}/{}^7\text{Li}$.

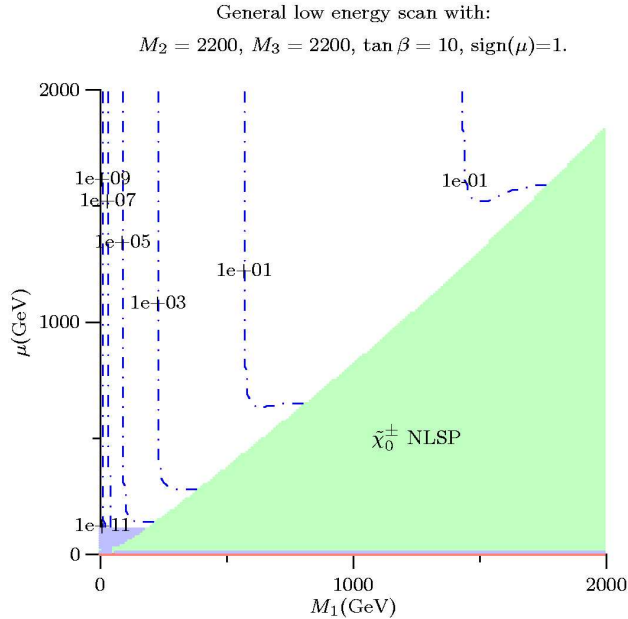


Figure 5.3: Parameter space of a bino-Higgsino neutralino in the M_1 - μ plane. The blue (dark grey) region is excluded by the LEP searches and in the green (light grey) region the light chargino is the NLSP. In the red (darker grey) region radiative electroweak symmetry breaking fails. There are depicted also neutralino lifetime contours for a gravitino mass $m_{3/2} = 1$ GeV.

GeV all neutralinos with mass $m_\chi > 1.6$ TeV are allowed. Then there is a mass window around 500 GeV for binos with a wino component that lowers the relic density. In contrast, at $m_{3/2} = 10$ GeV the bino is practically excluded, whereas the wino 4-vertex reduces the lifetime of the heavy wino so efficient that it decays early enough. Thus at large masses a dominant wino component is preferred to escape the BBN bounds. In addition there are some wino points left at $m_\chi \approx 500$ GeV.

Another feature in the plot is the dip that corresponds to a neutralino mass $m_\chi = 1100$ GeV, where the non-zero higgsino component annihilates resonantly via the heavy CP-odd Higgs boson A . Although it is suppressed by the mixing, this effect is efficient enough to bring down the bino relic density at that point in the parameter space.

From the upper to the lower plots of Figure 5.2 we can see, that the main effect of a variation of the gravitino mass is a horizontal shift of all points. Thus it is easy to infer, that the scenario of bino-wino NLSP with a mass $m_\chi \lesssim 2$ TeV and gravitino dark matter with a high mass of $O(100$ GeV) is excluded by BBN.

Besides one can infer from Figure 5.2 that even with lighter gravitino, e.g. $m_{3/2} = 100$ MeV, a bino NLSP scenario stays constrained due to the hadronic BBN bounds.

5.2 Bino-Higgsino

In order to study the bino-Higgsino case we fix the soft wino mass at a large value $M_2 = 2200$ GeV and scan the M_1 - μ plane as shown in Figure 5.3. Again, the composition changes continuously from approximately pure bino in the upper left corner along the diagonal with $M_1 = \mu$ to Higgsino, but a low μ parameter and comparable large M_1 leads to a chargino NLSP. Thus a large Higgsino component is achieved in a comparatively small band near to the chargino NLSP region giving the blue points in Figure 5.4 that is generated quite similar to the previous plots on bino-wino NLSP.

Resonant annihilation via the heavy Higgses A and H , which are nearly mass degenerate for our choice of parameters, proceeds naturally more strongly for a Higgsino NLSP. In Figure 5.4 this effect provides the only possibility to have a gravitino with a mass $m_{3/2} = 10$ GeV. All other points are surely excluded.

Even at $m_{3/2} = 1$ GeV the scenario is again strongly constrained by the hadronic bounds. We can identify three allowed regions. For sure, a heavy neutralino with a mass $m_\chi \gtrsim 1.6$ TeV decays early enough. Then there is the resonance and some Higgsino points around $m_\chi \approx 1100$ GeV.

From the hadronic bounds on the scenario with a gravitino mass $m_{3/2} = 10$ GeV, we can infer that the Higgs resonance is not strong enough to allow any bino-Higgsino neutralino at low masses with a gravitino in the $O(100)$ GeV mass range, since then as stated before all points are shifted to the right. Furthermore, we can use Eq. (4.18) and (4.28) with Eq. (4.23) to conclude that in the case of bino-Higgsino at large masses even a tiny wino component lets the neutralino decay dominantly via the wino 4-vertex.

Besides, we can compute from the results of Chapter 4 that the neutralino lifetime becomes shorter than 0.1 s in any composition at a gravitino mass of $m_{3/2} = 1$ GeV when the neutralino mass becomes larger than $m_\chi = 1600$ GeV. In this way any neutralino circumvents the BBN bounds. This can also be seen in the BBN bound plots of this chapter and sets the upper bound of the neutralino mass range considered in the branching ratio plots of Chapter 4.

5.3 Wino-Higgsino

In the case of wino-Higgsino we fix the soft bino mass at a large value $M_1 = 2200$ GeV and scan the M_2 - μ plane as shown in Figure 5.5. Here, the composition changes continuously from approximately pure wino in the upper left corner along the diagonal with $M_2 = \mu$ to Higgsino until at large values of the soft wino mass M_2 the light chargino

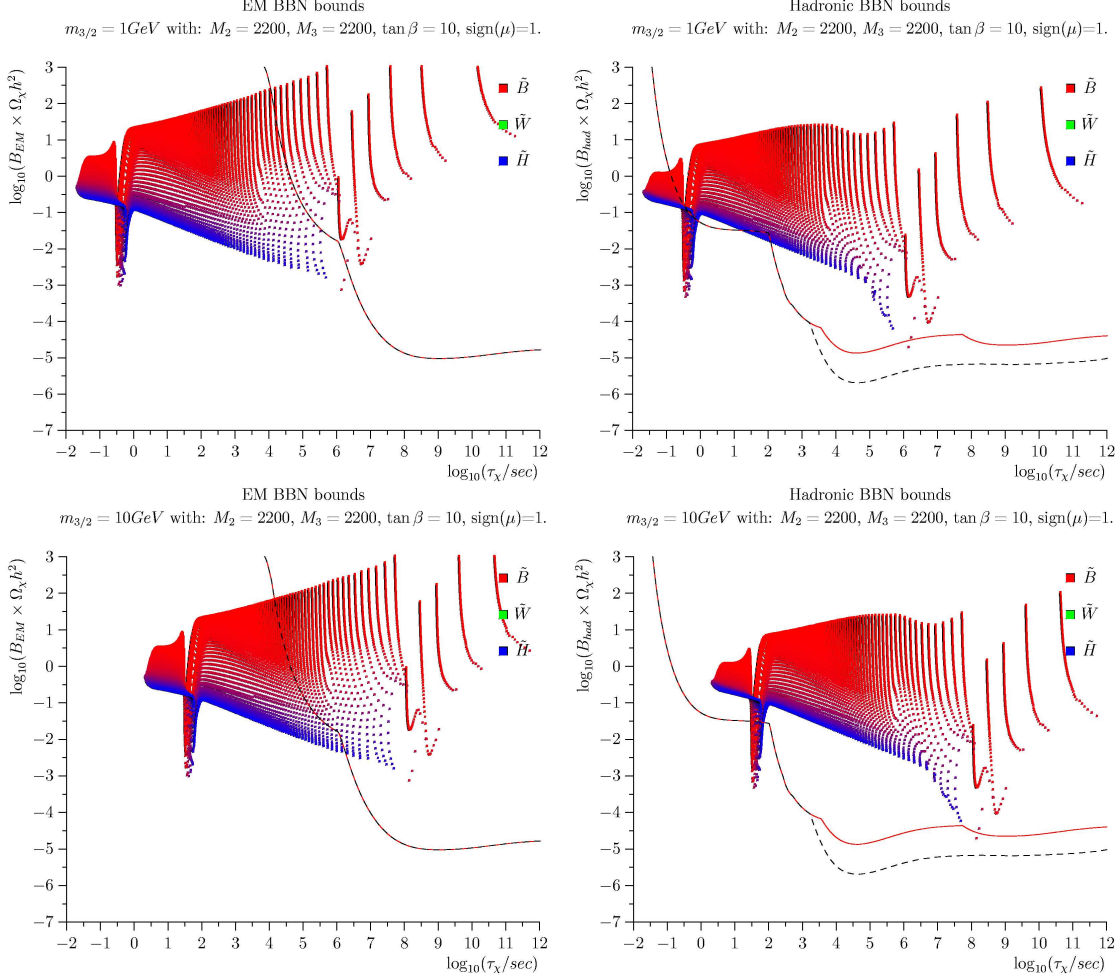


Figure 5.4: Bino-Higgsino neutralino in the $B_i \times \Omega_\chi h^2$ vs. τ plane compared with electromagnetic and hadronic BBN constraints for the case of 1 (upper) and 10 (lower) GeV gravitino mass. The neutralino mass decreases from left to right from 2 TeV to a few GeV for bino neutralino. The composition is chroma coded, whereby red indicates bino and blue indicates Higgsino. The deformation between the left and right plots is due to the different branching ratios. Bounds are taken from [11], thereby the dashed line corresponds to less conservative bounds from ${}^6\text{Li}/{}^7\text{Li}$.

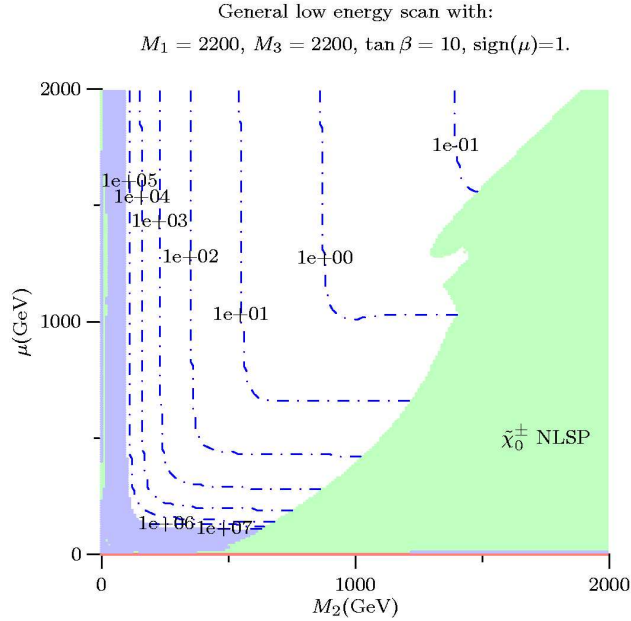


Figure 5.5: Parameter space of a wino-higgsino neutralino in the M_2 - μ plane. The blue region is excluded by the LEP searches and in the green region the light chargino is the NLSP. In the red region radiative electroweak symmetry breaking fails. Depicted are also neutralino lifetime contours for a gravitino mass $m_{3/2} = 1$ GeV.

becomes the NLSP. Furthermore, the LEP bounds on μ and M_2 exclude wino-higgsino neutralinos with a mass $m_\chi \lesssim 100$ GeV.

Figure 5.6 combines the former mentioned properties of wino and Higgsino. Compared to the bino case both have a lower relic density. At large masses the wino 4-vertex is efficient for wino NLSP and the Higgsino component brings the relic density down in the resonance region. We do not see resonant annihilation with the light Higgs $m_h = 115$ GeV, since a light wino-higgsino with mass $m_\chi \sim 55$ GeV that could annihilate resonantly via h is excluded by the LEP searches.

However, with a gravitino mass $m_{3/2} = 1$ GeV at least wino NLSP is allowed down to masses $m_\chi \approx 450$ GeV. But, for sure, there is also the window around $m_\chi = 1100$ GeV for the Higgsino again.

The only way to overcome the BBN bounds with $m_{3/2} = 10$ GeV is again the resonance case. A light wino NLSP seems to escape from the hadronic bounds due to the low hadronic branching ratio, but, again, it is excluded by the electromagnetic bounds anyway. The interplay of the two types of bounds is of particular importance in the case of wino-higgsino NLSP with heavy gravitino of $O(100)$ GeV as shown in Figure 5.7. As discussed in Section 4.4 the Z threshold is shifted to higher neutralino masses. There-

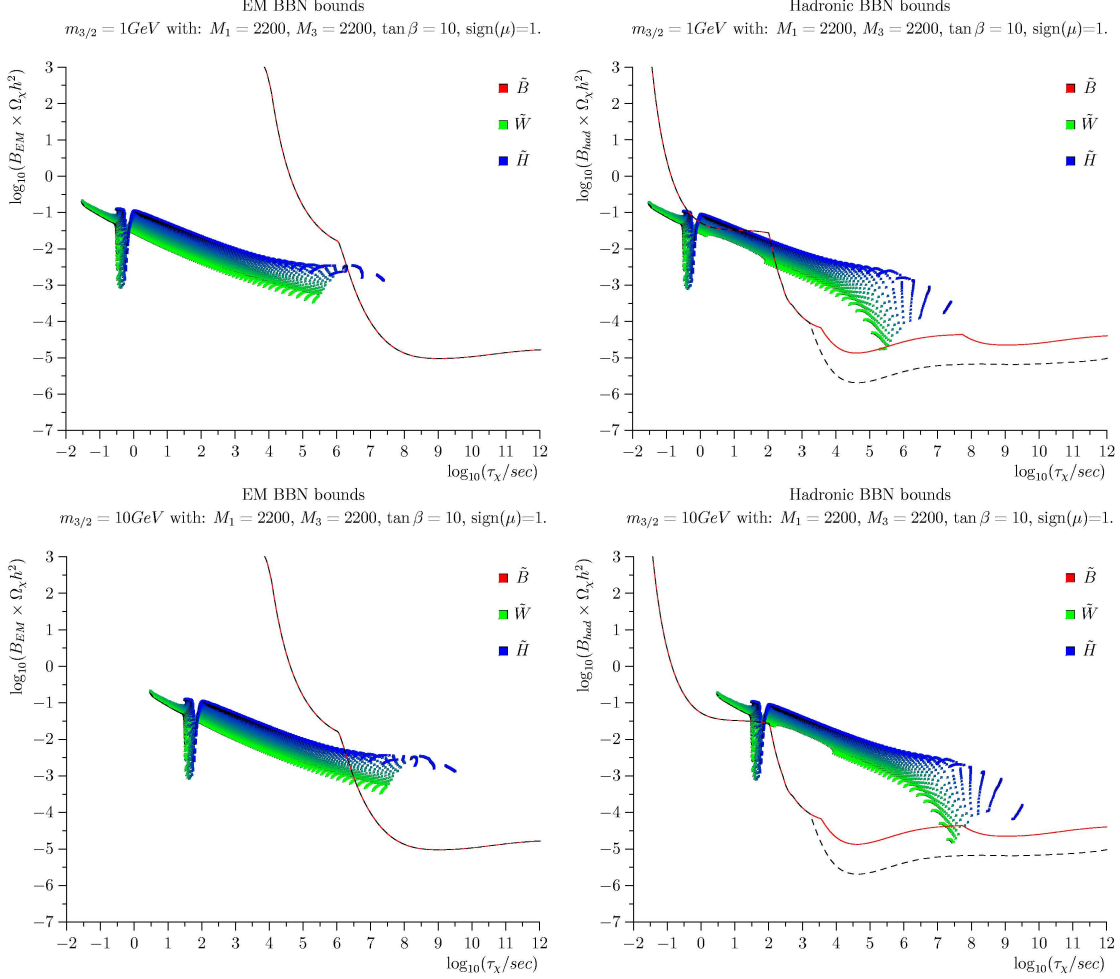


Figure 5.6: Wino-Higgsino neutralino in the $B_i \times \Omega_\chi h^2$ vs. τ plane compared with electromagnetic and hadronic BBN constraints for the case of 1 (upper) and 10 (lower) GeV gravitino mass. The neutralino mass decreases from left to right from 2 TeV to ~ 100 GeV. The composition is chroma coded, whereby green indicates wino and blue indicates Higgsino. The deformation between the left and right plots is due to the different branching ratios. Bounds are taken from [11], thereby the dashed line corresponds to less conservative bounds from ${}^6\text{Li}/{}^7\text{Li}$.

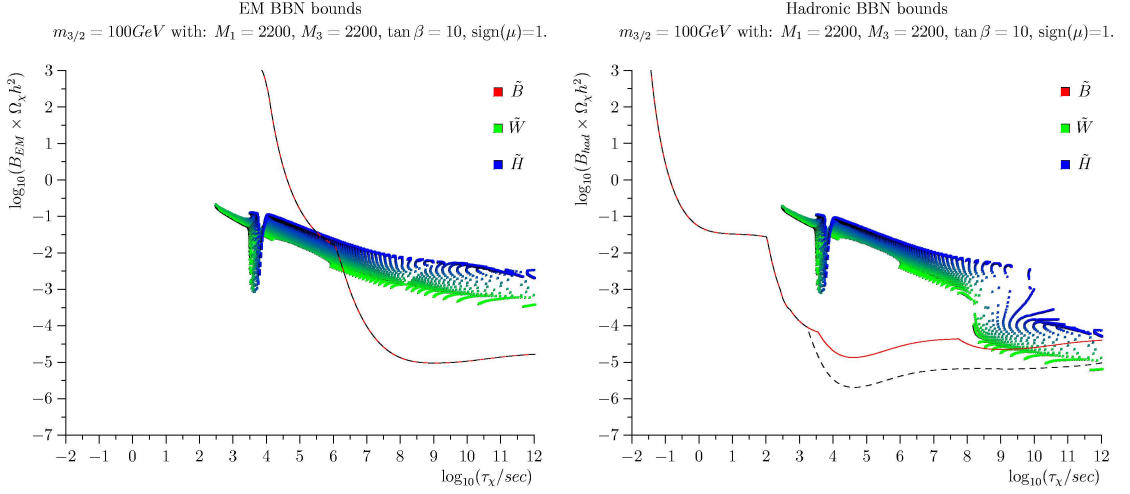


Figure 5.7: Wino-Higgsino neutralino in the $B_i \times \Omega_\chi h^2$ vs. τ plane compared with electromagnetic and hadronic BBN constraints for the case of 100 GeV gravitino mass. The neutralino mass decreases from left to right from 2 TeV to ~ 100 GeV. The composition is chroma coded, whereby green indicates wino and blue indicates Higgsino. The deformation between the left and right plots is due to the different branching ratios. Bounds are taken from [11], thereby the dashed line corresponds to less conservative bounds from ${}^6\text{Li}/{}^7\text{Li}$.

fore, winos and higgsinos appear with a hadronic branching ratio $B_{had} \approx 0.03$. In this way the light wino escapes the hadronic BBN bounds, but not the electromagnetic ones, since the electromagnetic branching ratio B_{em} is always near to one. So we conclude that gravitino dark matter with $m_{3/2} = O(100)$ GeV and neutralino NLSP up to $m_\chi = 3$ TeV is excluded by big bang nucleosynthesis. Thanks to the wino 4-vertex, the wino decays relatively fast at large masses making it the best case for large gravitino and neutralino masses. Note that a 100 GeV gravitino is already allowed with a 3.6 TeV wino NLSP.

Chapter 6

Conclusions

We have considered constraints by big bang nucleosynthesis on gravitino dark matter with a general neutralino NLSP. At first, we computed analytically all 2- and 3-body decays of the neutralino NLSP into gravitino and Standard Model particles, whereby we have maintained the impact of the gravitino mass, giving us the possibility to consider also heavy gravitinos in a safe way. We have determined the electromagnetic and hadronic branching ratio to a high accuracy, whereby we regarded all six quark flavour and their corresponding masses. Thus we found that the minimal hadronic branching ratio is ~ 0.03 , which is more than an order of magnitude larger than estimated in earlier studies.

In the process we have regarded thresholds exactly and investigated all possible interferences. As a mixing effect we found that a photino-like neutralino has a favourable low hadronic branching ratio.

In the course of the decay width calculations, we have derived all Feynman rules necessary for the calculation of the neutralino partial decay widths. Thereby we found Higgsino-Higgs 4-vertices and a wino 4-vertex from the non-abelian part of the gravitino interaction Lagrangian. These 4-vertices have been neglected in the literature so far. In fact, we have found that a wino-like neutralino decays even dominantly via its 4-vertex at masses larger than 1 TeV.

Then independently from any model at high-energies, we have investigated the bounds by big bang nucleosynthesis. We found that the bounds are, in general, slightly weaker for the case of a wino or Higgsino neutralino due to the lower relic density, but they are not weak enough to allow a gravitino with a mass of 100 GeV at low neutralino masses. Especially in the case of heavy gravitino, the interplay between hadronic bounds at larger masses ~ 1 TeV and electromagnetic bounds at masses relatively near to the

gravitino mass exclude wide ranges of the parameter space. We confirmed that a bino NLSP in the few TeV range with gravitino masses larger than 10 GeV is excluded. Furthermore, we exclude the possibility that neutralino NLSP decays produce the whole dark matter density. Either the gravitino-to-neutralino mass ratio is too small or the desired neutralino relic density clashes with the BBN bounds.

Nevertheless, we found that gravitino masses in the 10 – 20 GeV window are possible in the case of resonant annihilation via the heavy Higgs bosons for neutralino masses $m_\chi \approx m_A/2$ or $m_H/2 \sim 1100$ GeV. Since the resonance happens via the Higgsino component, this emphasizes a Higgsino NLSP. A gravitino mass of 10 – 20 GeV may still be marginally in agreement with thermal leptogenesis, so that the gravitino can be the dark matter of the universe, while the lightest neutralino is the next-to-lightest supersymmetric particle. This region is a difficult part of parameter space to investigate at the Large Hadron Collider (LHC), because it necessitates a very precise measurement of the lightest neutralino mass and Higgs masses to disentangle the neutralino LSP and thus neutralino dark matter case from the one we discussed here.

Moreover, we found that the non-abelian wino 4-vertex opens up another possibility. Heavy winos decay dominantly via this new vertex, so that a heavy gravitino with a mass of 100 GeV is already allowed for a wino-like neutralino NLSP with a mass of 3.5 TeV. This seems to favour at least at large masses a wino NLSP.

With this thesis we have closed any gap in the study of gravitino dark matter scenarios with neutralino NLSP coming from approximations in the calculation of the neutralino decay rates and hadronic branching ratio.

Appendix A

Notation and Conventions

In this thesis we use *natural units* [22]. In these units the reduced Planck constant, the speed of light and the Boltzmann constant obey

$$\hbar = c = k = 1. \tag{A.1}$$

We choose the metric of Minkowski space to be given by

$$g_{\mu\nu} = \eta_{\mu\nu} = \eta^{\mu\nu} = \text{diag}(+1, -1, -1, -1). \tag{A.2}$$

Greek indices $\mu, \nu, \dots = 0, \dots, 3$ denote space-time indices. We fix the sign of the completely antisymmetric tensor $\varepsilon_{\mu\nu\rho\sigma}$ by choosing

$$\varepsilon_{0123} \equiv -1. \tag{A.3}$$

We use the Einstein summation convention

$$a^\mu b_\mu = \sum_{\mu=0}^3 a^\mu b_\mu \tag{A.4}$$

and the Feynman slash notation

$$\not{p} \equiv \gamma^\mu p_\mu. \tag{A.5}$$

Even though we adopt many of the conventions in [35], we give our notation here explicitly since there are many different notations in the literature. Especially, our notation differs from that used by Wess and Bagger [40].

Weyl Spinors A two-component complex undotted spinor (left-handed Weyl spinor) ξ_α transforms in the $(\frac{1}{2}, \mathbf{0})$ matrix representation of the Lorentz group $\text{SO}(3,1)$, i.e. under $\text{SL}(2, \mathbb{C})$, while the dotted spinor (right-handed Weyl spinor) $\bar{\xi}_{\dot{\alpha}}$ is in the conjugate representation $(\mathbf{0}, \frac{1}{2})$. Both spinors are related by hermitian conjugation, i.e. $(\xi_\alpha)^\dagger = \bar{\xi}_{\dot{\alpha}}$ and $(\bar{\xi}_{\dot{\alpha}})^\dagger = \xi_\alpha$. Spinor indices are pulled by the Lorentz invariant ε -tensors

$$\varepsilon_{\alpha\beta} \equiv \begin{pmatrix} 0 & -1 \\ 1 & 0 \end{pmatrix}, \quad \varepsilon^{\alpha\beta} \equiv \begin{pmatrix} 0 & 1 \\ -1 & 0 \end{pmatrix}, \quad (\text{A.6a})$$

$$\varepsilon_{\dot{\alpha}\dot{\beta}} \equiv \begin{pmatrix} 0 & -1 \\ 1 & 0 \end{pmatrix}, \quad \varepsilon^{\dot{\alpha}\dot{\beta}} \equiv \begin{pmatrix} 0 & 1 \\ -1 & 0 \end{pmatrix}, \quad (\text{A.6b})$$

namely,

$$\xi_\alpha = \varepsilon_{\alpha\beta} \xi^\beta, \quad \xi^\alpha = \varepsilon^{\alpha\beta} \xi_\beta, \quad (\text{A.7a})$$

$$\bar{\xi}_{\dot{\alpha}} = \varepsilon_{\dot{\alpha}\dot{\beta}} \bar{\xi}^{\dot{\beta}}, \quad \bar{\xi}^{\dot{\alpha}} = \varepsilon^{\dot{\alpha}\dot{\beta}} \bar{\xi}_{\dot{\beta}}. \quad (\text{A.7b})$$

We define the Pauli sigma matrices (index 1,2,3) with lower Lorentz indices σ_μ as

$$\begin{aligned} \sigma_0 &\equiv \begin{pmatrix} 1 & 0 \\ 0 & 1 \end{pmatrix}, & \sigma_1 &\equiv \begin{pmatrix} 0 & 1 \\ 1 & 0 \end{pmatrix}, \\ \sigma_2 &\equiv \begin{pmatrix} 0 & -i \\ i & 0 \end{pmatrix}, & \sigma_3 &\equiv \begin{pmatrix} 1 & 0 \\ 0 & -1 \end{pmatrix}. \end{aligned} \quad (\text{A.8})$$

The standard convention for the contraction of anticommuting Weyl spinors is

$$\xi\eta \equiv \xi^\alpha \eta_\alpha = \varepsilon^{\alpha\beta} \xi_\beta \eta_\alpha = -\varepsilon^{\alpha\beta} \eta_\alpha \xi_\beta = \eta\xi, \quad (\text{A.9a})$$

$$\bar{\xi}\bar{\eta} \equiv \bar{\xi}_{\dot{\alpha}} \bar{\eta}^{\dot{\alpha}} = \varepsilon^{\dot{\alpha}\dot{\beta}} \bar{\xi}_{\dot{\beta}} \bar{\eta}^{\dot{\alpha}} = -\varepsilon^{\dot{\alpha}\dot{\beta}} \bar{\eta}^{\dot{\alpha}} \bar{\xi}_{\dot{\beta}} = \bar{\eta}\bar{\xi}. \quad (\text{A.9b})$$

The spinor index structure of the sigma matrices $\sigma^\mu_{\alpha\dot{\alpha}}$ is fixed via the definitions

$$\bar{\sigma}^{\mu\dot{\alpha}\alpha} \equiv \varepsilon^{\dot{\alpha}\dot{\beta}} \varepsilon^{\alpha\beta} \sigma^\mu_{\beta\dot{\beta}}, \quad (\text{A.10})$$

and

$$\sigma^{\mu\nu\alpha\beta} \equiv \frac{1}{4} \left(\sigma^\mu_{\alpha\dot{\alpha}} \bar{\sigma}^{\nu\dot{\alpha}\beta} - \sigma^\nu_{\alpha\dot{\alpha}} \bar{\sigma}^{\mu\dot{\alpha}\beta} \right), \quad (\text{A.11a})$$

$$\bar{\sigma}^{\mu\nu\dot{\alpha}\dot{\beta}} \equiv \frac{1}{4} \left(\bar{\sigma}^{\mu\dot{\alpha}\alpha} \sigma^\nu_{\alpha\dot{\beta}} - \bar{\sigma}^{\nu\dot{\alpha}\alpha} \sigma^\mu_{\alpha\dot{\beta}} \right). \quad (\text{A.11b})$$

Four-component Spinors In the *Weyl* or *chiral representation*, the Dirac matrices γ read

$$\gamma^\mu = \begin{pmatrix} 0 & \sigma^\mu \\ \bar{\sigma}^\mu & 0 \end{pmatrix}. \quad (\text{A.12})$$

They satisfy the Clifford algebra

$$\{\gamma^\mu, \gamma^\nu\} = 2\eta^{\mu\nu} \quad (\text{A.13})$$

and anticommute with $\gamma^5 \equiv i\gamma^0\gamma^1\gamma^2\gamma^3$, i.e. $\{\gamma^\mu, \gamma^5\} = 0$. In this representation

$$\gamma^5 = \begin{pmatrix} -\mathbb{1} & 0 \\ 0 & \mathbb{1} \end{pmatrix}. \quad (\text{A.14})$$

A *Dirac spinor* is written in terms of a left-handed and a right-handed Weyl spinor

$$\psi_{(\text{D})} = \begin{pmatrix} \xi_\alpha \\ \bar{\eta}^{\dot{\alpha}} \end{pmatrix} \quad (\text{A.15})$$

and its adjoint spinor is

$$\bar{\psi}_{(\text{D})} \equiv \psi_{(\text{D})}^\dagger \gamma^0 = \left(\eta^\alpha \quad \bar{\xi}_{\dot{\alpha}} \right) \quad (\text{A.16})$$

With the chiral projectors

$$P_L = \frac{1}{2}(\mathbb{1} - \gamma^5) \quad \text{and} \quad P_R = \frac{1}{2}(\mathbb{1} + \gamma^5) \quad (\text{A.17})$$

pure left-handed and right-handed (chiral) four-spinors are given by

$$\psi_L \equiv P_L \psi_{(\text{D})} = \begin{pmatrix} \mathbb{1} & 0 \\ 0 & 0 \end{pmatrix} \begin{pmatrix} \xi_\alpha \\ \bar{\eta}^{\dot{\alpha}} \end{pmatrix} = \begin{pmatrix} \xi_\alpha \\ 0 \end{pmatrix} \quad (\text{A.18a})$$

and

$$\psi_R \equiv P_R \psi_{(\text{D})} = \begin{pmatrix} 0 & 0 \\ 0 & \mathbb{1} \end{pmatrix} \begin{pmatrix} \xi_\alpha \\ \bar{\eta}^{\dot{\alpha}} \end{pmatrix} = \begin{pmatrix} 0 \\ \bar{\eta}^{\dot{\alpha}} \end{pmatrix}, \quad (\text{A.18b})$$

respectively. For the adjoints of the chiral spinors one finds

$$\bar{\psi}_L = \bar{\psi}_{(\text{D})} P_R = \left(0 \quad \bar{\xi}_{\dot{\alpha}} \right) \quad (\text{A.19a})$$

and

$$\bar{\psi}_R = \bar{\psi}_{(\text{D})} P_L = \left(\eta^\alpha \quad 0 \right). \quad (\text{A.19b})$$

The charge conjugation matrix C can be written as

$$C = i\gamma^2\gamma^0 = \begin{pmatrix} \varepsilon_{\alpha\beta} & 0 \\ 0 & \varepsilon^{\dot{\alpha}\dot{\beta}} \end{pmatrix}, \quad (\text{A.20})$$

with

$$C^\dagger = C^T = C^{-1} = -C \quad \text{and} \quad C^2 = -\mathbb{1}. \quad (\text{A.21})$$

The charge-conjugated Dirac spinor of (A.15) then reads

$$\psi_{(\text{D})}^c \equiv C \bar{\psi}_{(\text{D})}^T = \begin{pmatrix} \eta_\alpha \\ \bar{\xi}^{\dot{\alpha}} \end{pmatrix}. \quad (\text{A.22})$$

A *Majorana spinor* has the property $\eta = \xi$, so that it is equal to its own charge-conjugate, i.e. $\psi_{(\text{M})} = \psi_{(\text{M})}^c$. A Majorana spinor can be written as

$$\psi_{(\text{M})} = \begin{pmatrix} \xi_\alpha \\ \bar{\xi}^{\dot{\alpha}} \end{pmatrix}, \quad (\text{A.23})$$

so that its adjoint

$$\bar{\psi}_{(\text{M})} = \left(\xi^\alpha \quad \bar{\xi}_{\dot{\alpha}} \right). \quad (\text{A.24})$$

Note that the matrix C fulfills

$$C \Gamma_i^T C^{-1} = \eta_i \Gamma_i \quad (\text{no sum}) \quad (\text{A.25})$$

with

$$\eta_i = \begin{cases} 1 & \text{for } \Gamma_i = 1, i\gamma^5, \gamma^\mu \gamma^5 \\ -1 & \text{for } \Gamma_i = \gamma^\mu, \sigma^{\mu\nu} \end{cases}, \quad (\text{A.26})$$

where Γ stems from an interaction Lagrangian, i.e. $\mathcal{L}_{int} = \dots (\bar{\chi} \Gamma \chi) \dots$.

Appendix B

Example Calculation

To give an example, we sketch in this appendix how to compute the decay width of the process $\chi \rightarrow \Psi_\mu \gamma$. Starting from the interaction Lagrangian $\mathcal{L}_{\Psi, \text{int}}^{(\alpha)}$ (3.49) we see that its third term,

$$-\frac{i}{8M_p} \bar{\psi}_\mu[\gamma^\rho, \gamma^\sigma] \gamma^\mu \lambda^{(\alpha)a} F_{\rho\sigma}^{(\alpha)a}, \quad (\text{B.1})$$

will be relevant for this process, since it will give Feynman rules containing gauginos $\lambda^{(\alpha)a}$. Furthermore, we will need only the abelian part of the field strength tensor (3.52), which brings us to

$$\rightarrow -\frac{i}{8M_p} \bar{\psi}_\mu[\gamma^\rho, \gamma^\sigma] \gamma^\mu \lambda^{(\alpha)a} (\partial_\rho A_\sigma^{(\alpha)a} - \partial_\sigma A_\rho^{(\alpha)a}). \quad (\text{B.2})$$

This can be simplified using $[A, B] = -[B, A]$ with a relabeling of dummy indices,

$$= -\frac{i}{4M_p} \bar{\psi}_\mu[\gamma^\rho, \gamma^\sigma] \gamma^\mu \lambda^{(\alpha)a} \partial_\rho A_\sigma^{(\alpha)a}. \quad (\text{B.3})$$

Here, $\alpha = 1, 2 \neq 3$ and we are looking for the electromagnetically neutral part, which gives us, following Table 3.3,

$$\rightarrow -\frac{i}{4M_p} \bar{\psi}_\mu[\gamma^\rho, \gamma^\sigma] \gamma^\mu (\widetilde{W}^0 \partial_\rho W_\sigma^0 + \widetilde{B} \partial_\rho B_\sigma), \quad (\text{B.4})$$

where we replace W_σ^0 and B_σ via the inversion of Eq. (3.24) with Z_σ^0 and A_σ of Section 3.3.2. This gives

$$\begin{aligned} &= -\frac{i}{4M_p} \bar{\psi}_\mu[\gamma^\rho, \gamma^\sigma] \gamma^\mu \\ &\quad \times (\widetilde{W}^0 \partial_\rho (\cos \Theta_W Z_\sigma^0 + \sin \Theta_W A_\sigma) + \widetilde{B} \partial_\rho (-\sin \Theta_W Z_\sigma^0 + \cos \Theta_W A_\sigma)). \end{aligned} \quad (\text{B.5})$$

If we rewrite this expression,

$$= -\frac{i}{4M_p}\bar{\psi}_\mu[\gamma^\rho, \gamma^\sigma]\gamma^\mu(\tilde{B}\cos\Theta_W + \tilde{W}^0\sin\Theta_W)\partial_\rho A_\sigma \quad (\text{B.6})$$

$$-\frac{i}{4M_p}\bar{\psi}_\mu[\gamma^\rho, \gamma^\sigma]\gamma^\mu(-\tilde{B}\sin\Theta_W + \tilde{W}^0\cos\Theta_W)\partial_\rho Z_\sigma^0, \quad (\text{B.7})$$

we can read-off the gaugino-gravitino-photon vertex rule from Eq. (B.6) following the method proposed in [50]. Since \mathbf{N} is real, $\mathbf{N}_{11}^* = \mathbf{N}_{11}$.

However, with given Feynman rules the first step is to draw the desired Feynman diagram, see Figure 4.1. Then we use the Feynman rules of Appendix D to write down the amplitude, i.e.

$$i\mathcal{M} = \epsilon_\rho^*(p_1)\mathcal{M}^\rho(p_1) \quad (\text{B.8})$$

with

$$\mathcal{M}^\rho(p_1) = \frac{1}{4M_p}(N_{11}c_W + N_{12}s_W)\bar{\Psi}_\nu^r(p)[\gamma^\rho, \not{p}_1]\gamma^\nu u^s(k). \quad (\text{B.9})$$

After squaring the amplitude, with

$$\mathcal{M}^{*\sigma}(p_1) = \frac{1}{4M_p}(N_{11}c_W + N_{12}s_W)^*\bar{u}^s(k)\gamma^\mu[\not{p}_1, \gamma^\sigma]\Psi_\mu^r(p), \quad (\text{B.10})$$

getting

$$|\mathcal{M}|^2 = \sum_\epsilon \epsilon_\rho^* \epsilon_\sigma \mathcal{M}^\rho(p_1) \mathcal{M}^{*\sigma}(p_1), \quad (\text{B.11})$$

we sum over photon polarizations and gravitino helicities and average over the neutralino spin using the known relations,

$$\sum_r u^r(k)\bar{u}^r(k) = \not{k} + m, \quad \sum_\epsilon \epsilon_\mu^* \epsilon_\nu \rightarrow -g_{\mu\nu} \quad (\text{B.12})$$

and the gravitino polarization tensor $\Pi_{\mu\nu}$ (3.46). This gives

$$\frac{1}{2} \sum_{s,r,\epsilon} |\mathcal{M}|^2 = -\frac{1}{2} \frac{|N_{11}c_W + N_{12}s_W|^2}{(4M_p)^2} \text{Tr}[\Pi_{\mu\nu}(p)[\gamma_\sigma, \not{p}_1]\gamma^\nu(\not{k} + m_\chi)\gamma^\mu[\not{p}_1, \gamma^\sigma]]. \quad (\text{B.13})$$

After the evaluation of the Dirac traces, Eq. (B.13) reads

$$= \frac{1}{2} \frac{|N_{11}c_W + N_{12}s_W|^2}{(4M_p)^2} \left\{ (128 - \frac{128}{3})(p \cdot p_1)(k \cdot p_1) + \frac{256}{3} \frac{(p_1 \cdot p)^2}{m_{3/2}^2} (k \cdot p) \right\}. \quad (\text{B.14})$$

This result for $|\mathcal{M}|^2$ we plug in Eq. (C.5), whereby the scalar products are given by Eq. (C.6). Thus we arrive at the final result

$$\Gamma(\tilde{G} \rightarrow \Psi_\mu \gamma) = \frac{|N_{11}\cos\Theta_W + N_{12}\sin\Theta_W|^2}{48\pi M_p^2} \left(\frac{m_\chi^5}{m_{3/2}^2} - 6m_{3/2}m_\chi + 8\frac{m_{3/2}^4}{m_\chi} - 3\frac{m_{3/2}^6}{m_\chi^3} \right), \quad (\text{B.15})$$

which is, with the parameterization of Eq. (E.5), also given in Eq. (E.6).

Appendix C

Kinematics and Parametrisation

The energy E and 3-momentum \vec{p} of a particle of mass m form a 4-vector $p = (E, \vec{p})$ whose square $p^2 \equiv E^2 - |\vec{p}|^2 = m^2$. The Lorentz transformation converts 4-vectors between two different reference frames, where one is in constant motion with respect to the other. Since the scalar product of two 4-momenta $p_1 \cdot p_2 = E_1 E_2 - \vec{p}_1 \cdot \vec{p}_2$ is invariant under Lorentz transformations, it is frame independent.

In the course of the calculation of decay widths we need to calculate 4-momentum scalar products, i.e. scalar products of the 4-momenta of the considered particles. These 4-momenta are given explicitly by the kinematics of the process under consideration. Since scalar products are frame independent, we can choose a particular frame to describe the kinematics. We choose the frame to make the calculation as simple as possible.

Particle Decays The partial decay width of a particle of mass M into n bodies in its rest frame $p = (M, 0, 0, 0)$ is given in terms of the Lorentz-invariant matrix element \mathcal{M} by [22]

$$d\Gamma = \frac{(2\pi)^4}{2M} |\mathcal{M}|^2 d\Phi_n(p; p_1, \dots, p_n), \quad (\text{C.1})$$

where $d\Phi_n$ is an element of the n -body phase space given by

$$d\Phi_n(p; p_1, \dots, p_n) = \delta^4\left(p - \sum_{i=1}^n p_i\right) \prod_{i=1}^n \frac{d^3 p_i}{(2\pi)^3 2E_i}. \quad (\text{C.2})$$

The δ -distribution implements 4-momentum conservation. To get the total decay width Γ we integrate over phase space.

C.1 2-body decays

In the rest frame of a particle with 4-momentum $p = (M, 0, 0, 0)$, decaying into two particles labeled 1 and 2, the absolute value of the 3-momenta of the decay products is determined by 4-momentum conservation,

$$|\vec{p}_1| = |\vec{p}_2| = \frac{1}{2M}[(M^2 - (m_1 + m_2)^2)(M^2 - (m_1 - m_2)^2)]^{1/2}. \quad (\text{C.3})$$

The partial decay width becomes

$$d\Gamma = \frac{1}{32\pi^2} |\mathcal{M}|^2 \frac{|\vec{p}_1|}{M^2} d\Omega, \quad (\text{C.4})$$

where $d\Omega = d\Phi_1 d(\cos \Theta_1)$ is the solid angle of particle 1. In fact this solid angle is the only degree of freedom left ($\vec{p}_1 = -\vec{p}_2$) and its integration is trivial. We get

$$\Gamma = \frac{1}{8\pi} |\mathcal{M}|^2 \frac{|\vec{p}_1|}{M^2}. \quad (\text{C.5})$$

The scalar products are given by the particle masses, i.e.

$$\begin{aligned} (p \cdot p_1) &= \frac{M^2 + m_1^2 - m_2^2}{2}, \\ (p \cdot p_2) &= \frac{M^2 - m_1^2 + m_2^2}{2}, \\ (p_1 \cdot p_2) &= \frac{M^2 - m_1^2 - m_2^2}{2}. \end{aligned} \quad (\text{C.6})$$

C.2 3-body decays

In the rest frame of a decaying particle with 4-momentum p , decaying into three particles labeled 1, 2 and 3, we write the 4-momenta as

$$p = \begin{pmatrix} M \\ 0 \\ 0 \\ 0 \end{pmatrix}, \quad p_3 = \begin{pmatrix} p_3^0 \\ 0 \\ 0 \\ p_3^3 \end{pmatrix}, \quad p_1 = \begin{pmatrix} p_1^0 \\ p_1^3 \sin \xi \\ 0 \\ p_1^3 \cos \xi \end{pmatrix}, \quad p_2 = \begin{pmatrix} p_2^0 \\ -p_1^3 \sin \xi \\ 0 \\ -p_3^3 - p_1^3 \cos \xi \end{pmatrix}.$$

Due to momentum conservation $p = p_1 + p_2 + p_3$, the momenta of the three decay particles lie in a plane and the angle ξ is fixed if the energies p_i^0 are known.

It is convenient to introduce the following parametrisation. For the masses $m_i^2 = p_i^2$ we use dimensionless variables

$$a = \frac{(p_1)^2}{M^2}, \quad b = \frac{(p_2)^2}{M^2}, \quad c = \frac{(p_3)^2}{M^2}.$$

Energy and momentum are normalised to the half of the mass of the decaying particle:

$$\begin{aligned}
 x_1 &= \frac{2p_1^0}{M}, \quad y_1 = \frac{2|\vec{p}_1|}{M} = \sqrt{x_1^2 - 4a} \\
 x_2 &= \frac{2p_2^0}{M}, \quad y_2 = \frac{2|\vec{p}_2|}{M} = \sqrt{x_2^2 - 4b} \\
 x_3 &= \frac{2p_3^0}{M}, \quad y_3 = \frac{2|\vec{p}_3|}{M} = \sqrt{x_3^2 - 4c}.
 \end{aligned} \tag{C.7}$$

Then energy conservation reads $x_1 + x_2 + x_3 = 2$ and the angle ξ is given by

$$\cos \xi = \frac{x_1 x_3 - 2(x_1 + x_3 - 1 - a + b - c)}{y_1 y_3}.$$

After integrations using the δ -distribution and angle integrations the phase space element (C.2) becomes

$$d\Phi_3 = \frac{M^2 \pi^2}{4} dx_1 dx_3 \tag{C.8}$$

with the following integration limits:

$$\begin{aligned}
 x_3^- = 2\sqrt{c} \leq x_3 &\leq 1 + c - a - b - 2\sqrt{a}\sqrt{b} = x_3^+ \\
 x_1^- \leq x_1 &\leq x_1^+ \\
 x_1^\pm &= 1 + a - b + c - x_3 - \frac{1}{2}(2c - x_3)\left(1 + \frac{a - b}{1 + c - x_3}\right) \\
 &\quad \pm \frac{1}{2}y_3 \sqrt{1 - 2\frac{a + b}{1 + c - x_3} + \frac{(a - b)^2}{(1 + c - x_3)^2}}
 \end{aligned} \tag{C.9}$$

If two masses are equal ($a = b$), the inequalities become simpler,

$$\begin{aligned}
 2\sqrt{c} \leq x_3 &\leq 1 + c - 4a \\
 x_1^- \leq x_1 &\leq x_1^+ \\
 x_1^\pm &= \frac{1}{2}(2 - x_3 \pm y_3 \sqrt{1 - \frac{4a}{1 + c - x_3}}).
 \end{aligned} \tag{C.10}$$

Note, that there are only two degrees of freedom left. But the remaining integrations are non-trivial. x_1^\pm depends in a complex way on x_3 making it generally more than uncomfortable to calculate the last integral analytically.

Starting from eq. (C.1) using eq. (C.8) with the definitions (C.7), the partial decay width becomes

$$d\Gamma = \frac{M}{32(2\pi)^3} |\mathcal{M}(x_1, x_3)|^2 dx_1 dx_3. \tag{C.11}$$

To get the total decay width we integrate x_1 and x_3 with the appropriate integration limits (C.9) or (C.10). Here, as indicated in (C.11) \mathcal{M} is a function $\mathcal{M}(x_1, x_3)$.

The scalar products written in integration variables are:

$$\begin{aligned}(p_1 \cdot p_2) &= \frac{M^2}{2}(1 - a - b + c - x_3) \\(p_1 \cdot p_3) &= \frac{M^2}{2}(-1 - a + b - c + x_1 + x_3) \\(p_2 \cdot p_3) &= \frac{M^2}{2}(1 + a - b - c - x_1) \\(p \cdot p_1) &= \frac{M^2}{2}x_1 \\(p \cdot p_2) &= \frac{M^2}{2}(2 - x_1 - x_3) \\(p \cdot p_3) &= \frac{M^2}{2}x_3\end{aligned}\tag{C.12}$$

Appendix D

Feynman rules

We provide the complete set of Feynman rules necessary for the computations performed in Chapter 4. If they are standard vertices of Glashow-Weinberg-Salam (GWS) theory of weak interaction, they are derived/taken from [48] and checked against [41]. Otherwise they are derived from the Lagrangian as given in Eq. (25.24) and Eq. (G.2) in the book of Wess and Bagger [40]. Especially gravitino vertices are checked in the high-energy limit against the Feynman rules as they are given in [35].

The gravitino Ψ_μ is represented as a double solid line and gauge bosons are drawn as wiggled lines. The neutralino is always depicted as its corresponding gauge eigenstate. Bino \tilde{B} and wino \tilde{W}^0 are gauginos (\tilde{G}^0 refers to an electromagnetically neutral mixed state of gauginos). Gauginos are depicted as wiggled lines with additional straight solid lines, whereas the Higgsino \tilde{H}^0 is a chiral fermion that are drawn as single solid lines.

The method of continuous fermion flow [50] is addressed in Section 3.3.3. The fermion flow is independent of the fermion number flow and the direction of momenta. The fermion flow is represented by additional arrow lines close to the fermion lines, whereas the fermion number flow is as usual represented by an arrow on the chiral fermion lines. For the negative frequency solution of the gravitino see [36].

For the external lines and propagators shown below the momentum P flows from the left to the right. Furthermore, momenta are assumed to flow towards the vertices.

External Lines

- Scalar particles

$$\begin{array}{c}
 \text{---} \blacktriangleright \text{---} \bullet \bullet \text{---} \blacktriangleright \text{---} \quad \text{---} \blacktriangleleft \text{---} \bullet \bullet \text{---} \blacktriangleleft \text{---} \quad = \quad 1
 \end{array}$$

- Gauginos and matter fermions

$$\begin{array}{llll}
 \begin{array}{c} \longrightarrow \\ \text{~~~~~} \bullet \end{array} & \begin{array}{c} \longrightarrow \\ \longrightarrow \\ \bullet \end{array} & \begin{array}{c} \longrightarrow \\ \longleftarrow \\ \bullet \end{array} & = u^s(p) \\
 \begin{array}{c} \longrightarrow \\ \bullet \text{~~~~~} \end{array} & \begin{array}{c} \longrightarrow \\ \longrightarrow \\ \bullet \end{array} & \begin{array}{c} \longrightarrow \\ \longleftarrow \\ \bullet \end{array} & = \bar{u}^s(p) \\
 \begin{array}{c} \longleftarrow \\ \bullet \text{~~~~~} \end{array} & \begin{array}{c} \longleftarrow \\ \longleftarrow \\ \bullet \end{array} & \begin{array}{c} \longleftarrow \\ \longleftarrow \\ \bullet \end{array} & = v^s(p) \\
 \begin{array}{c} \longleftarrow \\ \text{~~~~~} \bullet \end{array} & \begin{array}{c} \longleftarrow \\ \longrightarrow \\ \bullet \end{array} & \begin{array}{c} \longleftarrow \\ \longrightarrow \\ \bullet \end{array} & = \bar{v}^s(p)
 \end{array}$$

- Gauge bosons

$$\mu, a \text{ ~~~~~ } \bullet = \epsilon_\mu^a(p), \quad \bullet \text{ ~~~~~ } \mu, a = \epsilon_\mu^{*a}(p).$$

- Gravitino

$$\begin{array}{ll}
 \mu \begin{array}{c} \longrightarrow \\ \longrightarrow \\ \bullet \end{array} = \psi_\mu^{+s}(p), & \begin{array}{c} \longrightarrow \\ \longrightarrow \\ \bullet \end{array} \mu = \bar{\psi}_\mu^{+s}(p) \\
 \begin{array}{c} \longleftarrow \\ \longleftarrow \\ \bullet \end{array} \mu = \psi_\mu^{-s}(p), & \mu \begin{array}{c} \longleftarrow \\ \longleftarrow \\ \bullet \end{array} = \bar{\psi}_\mu^{-s}(p)
 \end{array}$$

Propagators

- Scalar particles

$$i \bullet \text{ --- } \longrightarrow \text{ --- } \bullet j = \frac{i}{p^2 - m_\phi^2} \delta^{ij}$$

- Matter fermions

$$\begin{array}{l}
 i \bullet \begin{array}{c} \longrightarrow \\ \longrightarrow \\ \bullet \end{array} j = \frac{i(\not{p} + m_\chi)}{p^2 - m_\chi^2} \delta^{ij} \\
 i \bullet \begin{array}{c} \longleftarrow \\ \longrightarrow \\ \bullet \end{array} j = \frac{i(-\not{p} + m_\chi)}{p^2 - m_\chi^2} \delta^{ij}
 \end{array}$$

- Gauginos

$$a \bullet \begin{array}{c} \longrightarrow \\ \text{~~~~~} \\ \bullet \end{array} b = \frac{i(\not{p} + m_\lambda)}{p^2 - m_\lambda^2} \delta^{ab}$$

- Massless gauge bosons in Feynman gauge ($\xi = 1$)

$$a, \mu \text{ --- } \text{wavy line} \text{ --- } b, \nu = -\frac{ig_{\mu\nu}}{p^2} \delta^{ab}$$

- Massive gauge bosons in unitary gauge ($\xi \rightarrow \infty$)
with this the Goldstone propagator vanishes

$$a, \mu \text{ --- } \text{wavy line} \text{ --- } b, \nu = \frac{-i(g_{\mu\nu} - p_\mu p_\nu / m_A^2)}{p^2 - m_A^2} \delta^{ab}$$

Relevant Gauge and Yukawa Vertices

We use abbreviations $s_\alpha \equiv \sin \alpha$, $c_\alpha \equiv \cos \alpha$, $s_W \equiv \sin \Theta_W$ and others listed in Appendix E.

Vertex rules $i\Gamma$ for reversed fermion flow $i\Gamma'$ can be computed with

$$\Gamma' = C\Gamma^T C^{-1} \tag{D.1}$$

using eq. (A.25).

$$\begin{array}{l}
 \begin{array}{c} \gamma_\mu \\ \text{---} \\ f \text{ ---} \bullet \text{ ---} f \\ \text{---} \end{array} = -ieQ\gamma^\mu \\
 \\
 \begin{array}{c} Z_\mu^0 \\ \text{---} \\ f \text{ ---} \bullet \text{ ---} f \\ \text{---} \end{array} = -ig_Z((T_3 - Qs_W^2)P_L - Qs_W^2 P_R)\gamma^\mu
 \end{array}$$

$$\begin{array}{l}
 \begin{array}{c}
 \text{---} u \text{---} \bullet \text{---} h^0 \\
 \text{---} u \text{---} \bullet \text{---} u \\
 \text{---} u \text{---} \bullet \text{---} u
 \end{array} = -i \frac{m_u g_Z c_\alpha}{m_Z \sqrt{2} s_\beta} \qquad \begin{array}{c}
 \text{---} d, l \text{---} \bullet \text{---} h^0 \\
 \text{---} d, l \text{---} \bullet \text{---} d, l \\
 \text{---} d, l \text{---} \bullet \text{---} d, l
 \end{array} = -i \frac{m_d g_Z -s_\alpha}{m_Z \sqrt{2} c_\beta} \\
 \\
 \begin{array}{c}
 \text{---} u \text{---} \bullet \text{---} H^0 \\
 \text{---} u \text{---} \bullet \text{---} u \\
 \text{---} u \text{---} \bullet \text{---} u
 \end{array} = -i \frac{m_u g_Z s_\alpha}{m_Z \sqrt{2} s_\beta} \qquad \begin{array}{c}
 \text{---} d, l \text{---} \bullet \text{---} H^0 \\
 \text{---} d, l \text{---} \bullet \text{---} d, l \\
 \text{---} d, l \text{---} \bullet \text{---} d, l
 \end{array} = -i \frac{m_d g_Z c_\alpha}{m_Z \sqrt{2} c_\beta} \\
 \\
 \begin{array}{c}
 \text{---} u \text{---} \bullet \text{---} A^0 \\
 \text{---} u \text{---} \bullet \text{---} u \\
 \text{---} u \text{---} \bullet \text{---} u
 \end{array} = -i \frac{m_u g_Z c_\beta}{m_Z \sqrt{2} s_\beta} \underbrace{(P_R - P_L)}_{=\gamma^5} \\
 \\
 \begin{array}{c}
 \text{---} d, l \text{---} \bullet \text{---} A^0 \\
 \text{---} d, l \text{---} \bullet \text{---} d, l \\
 \text{---} d, l \text{---} \bullet \text{---} d, l
 \end{array} = -i \frac{m_d g_Z s_\beta}{m_Z \sqrt{2} c_\beta} \underbrace{(P_R - P_L)}_{=\gamma^5} \\
 \\
 \begin{array}{c}
 \text{---} \tilde{f}_L \\
 \text{---} \tilde{G}^0 \text{---} \bullet \text{---} f \\
 \text{---} \tilde{G}^0 \text{---} \bullet \text{---} f \\
 \text{---} \tilde{G}^0 \text{---} \bullet \text{---} f
 \end{array} = -i \frac{g_Z}{\sqrt{2}} (Y_{\tilde{f}_L} N_{11sW} \pm_{f=d,l}^{f=u} N_{12cW}) P_L \\
 \\
 \begin{array}{c}
 \text{---} \tilde{f}_L \\
 \text{---} \tilde{G}^0 \text{---} \bullet \text{---} f \\
 \text{---} \tilde{G}^0 \text{---} \bullet \text{---} f \\
 \text{---} \tilde{G}^0 \text{---} \bullet \text{---} f
 \end{array} = -i \frac{g_Z}{\sqrt{2}} (Y_{\tilde{f}_L} N_{11sW} \pm_{f=d,l}^{f=u} N_{12cW}) P_R
 \end{array}$$

$$\begin{aligned}
\begin{array}{c} \tilde{G}^0 \\ \swarrow \\ \text{---} \\ \searrow \\ f \end{array} \begin{array}{c} \tilde{f}_R \\ \nearrow \\ \bullet \\ \searrow \\ f \end{array} &= \pm_{f=d,l}^{f=u} i \frac{g_Z}{\sqrt{2}} Y_{\tilde{f}_R} N_{11} s_W P_R \\
\begin{array}{c} \tilde{G}^0 \\ \swarrow \\ \text{---} \\ \searrow \\ f \end{array} \begin{array}{c} \tilde{f}_R \\ \nearrow \\ \bullet \\ \searrow \\ f \end{array} &= \pm_{f=d,l}^{f=u} i \frac{g_Z}{\sqrt{2}} Y_{\tilde{f}_R} N_{11} s_W P_L
\end{aligned}$$

$$\begin{array}{c} \tilde{H}^0 \\ \swarrow \\ \text{---} \\ \searrow \\ u \end{array} \begin{array}{c} \tilde{u}_L \\ \nearrow \\ \bullet \\ \searrow \\ u \end{array} = -i \frac{m_u}{m_Z} \frac{g_Z}{\sqrt{2}} \frac{N_{14}}{s_\beta} P_L$$

$$\begin{array}{c} \tilde{H}^0 \\ \swarrow \\ \text{---} \\ \searrow \\ d,l \end{array} \begin{array}{c} \tilde{d}_L, \tilde{l}_L \\ \nearrow \\ \bullet \\ \searrow \\ d,l \end{array} = -i \frac{m_d}{m_Z} \frac{g_Z}{\sqrt{2}} \frac{N_{13}}{c_\beta} P_L$$

$$\begin{array}{c} \tilde{H}^0 \\ \swarrow \\ \text{---} \\ \searrow \\ u \end{array} \begin{array}{c} \tilde{u}_R \\ \nearrow \\ \bullet \\ \searrow \\ u \end{array} = -i \frac{m_u}{m_Z} \frac{g_Z}{\sqrt{2}} \frac{N_{14}}{s_\beta} P_R$$

$$\begin{array}{c} \tilde{H}^0 \\ \swarrow \\ \text{---} \\ \searrow \\ d,l \end{array} \begin{array}{c} \tilde{d}_R, \tilde{l}_R \\ \nearrow \\ \bullet \\ \searrow \\ d,l \end{array} = -i \frac{m_d}{m_Z} \frac{g_Z}{\sqrt{2}} \frac{N_{13}}{c_\beta} P_R$$

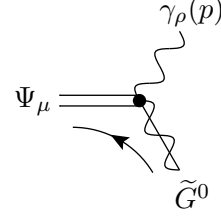
$$\begin{array}{c} \tilde{H}^0 \\ \swarrow \\ \text{---} \\ \searrow \\ u \end{array} \begin{array}{c} \tilde{u}_L \\ \nearrow \\ \bullet \\ \searrow \\ u \end{array} = -i \frac{m_u}{m_Z} \frac{g_Z}{\sqrt{2}} \frac{N_{14}}{s_\beta} P_R$$

$$\begin{array}{c} \tilde{H}^0 \\ \swarrow \\ \text{---} \\ \searrow \\ d,l \end{array} \begin{array}{c} \tilde{d}_L, \tilde{l}_L \\ \nearrow \\ \bullet \\ \searrow \\ d,l \end{array} = -i \frac{m_d}{m_Z} \frac{g_Z}{\sqrt{2}} \frac{N_{13}}{c_\beta} P_R$$

$$\begin{array}{c} \tilde{H}^0 \\ \swarrow \\ \text{---} \\ \searrow \\ u \end{array} \begin{array}{c} \tilde{u}_R \\ \nearrow \\ \bullet \\ \searrow \\ u \end{array} = -i \frac{m_u}{m_Z} \frac{g_Z}{\sqrt{2}} \frac{N_{14}}{s_\beta} P_L$$

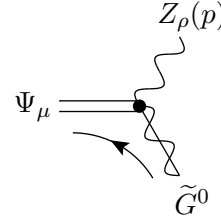
$$\begin{array}{c} \tilde{H}^0 \\ \swarrow \\ \text{---} \\ \searrow \\ d,l \end{array} \begin{array}{c} \tilde{d}_R, \tilde{l}_R \\ \nearrow \\ \bullet \\ \searrow \\ d,l \end{array} = -i \frac{m_d}{m_Z} \frac{g_Z}{\sqrt{2}} \frac{N_{13}}{c_\beta} P_L$$

Gravitino Vertices



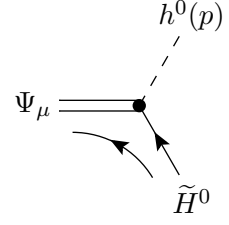
A Feynman diagram showing a vertex where a gravitino line (double line with arrow) enters from the left, a photon line (wavy line) enters from the top, and a graviton line (wavy line) exits to the right. The photon is labeled $\gamma_\rho(p)$ and the graviton is labeled \tilde{G}^0 .

$$= -\frac{i}{4M_p}(N_{11}c_W + N_{12}s_W) [\not{p}, \gamma^\rho] \gamma^\mu$$



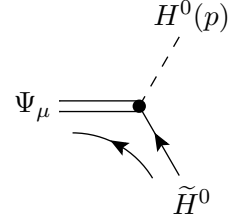
A Feynman diagram showing a vertex where a gravitino line (double line with arrow) enters from the left, a Z boson line (wavy line) enters from the top, and a graviton line (wavy line) exits to the right. The Z boson is labeled $Z_\rho(p)$ and the graviton is labeled \tilde{G}^0 .

$$= -\frac{i}{4M_p}(-N_{11}s_W + N_{12}c_W) [\not{p}, \gamma^\rho] \gamma^\mu$$



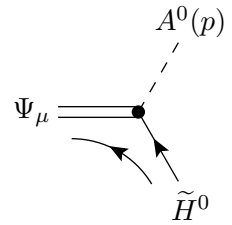
A Feynman diagram showing a vertex where a gravitino line (double line with arrow) enters from the left, a Higgs boson line (dashed line) enters from the top, and a graviton line (wavy line) exits to the right. The Higgs boson is labeled $h^0(p)$ and the graviton is labeled \tilde{H}^0 .

$$= \frac{i}{2M_p}(-N_{13}s_\alpha + N_{14}c_\alpha) \not{p} \gamma^\mu$$



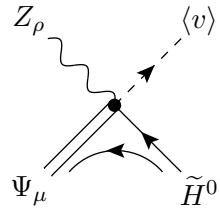
A Feynman diagram showing a vertex where a gravitino line (double line with arrow) enters from the left, a Higgs boson line (dashed line) enters from the top, and a graviton line (wavy line) exits to the right. The Higgs boson is labeled $H^0(p)$ and the graviton is labeled \tilde{H}^0 .

$$= \frac{i}{2M_p}(N_{13}c_\alpha + N_{14}s_\alpha) \not{p} \gamma^\mu$$



A Feynman diagram showing a vertex where a gravitino line (double line with arrow) enters from the left, a Higgs boson line (dashed line) enters from the top, and a photon line (wavy line) exits to the right. The Higgs boson is labeled \tilde{H}^0 and the photon is labeled $A^0(p)$.

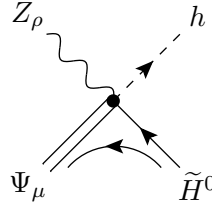
$$= -\frac{1}{2M_p}(N_{13}s_\beta + N_{14}c_\beta) \not{p} \gamma^\mu \underbrace{(P_R - P_L)}_{=-\gamma^5}$$



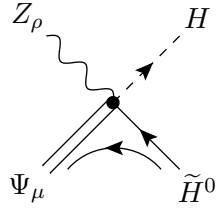
A Feynman diagram showing a vertex where a gravitino line (double line with arrow) enters from the left, a Z boson line (wavy line) enters from the top, and a graviton line (wavy line) exits to the right. The Z boson is labeled Z_ρ and the graviton is labeled \tilde{H}^0 .

$$= -i\frac{m_Z}{2M_p}(-N_{13}c_\beta + N_{14}s_\beta)\gamma^\rho \gamma^\mu \underbrace{(P_L - P_R)}_{=-\gamma^5}$$

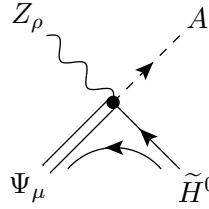
The vertex does not exist for the photon.



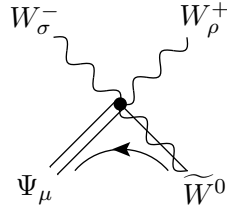
$$= i \frac{gZ}{4M_p} (N_{13}s_\alpha + N_{14}c_\alpha) \gamma^\rho \gamma^\mu \underbrace{(P_R - P_L)}_{=\gamma^5}$$



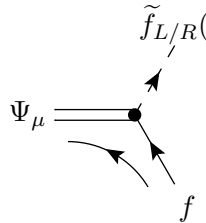
$$= i \frac{gZ}{4M_p} (-N_{13}c_\alpha + N_{14}s_\alpha) \gamma^\rho \gamma^\mu \underbrace{(P_R - P_L)}_{=\gamma^5}$$



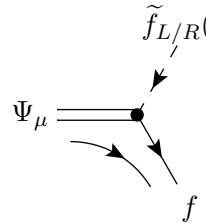
$$= -\frac{gZ}{4M_p} (-N_{13}s_\beta + N_{14}c_\beta) \gamma^\rho \gamma^\mu$$



$$= \frac{i}{4M_p} \frac{e}{s_W} [\gamma^\rho, \gamma^\sigma] \gamma^\mu$$



$$= \frac{i}{\sqrt{2}M_p} \not{p} \gamma^\mu P_{L/R}$$



$$= -\frac{i}{\sqrt{2}M_p} \not{p} \gamma^\mu P_{R/L}$$

Appendix E

Full Analytic Results

We list the analytic results for each partial decay width computed in the course of the preparation of this thesis. We consider all 3-body decays of the neutralino NLSP into gravitino and Standard Model particles. There are Feynman diagrams for each process under consideration.

We remind that we use the reduced Planck mass [22]

$$M_p = \frac{1}{\sqrt{8\pi G_N}} = 2.435 \times 10^{18} \text{ GeV}. \quad (\text{E.1})$$

The Higgs expectation values are given by

$$\langle H_u \rangle = v_u/\sqrt{2} \quad \text{and} \quad \langle H_d \rangle = v_d/\sqrt{2} \quad (\text{E.2})$$

so that

$$v_u^2 + v_d^2 = v^2 = \frac{4m_Z^2}{g^2 + g'^2} \approx (246 \text{ GeV})^2, \quad (\text{E.3})$$

where v denotes the Standard Model Higgs VEV. g and g' denote the known weak coupling and $U(1)_Y$ hypercharge coupling, respectively. So the mass of the Z boson is given by

$$m_Z = \frac{v}{2} g_Z \equiv \frac{v}{2} \sqrt{g^2 + g'^2}, \quad (\text{E.4})$$

where we have defined the Z boson coupling $g_Z = \sqrt{g^2 + g'^2}$.

e denotes as usual the electron charge. It is $e^2 = 4\pi\alpha_{QED}$, where α_{QED} is the known QED coupling constant.

E.1 2 body decays

Definitions For $m_A > m_B + m_C$ (in parametrisation $1 - x_B - x_C > 0$)

$$\beta_{A \rightarrow BC} \equiv [1 - 2(x_B^2 + x_C^2) + (x_B^2 - x_C^2)^2]^{\frac{1}{2}} \quad (\text{E.5})$$

and $\beta_{A \rightarrow BC} = 0$ otherwise. $x_i = \frac{m_i}{m_A}$ is the mass ratio between particle i and A .

Analytic Results Our results agree with those in [18] which differ slightly from the results in [19]. In addition, we checked the results in the goldstino limit by comparison with the results gained in the effective theory of a single goldstino provided in [55] and correctly transcribed to [35].

The Feynman diagrams of $\tilde{G} \rightarrow \Psi_\mu \gamma$ and $\tilde{G} \rightarrow \Psi_\mu Z$ are drawn in Figure 4.1.

$$\Gamma(\tilde{G} \rightarrow \Psi_\mu \gamma) = \frac{|\mathbf{N}_{11} \cos \Theta_W + \mathbf{N}_{12} \sin \Theta_W|^2 m_\chi^5}{48\pi M_p^2 m_{\frac{3}{2}}^2} \quad (\text{E.6})$$

$$\times \left(1 - x_{\frac{3}{2}}^2\right)^3 \left(1 + 3x_{\frac{3}{2}}^2\right) \quad (\text{E.7})$$

$$\Gamma(\tilde{G} \rightarrow \Psi_\mu Z) = \frac{|-\mathbf{N}_{11} \sin \Theta_W + \mathbf{N}_{12} \cos \Theta_W|^2 m_\chi^5}{48\pi M_p^2 m_{\frac{3}{2}}^2} \beta_{\chi \rightarrow \Psi_\mu Z}$$

$$\times \left[\left(1 - x_{\frac{3}{2}}^2\right)^2 \left(1 + 3x_{\frac{3}{2}}^2\right) - x_Z^2 \left\{ 3 + x_{\frac{3}{2}}^3 \left(x_{\frac{3}{2}} - 12\right) - x_Z^2 \left(3 - x_{\frac{3}{2}}^2 - x_Z^2\right) \right\} \right] \quad (\text{E.8})$$

The Feynman diagram of $\tilde{H} \rightarrow \Psi_\mu h$ is drawn in Figure 4.5. For the case of H and A it

is trivially obtained by replacing h by H and A , respectively.

$$\begin{aligned}
 \Gamma(\tilde{H} \rightarrow \Psi_\mu h) &= \frac{|-\mathbf{N}_{13} \sin \alpha + \mathbf{N}_{14} \cos \alpha|^2 m_\chi^5}{96\pi M_p^2 m_{\frac{3}{2}}^2} \beta_{\chi \rightarrow \Psi_\mu h} \\
 &\times [(1 - x_{\frac{3}{2}})^2 (1 + x_{\frac{3}{2}})^4 \\
 &- x_h^2 \{(1 + x_{\frac{3}{2}})^2 (3 - 2x_{\frac{3}{2}} + 3x_{\frac{3}{2}}^2) \\
 &- x_h^2 (3 + 2x_{\frac{3}{2}} + 3x_{\frac{3}{2}}^2 - x_h^2)\}] \quad (\text{E.9})
 \end{aligned}$$

$$\begin{aligned}
 \Gamma(\tilde{H} \rightarrow \Psi_\mu H) &= \frac{|\mathbf{N}_{13} \cos \alpha + \mathbf{N}_{14} \sin \alpha|^2 m_\chi^5}{96\pi M_p^2 m_{\frac{3}{2}}^2} \beta_{\chi \rightarrow \Psi_\mu H} \\
 &\times [(1 - x_{\frac{3}{2}})^2 (1 + x_{\frac{3}{2}})^4 \\
 &- x_H^2 \{(1 + x_{\frac{3}{2}})^2 (3 - 2x_{\frac{3}{2}} + 3x_{\frac{3}{2}}^2) \\
 &- x_H^2 (3 + 2x_{\frac{3}{2}} + 3x_{\frac{3}{2}}^2 - x_H^2)\}] \quad (\text{E.10})
 \end{aligned}$$

$$\begin{aligned}
 \Gamma(\tilde{H} \rightarrow \Psi_\mu A) &= \frac{|\mathbf{N}_{13} \sin \beta_0 + \mathbf{N}_{14} \cos \beta_0|^2 m_\chi^5}{96\pi M_p^2 m_{\frac{3}{2}}^2} \beta_{\chi \rightarrow \Psi_\mu A} \\
 &\times [(1 + x_{\frac{3}{2}})^2 (1 - x_{\frac{3}{2}})^4 \\
 &- x_A^2 \{(1 - x_{\frac{3}{2}})^2 (3 + 2x_{\frac{3}{2}} + 3x_{\frac{3}{2}}^2) \\
 &- x_A^2 (3 - 2x_{\frac{3}{2}} + 3x_{\frac{3}{2}}^2 - x_A^2)\}] \quad (\text{E.11})
 \end{aligned}$$

$$\begin{aligned}
 \Gamma(\tilde{H} \rightarrow \Psi_\mu Z) &= \frac{|-\mathbf{N}_{13} \cos \beta_0 + \mathbf{N}_{14} \sin \beta_0|^2 m_\chi^5}{96\pi M_p^2 m_{\frac{3}{2}}^2} \beta_{\chi \rightarrow \Psi_\mu Z} \\
 &\times [(1 + x_{\frac{3}{2}})^2 (1 - x_{\frac{3}{2}})^4 \\
 &- x_Z^2 \{(1 - x_{\frac{3}{2}})^2 (3 + 2x_{\frac{3}{2}} - 9x_{\frac{3}{2}}^2) \\
 &- x_Z^2 (3 - 2x_{\frac{3}{2}} - 9x_{\frac{3}{2}}^2 - x_Z^2)\}] \quad (\text{E.12})
 \end{aligned}$$

$$\Gamma(\chi \rightarrow \Psi_\mu Z) = \Gamma(\tilde{G} \rightarrow \Psi_\mu Z) + \Gamma(\tilde{H} \rightarrow \Psi_\mu Z) \quad (\text{E.13})$$

Eq. (E.13) shows that there is no interference between the two Z channels. Thus there are no gaugino-Higgsino interferences at the 2-body decays of general neutralino NLSP at all.

E.2 3 body decays

We provide explicit results for the decay rates into any quark pair. Since all considered decays are processes of quantum electrodynamics, it is trivial to derive the decay rates into any lepton pair from the given ones. Starting with a given decay rate this is done by: 1) Divide it by 3, because leptons are color singlets. 2) Use the right masses m_l and widths Γ_l . 3) Use appropriate quantum numbers.

For each result it is assumed that the process is kinematically allowed. Otherwise it is 0. Thresholds can be implemented by the Θ -function.

Definitions

$a = \frac{m_A^2}{m_\chi^2}$, $c = \frac{m_{\frac{3}{2}}^2}{m_\chi^2}$ and $d_D = \frac{m_D^2}{m_\chi^2}$ for a decay $\chi \rightarrow XD \rightarrow \Psi_\mu A \bar{A}$: phase space parametrization. Note $g_i = \frac{\Gamma_i^2}{m_\chi^2}$.

$(1 - \sqrt{c} - 2\sqrt{a}) > 0$: condition for 'kinematically allowed' ($m_\chi > m_{\frac{3}{2}} + 2m_A$) in parametrisation. The Θ -function implements thresholds.

$$Q(q) = \begin{cases} -\frac{1}{3}, & \text{for } q = d \\ +\frac{2}{3}, & \text{for } q = u \end{cases} : \text{electric charge quantum number}$$

$$T_3(q) = \begin{cases} -\frac{1}{2}, & \text{for } q = d \\ +\frac{1}{2}, & \text{for } q = u \end{cases} : \text{weak isospin eigenvalue}$$

$k_L = T_3(q) - Q(q) \sin^2 \Theta_W$: corresponding to the left-handed quark

$k_R = -Q(q) \sin^2 \Theta_W$: corresponding to the right-handed quark

$$Y_i = \begin{cases} \frac{1}{3}, & \text{for } i = \tilde{u}_L, \tilde{d}_L \\ -\frac{2}{3}, & \text{for } i = \tilde{d}_R \\ \frac{4}{3}, & \text{for } i = \tilde{u}_R \end{cases} : \text{hypercharge quantum number}$$

$$v(q) = \begin{cases} v_d, & \text{for } q = d \\ v_u, & \text{for } q = u \end{cases} : \text{Higgs vacuum expectation values}$$

$$k_h(q) = \begin{cases} \frac{-\sin \alpha}{\sqrt{2}}, & \text{for } q = d \\ \frac{\cos \alpha}{\sqrt{2}}, & \text{for } q = u \end{cases}$$

$$k_H(q) = \begin{cases} \frac{\cos \alpha}{\sqrt{2}}, & \text{for } q = d \\ \frac{\sin \alpha}{\sqrt{2}}, & \text{for } q = u \end{cases}$$

$$k_A(q) = \begin{cases} \frac{\sin \beta_0}{\sqrt{2}}, & \text{for } q = d \\ \frac{\cos \beta_0}{\sqrt{2}}, & \text{for } q = u \end{cases}$$

The Breit-Wigner approximation for propagators is

$$'D_i = \frac{1}{p_i^2 - m_i^2 + im_i\Gamma_i} \quad (\text{E.14})$$

with fixed $\Gamma \neq \Gamma(p_i^2)$. So it is

$$'D_{ij} = \frac{1}{2} ('D_i'D_j^* + 'D_i^*'D_j) = \frac{(p_i^2 - m_i^2)(p_j^2 - m_j^2) + m_i m_j \Gamma_i \Gamma_j}{[(p_i^2 - m_i^2)^2 + m_i^2 \Gamma_i^2][(p_j^2 - m_j^2)^2 + m_j^2 \Gamma_j^2]}. \quad (\text{E.15})$$

Define (dimensionless) in parametrization for $p_i = p_j = k - p$

$$D_{ij} = D_{ji} = \frac{(c - d_i - x_3 + 1)(c - d_j - x_3 + 1) + \sqrt{d_i d_j g_i g_j}}{[(c - d_i - x_3 + 1)^2 + d_i g_i][(c - d_j - x_3 + 1)^2 + d_j g_j]} \quad (\text{E.16})$$

,for instance (i=j),

$$D_{ii} = \frac{1}{(c - d_i - x_3 + 1)^2 + d_i g_i}. \quad (\text{E.17})$$

Define for $p_i = k - p_1$ and $p_j = k - p_2$

$$D_{ij}^{p_1 p_2} = \frac{(a - d_i - x_1 + 1)(a - d_j + x_1 + x_3 - 1) + \sqrt{d_i d_j g_i g_j}}{[(a - d_i - x_1 + 1)^2 + d_i g_i][(a - d_j + x_1 + x_3 - 1)^2 + d_j g_j]}. \quad (\text{E.18})$$

Define for $p_i = k - p$ and $p_j = k - p_1$

$$D_{ij}^{pp_1} = \frac{(c - d_i - x_3 + 1)(a - d_j - x_1 + 1) + \sqrt{d_i d_j g_i g_j}}{[(c - d_i - x_3 + 1)^2 + d_i g_i][(a - d_j - x_1 + 1)^2 + d_j g_j]}. \quad (\text{E.19})$$

Define for $p_i = k - p$ and $p_j = k - p_2$

$$D_{ij}^{pp_2} = \frac{(c - d_i - x_3 + 1)(a - d_j + x_1 + x_3 - 1) + \sqrt{d_i d_j g_i g_j}}{[(c - d_i - x_3 + 1)^2 + d_i g_i][(a - d_j + x_1 + x_3 - 1)^2 + d_j g_j]}. \quad (\text{E.20})$$

Wino 4-vertex

The Feynman diagram of $\widetilde{W} \rightarrow \Psi_\mu W^+ W^-$ is drawn in Figure 4.4.

$$\begin{aligned}
 \Gamma \left(\widetilde{W} \rightarrow \Psi_\mu W^+ W^- \right) &= \frac{|\mathbf{N}_{12}|^2}{32(2\pi)^3 M_p^2} \frac{g^2}{4} \frac{1}{9} \frac{m_\chi^9}{m_W^4 m_{\frac{3}{2}}^2} \\
 &\times \int_{\frac{2\sqrt{c}}{1+c-4a}}^{1+c-4a} dx_3 \frac{\sqrt{x_3^2 - 4c}}{c - x_3 + 1} \sqrt{1 - \frac{4a}{c - x_3 + 1}} \\
 &\{12c^{9/2} + (6x_3 - 8)c^4 - 12(4a + 3x_3 - 3)c^{7/2} \\
 &+ 2(-8x_3^2 + 15x_3 + 4a(3x_3 - 4) - 8)c^3 \\
 &- 12(24a^2 - 8(x_3 - 1)a - 3(x_3 - 1)^2)c^{5/2} \\
 &+ (15x_3^3 - 32x_3^2 + 26x_3 + a^2(64 - 48x_3) - 8a(5x_3^2 - 8x_3 + 4) - 8)c^2 \\
 &- 12(-24a^2 + 4(x_3 - 1)a + (x_3 - 1)^2)(x_3 - 1)c^{3/2} \\
 &+ 2x_3(-3x_3^3 + 6x_3^2 - 4x_3 + 8a^2(2x_3 - 1) + 2a(5x_3^2 - 6x_3 + 2) + 1)c \\
 &+ (-8a^2 - 4(x_3 - 1)a + (x_3 - 1)^2)x_3^3\} \quad (E.21)
 \end{aligned}$$

$$\lim_{c, a \rightarrow 0} \Gamma \left(\widetilde{W} \rightarrow \Psi_\mu W^+ W^- \right) = \frac{|\mathbf{N}_{12}|^2}{32(2\pi)^3 M_p^2} \frac{g^2}{4} \frac{1}{9} \frac{m_\chi^9}{m_W^4 m_{\frac{3}{2}}^2} \frac{1}{30} \quad (E.22)$$

Higgsino 4-vertices

The Feynman diagram of $\widetilde{H} \rightarrow \Psi_\mu Z h$ is drawn in Figure 4.6. The Feynman diagrams for the other Higgs bosons are trivially obtained by replacing h by H and A , respectively.

Since at the decays via the Higgsino 4-vertices three different masses ($m_{3/2}, m_Z, m_h$) appear in the phase space, the analytical expressions become very complicated after the first integration, even though, they are analytically doable. The integration limits are given by Eq. (C.9).

Here, the masses are parameterized as

$$a = \frac{m_Z^2}{m_\chi^2} \quad \text{and} \quad b = \frac{m_{h,H,A}^2}{m_\chi^2} \quad \text{and} \quad c = \frac{m_{3/2}^2}{m_\chi^2}.$$

$$\begin{aligned}
 \Gamma\left(\tilde{H} \rightarrow \Psi_\mu Zh\right) &= \frac{|\mathbf{N}_{13}s_\alpha + \mathbf{N}_{14}c_\alpha|^2 g_z^2}{32(2\pi)^3 M_p^2} \frac{m_\chi^7}{24 m_Z^2 m_{\frac{3}{2}}^2} \\
 &\times \int_{x_3^-}^{x_3^+} dx_3 \int_{x_1^-}^{x_1^+} dx_1 (2\sqrt{c} - x_3) \\
 &(a^2 - 2(b - 5c + x_1 + x_3 - 1)a + (b - c + x_1 + x_3 - 1)^2)
 \end{aligned} \tag{E.23}$$

$$\begin{aligned}
 \Gamma\left(\tilde{H} \rightarrow \Psi_\mu ZH\right) &= \frac{|\mathbf{N}_{13}c_\alpha - \mathbf{N}_{14}s_\alpha|^2 g_z^2}{32(2\pi)^3 M_p^2} \frac{m_\chi^7}{24 m_Z^2 m_{\frac{3}{2}}^2} \\
 &\times \int_{x_3^-}^{x_3^+} dx_3 \int_{x_1^-}^{x_1^+} dx_1 (2\sqrt{c} - x_3) \\
 &(a^2 - 2(b - 5c + x_1 + x_3 - 1)a + (b - c + x_1 + x_3 - 1)^2)
 \end{aligned} \tag{E.24}$$

$$\begin{aligned}
 \Gamma\left(\tilde{H} \rightarrow \Psi_\mu ZA\right) &= \frac{|\mathbf{N}_{13}s_\beta - \mathbf{N}_{14}c_\beta|^2 g_z^2}{32(2\pi)^3 M_p^2} \frac{m_\chi^7}{24 m_Z^2 m_{\frac{3}{2}}^2} \\
 &\times \int_{x_3^-}^{x_3^+} dx_3 \int_{x_1^-}^{x_1^+} dx_1 (x_3 + 2\sqrt{c}) \\
 &(a^2 - 2(b - 5c + x_1 + x_3 - 1)a + (b - c + x_1 + x_3 - 1)^2)
 \end{aligned} \tag{E.25}$$

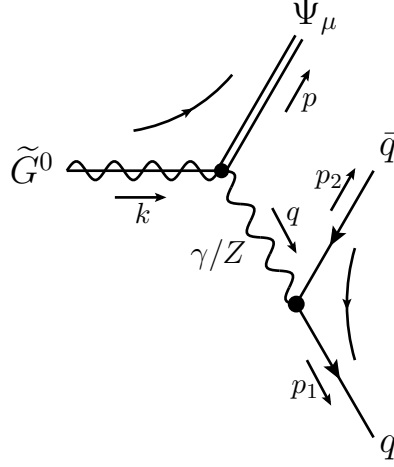


Figure E.1: Tree-level Feynman diagram of the gaugino \tilde{G}^0 3-body decay via γ or Z into gravitino and a pair of quark q and antiquark \bar{q} , i.e. $\tilde{G} \rightarrow \Psi_\mu \gamma/Z \rightarrow \Psi_\mu q \bar{q}$.

Gaugino via γ and Z

$$\begin{aligned}
 \Gamma \left(\tilde{G} \rightarrow \Psi_\mu \gamma/Z \rightarrow \Psi_\mu q \bar{q} \right) = & \\
 & \frac{|\mathbf{N}_{11} \cos \Theta_W + \mathbf{N}_{12} \sin \Theta_W|^2}{32(2\pi)^3 M_p^2} \frac{12}{9} (Q(q)e)^2 \frac{m_\chi^5}{m_{\frac{3}{2}}^2} \\
 & \times \int_{2\sqrt{c}}^{1+c-4a} dx_3 D_{\gamma\gamma} (2a + c - x_3 + 1) \\
 & \sqrt{1 - \frac{4a}{c - x_3 + 1} (x_3 + 2\sqrt{c})} \sqrt{x_3^2 - 4c} \\
 & \left(6c^2 - 4c^{\frac{3}{2}} + (6 - 4x_3)c - 2x_3 c^{\frac{1}{2}} + x_3^2 \right) \tag{E.26}
 \end{aligned}$$

$$\begin{aligned}
 + & \frac{|-\mathbf{N}_{11} \sin \Theta_W + \mathbf{N}_{12} \cos \Theta_W|^2}{32(2\pi)^3 M_p^2} \frac{6}{9} \left(\frac{g}{\cos \Theta_W} \right)^2 \frac{m_\chi^5}{m_{\frac{3}{2}}^2} \\
 & \times \int_{2\sqrt{c}}^{1+c-4a} dx_3 D_{ZZ} \left((c - a - x_3 + 1) k_L^2 + 6ak_L k_R + k_R^2 (c - a - x_3 + 1) \right) \\
 & \sqrt{1 - \frac{4a}{c - x_3 + 1} (x_3 + 2\sqrt{c})} \sqrt{x_3^2 - 4c} \\
 & \left(6c^2 - 4c^{\frac{3}{2}} + (6 - 4x_3)c - 2x_3 c^{\frac{1}{2}} + x_3^2 \right) \tag{E.27}
 \end{aligned}$$

$$\begin{aligned}
 & + \frac{\text{Re}[(\mathbf{N}_{11} \cos \Theta_W + \mathbf{N}_{12} \sin \Theta_W) (-\mathbf{N}_{11} \sin \Theta_W + \mathbf{N}_{12} \cos \Theta_W)^*]}{32(2\pi)^3 M_p^2} \\
 & \frac{12}{9} Q(q) g' g (k_L + k_R) \frac{m_\chi^5}{m_{\frac{3}{2}}^2} \\
 & \times \int_{2\sqrt{c}}^{1+c-4a} dx_3 D_{\gamma Z}(2a + c - x_3 + 1) \\
 & \sqrt{1 - \frac{4a}{c - x_3 + 1}} (x_3 + 2\sqrt{c}) \sqrt{x_3^2 - 4c} \\
 & \left(6c^2 - 4c^{\frac{3}{2}} + (6 - 4x_3) c - 2x_3 c^{\frac{1}{2}} + x_3^2 \right) \tag{E.28}
 \end{aligned}$$

In [3] they work in the limit $a \rightarrow 0$, but then Eq. (E.26) becomes divergent. The proposed solution is to take the limit on the integrand, while considering full integration limits. We checked that the numerical error due to that limit is in $O(10^{-2})$ compared to the full result.

Higgsino via h , H and A

$$\begin{aligned}
 \Gamma \left(\tilde{H} \rightarrow \Psi_\mu h/H/A \rightarrow \Psi_\mu q\bar{q} \right) = & \\
 & \frac{|-\mathbf{N}_{13} \sin \alpha + \mathbf{N}_{14} \cos \alpha|^2}{32(2\pi)^3 M_p^2} \frac{6}{6} \left(\frac{m_q}{v(q)} \right)^2 k_h^2(q) \frac{m_\chi^5}{m_{\frac{3}{2}}^2} \\
 & \times \int_{2\sqrt{c}}^{1+c-4a} dx_3 D_{hh}(-4a + c - x_3 + 1) \\
 & \sqrt{1 - \frac{4a}{c - x_3 + 1}} (x_3 + 2\sqrt{c}) \sqrt{x_3^2 - 4c} \\
 & (x_3 + 2\sqrt{c}) (x_3 - 2\sqrt{c}) \tag{E.29}
 \end{aligned}$$

$$\begin{aligned}
 + & \frac{|\mathbf{N}_{13} \cos \alpha + \mathbf{N}_{14} \sin \alpha|^2}{32(2\pi)^3 M_p^2} \frac{6}{6} \left(\frac{m_q}{v(q)} \right)^2 k_H^2(q) \frac{m_\chi^5}{m_{\frac{3}{2}}^2} \\
 & \times \int_{2\sqrt{c}}^{1+c-4a} dx_3 D_{HH}(-4a + c - x_3 + 1) \\
 & \sqrt{1 - \frac{4a}{c - x_3 + 1}} (x_3 + 2\sqrt{c}) \sqrt{x_3^2 - 4c} \\
 & (x_3 + 2\sqrt{c}) (x_3 - 2\sqrt{c}) \tag{E.30}
 \end{aligned}$$

$$\begin{aligned}
 + & \frac{|\mathbf{N}_{13} \sin \beta_0 + \mathbf{N}_{14} \cos \beta_0|^2}{32(2\pi)^3 M_p^2} \frac{6}{6} \left(\frac{m_q}{v(q)} \right)^2 k_A^2(q) \frac{m_\chi^5}{m_{\frac{3}{2}}^2} \\
 & \times \int_{2\sqrt{c}}^{1+c-4a} dx_3 D_{AA}(c - x_3 + 1) \\
 & \sqrt{1 - \frac{4a}{c - x_3 + 1}} (x_3 + 2\sqrt{c}) \sqrt{x_3^2 - 4c} \\
 & (x_3 - 2\sqrt{c})^2 \tag{E.31}
 \end{aligned}$$

$$\begin{aligned}
 + & \frac{\text{Re}[(-\mathbf{N}_{13} \sin \alpha + \mathbf{N}_{14} \cos \alpha) (\mathbf{N}_{13} \cos \alpha + \mathbf{N}_{14} \sin \alpha)^*]}{32(2\pi)^3 M_p^2} \\
 & \frac{12}{6} \left(\frac{m_q}{v(q)} \right)^2 k_h(q) k_H(q) \frac{m_\chi^5}{m_{\frac{3}{2}}^2} \\
 & \times \int_{2\sqrt{c}}^{1+c-4a} dx_3 D_{hH}(-4a + c - x_3 + 1) \\
 & \sqrt{1 - \frac{4a}{c - x_3 + 1}} (x_3 + 2\sqrt{c}) \sqrt{x_3^2 - 4c} \\
 & (x_3 + 2\sqrt{c}) (x_3 - 2\sqrt{c}) \tag{E.32}
 \end{aligned}$$

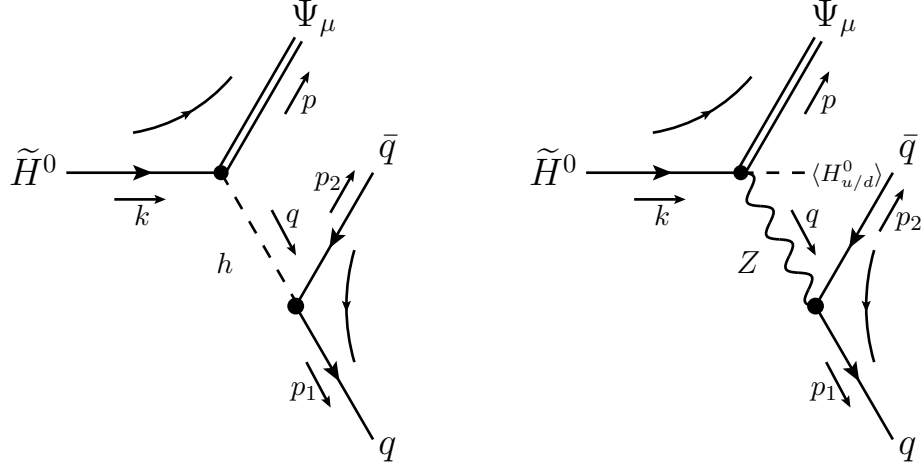


Figure E.2: Tree-level Feynman diagrams of the Higgsino \tilde{H}^0 3-body decay via h or Z into gravitino and a pair of quark q and antiquark \bar{q} , i.e. $\tilde{H} \rightarrow \Psi_\mu h/Z \rightarrow \Psi_\mu q\bar{q}$. The Feynman diagram with intermediate H and A are trivially obtained by replacing h by H and A respectively.

Higgsino via Z

$$\begin{aligned}
 \Gamma \left(\tilde{H} \rightarrow v\Psi_\mu Z \rightarrow \Psi_\mu q\bar{q} \right) = & \\
 & \frac{|-\mathbf{N}_{13} \cos \beta_0 + \mathbf{N}_{14} \sin \beta_0|^2}{32(2\pi)^3 M_p^2} \frac{3}{9} \left(\frac{g_Z}{m_z} \right)^2 \frac{m_\chi^7}{m_{\frac{3}{2}}^2} \\
 & \times \int_{\frac{2\sqrt{c}}{2\sqrt{c}}}^{1+c-4a} dx_3 D_{ZZ} \\
 & \sqrt{1 - \frac{4a}{c-x_3+1}} (x_3 - 2\sqrt{c}) \sqrt{x_3^2 - 4c} \\
 & \left\{ \frac{k_L^2 + k_R^2}{c-x_3+1} [12(d_Z^2 - a)c^3 + (4d_Z^2(5-6x_3) - 3a(4d_Z^2 - 8d_Z - x_3^2 - 8x_3 + 8))c^2 \right. \\
 & + ((13x_3^2 - 20x_3 + 8)d_Z^2 + 2a(2(3x_3 - 5)d_Z^2 \\
 & - 3(x_3^2 + 4x_3 - 4)d_Z - 3(x_3^3 + x_3^2 - 4x_3 + 2)))c \\
 & + (a(2d_Z^2 + 6(x_3 - 1)d_Z + 3(x_3 - 1)^2) - d_Z^2(x_3 - 1))x_3^2] \\
 & \left. + 6ak_L k_R [4c^2 + (12d_Z^2 - 8d_Z - x_3^2 - 4x_3 + 4)c + (2d_Z + x_3 - 1)x_3^2] \right\} \quad (\text{E.33})
 \end{aligned}$$

The different power of m_χ is due to $\propto d_Z^{-2} = \frac{m_\chi^4}{m_{\frac{3}{2}}^4}$. Since it is hard to count powers in

Eq. (E.33), we provide the limit of vanishing quark masses

$$\begin{aligned}
 \lim_{a \rightarrow 0} \Gamma \left(\tilde{H} \rightarrow v \Psi_\mu Z \rightarrow \Psi_\mu q \bar{q} \right) = & \\
 & \frac{|-\mathbf{N}_{13} \cos \beta_0 + \mathbf{N}_{14} \sin \beta_0|^2}{32(2\pi)^3 M_p^2} \frac{3}{9} (g_Z m_Z)^2 (k_L^2 + k_R^2) \frac{m_\chi^3}{m_{\frac{3}{2}}^2} \\
 & \times \int_{2\sqrt{c}}^{1+c} dx_3 D_{ZZ}(x_3 - 2\sqrt{c}) \\
 & \sqrt{x_3^2 - 4c} (12c^2 + (8 - 12x_3)c + x_3^2) . \tag{E.34}
 \end{aligned}$$

With the limit we see, that all the terms really $\propto d_Z^{-2}$ are also $\propto a$. So the diagram is not enhanced against other diagrams.

Between the Higgsino via h , H , A and Higgsino via Z there is interference between A and Z only, i.e.

$$\begin{aligned}
 \Gamma \left(\tilde{H} \rightarrow \Psi_\mu v(h^*/Z^*) \rightarrow \Psi_\mu q \bar{q} \right) &= 0 \\
 \Gamma \left(\tilde{H} \rightarrow \Psi_\mu v(H^*/Z^*) \rightarrow \Psi_\mu q \bar{q} \right) &= 0 \tag{E.35}
 \end{aligned}$$

and

$$\begin{aligned}
 \Gamma \left(\chi \rightarrow v \Psi_\mu (A^*/Z^*) \rightarrow \Psi_\mu q \bar{q} \right) = & \\
 & \frac{Re[(\mathbf{N}_{13} \sin \beta_0 + \mathbf{N}_{14} \cos \beta_0)(-\mathbf{N}_{13} \cos \beta_0 + \mathbf{N}_{14} \sin \beta_0)^*]}{32(2\pi)^3 M_p^2} \\
 & \times \int_{2\sqrt{c}}^{1+c-4a} dx_3 D_{AZ}(x_3 - \sqrt{c}) \\
 & \sqrt{1 - \frac{4a}{c - x_3 + 1}} (x_3 + 2\sqrt{c}) \sqrt{x_3^2 - 4c} \\
 & \left(2c^2 - x_3 c^{\frac{3}{2}} + (2 - 2d_Z - 2x_3)c + (x_3^2 + d_Z x_3 - x_3)c^{\frac{1}{2}} \right) . \tag{E.36}
 \end{aligned}$$

Gaugino and Higgsino via \tilde{q}

For many calculations with intermediate squarks, the usage of generalized Fierz identities became necessary. In the course of these calculations helpful references are [56, 57].

Definitions

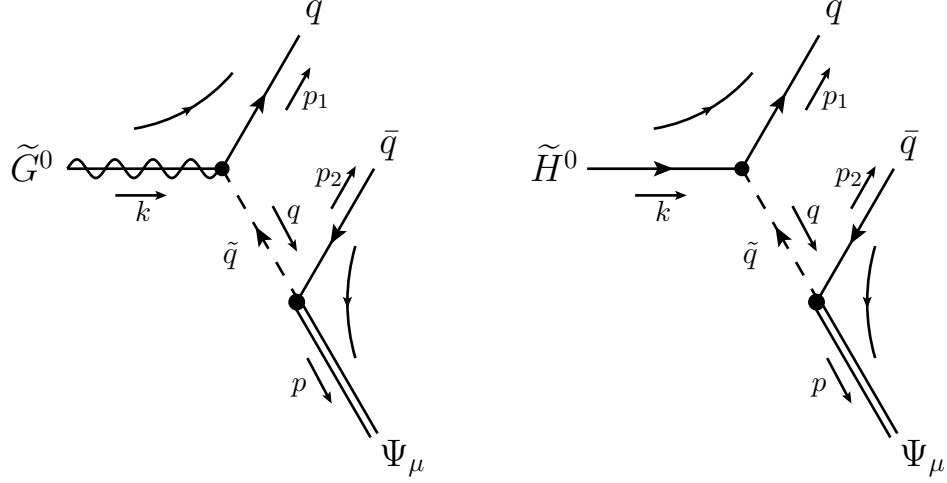


Figure E.3: Tree-level Feynman diagrams of the gaugino and Higgsino 3-body decays via intermediate squark \tilde{q} into gravitino and a pair of quark q and antiquark \bar{q} , i.e. $\chi \rightarrow q\tilde{q} \rightarrow \Psi_\mu q\bar{q}$. The Feynman diagram of $\chi \rightarrow \bar{q}\tilde{q} \rightarrow \Psi_\mu q\bar{q}$ is obtained by inversion of the fermion number flow arrows at the quark and squark lines.

$$I_{ij}^a = I_{ji}^a = \frac{1}{6} \int_{2\sqrt{a}}^{1-c-2\sqrt{c}\sqrt{a}} dx_3 D_{ij}(c \rightarrow a) x_3 \frac{(-c - x_3 + 1)}{a - x_3 + 1} \sqrt{x_3^2 - 4a} (c^2 + (-4a + 2x_3 - 2)c + (x_3 - 1)^2)^{3/2} \quad (\text{E.37})$$

$$I_{ij}^b = I_{ji}^b = \frac{4\sqrt{a}}{6} \int_{2\sqrt{a}}^{1-c-2\sqrt{c}\sqrt{a}} dx_3 D_{ij}(c \rightarrow a) \frac{(-c - x_3 + 1)}{a - x_3 + 1} \sqrt{x_3^2 - 4a} (c^2 + (-4a + 2x_3 - 2)c + (x_3 - 1)^2)^{3/2} \quad (\text{E.38})$$

$$I_{ij}^c = I_{ji}^c = \frac{2\sqrt{a}}{3} \int_{2\sqrt{a}}^{1-c-2\sqrt{c}\sqrt{a}} dx_3 D_{ij}(c \rightarrow a) \frac{-x_3}{a - x_3 + 1} \sqrt{x_3^2 - 4a} (c^2 + (-4a + 2x_3 - 2)c + (x_3 - 1)^2)^{3/2} \quad (\text{E.39})$$

$$I_{ij}^d = I_{ji}^d = \frac{4a}{3} \int_{\frac{1-c-2\sqrt{c}\sqrt{a}}{2\sqrt{a}}}^{1-c-2\sqrt{c}\sqrt{a}} dx_3 D_{ij}(c \rightarrow a) \frac{-1}{a-x_3+1} \sqrt{x_3^2-4a} (c^2 + (-4a+2x_3-2)c + (x_3-1)^2)^{3/2} \quad (\text{E.40})$$

$$x_1^\pm = \frac{1}{2} \left(2 - x_3 \pm \sqrt{x_3^2 - 4a} \sqrt{1 - \frac{4a}{1+c-x_3}} \right) \quad (\text{E.41})$$

$$I_{ij}^{f1} = \frac{1}{3} \int_{\frac{1+c-4a}{2\sqrt{c}}}^{1+c-4a} dx_3 \int_{x_1^-}^{x_1^+} dx_1 D_{ij}^{p_1 p_2} (c - (a+1)x_3 + x_1(x_1 + x_3 - 2) + 1) (c^2 - (4a + x_3 - 2)c + (x_1 - 1)(x_1 + x_3 - 1)) \quad (\text{E.42})$$

$$I_{ij}^{f2} = \frac{-2a}{3} \int_{\frac{1+c-4a}{2\sqrt{c}}}^{1+c-4a} dx_3 \int_{x_1^-}^{x_1^+} dx_1 D_{ij}^{p_1 p_2} (c^2 - (4a + x_3 - 2)c + (x_1 - 1)(x_1 + x_3 - 1)) \quad (\text{E.43})$$

$$I_{ij}^{f3} = \frac{-a}{3} \int_{\frac{1+c-4a}{2\sqrt{c}}}^{1+c-4a} dx_3 \int_{x_1^-}^{x_1^+} dx_1 D_{ij}^{p_1 p_2} x_3 (c^2 - (4a + x_3 - 2)c + (x_1 - 1)(x_1 + x_3 - 1)) \quad (\text{E.44})$$

$$I_{ij}^{f4} = \frac{\sqrt{a}}{3} \int_{\frac{1+c-4a}{2\sqrt{c}}}^{1+c-4a} dx_3 \int_{x_1^-}^{x_1^+} dx_1 D_{ij}^{p_1 p_2} (c - x_1 - x_3 + 1) (c^2 - (4a + x_3 - 2)c + (x_1 - 1)(x_1 + x_3 - 1)) \quad (\text{E.45})$$

$$\begin{aligned}
 I_{ij}^{f5} &= \frac{-\sqrt{a}}{3} \int_{2\sqrt{c}}^{1+c-4a} dx_3 \int_{x_1^-}^{x_1^+} dx_1 D_{ij}^{p_1 p_2} \\
 &\quad \{(3x_1 + 3x_3 - 7)c^2 - ((x_1 + x_3)(x_1 + 3x_3) + 4a(3x_1 + 3x_3 - 7) \\
 &\quad - 2(4x_1 + 7x_3 - 7))c - (a - 4x_1 + 4)x_3^2 \\
 &\quad + (x_1 - 1)^2(3x_1 - 7) + (x_1 - 1)(7x_1 - 11)x_3\} \quad (E.46)
 \end{aligned}$$

$$\begin{aligned}
 I_{ij}^{f6} &= \frac{-1}{3} \int_{2\sqrt{c}}^{1+c-4a} dx_3 \int_{x_1^-}^{x_1^+} dx_1 D_{ij}^{p_1 p_2} (c - x_1 - x_3 + 1)(x_1 + x_3 - 2) \\
 &\quad (c^2 - (4a + x_3 - 2)c + (x_1 - 1)(x_1 + x_3 - 1)) \quad (E.47)
 \end{aligned}$$

$$\begin{aligned}
 I_{ij}^{f7} &= \frac{\sqrt{a}}{3} \int_{2\sqrt{c}}^{1+c-4a} dx_3 \int_{x_1^-}^{x_1^+} dx_1 D_{ij}^{p_1 p_2} \\
 &\quad \{-2(c+2)x_1^2 + 4cx_1 + 8x_1 - (2a+c-3x_1+3)x_3^2 - 4c(-4a+c+2) \\
 &\quad + (3x_1^2 - 2(c+5)x_1 + c(-4a+c+8))x_3 + 7x_3 - 4\} \quad (E.48)
 \end{aligned}$$

$$\begin{aligned}
 I_{ij}^{f8} &= \frac{-1}{3} \int_{2\sqrt{c}}^{1+c-4a} dx_3 \int_{x_1^-}^{x_1^+} dx_1 D_{ij}^{p_1 p_2} \\
 &\quad \{8ca^2 + (x_3^2 + 2(3c - x_1 + 1)x_3 - 2((x_1 - 1)^2 + 3c(c + 2)))a \\
 &\quad + (c - x_3 + 1)(c^2 - (x_3 - 3)c + 2(x_1 - 1)(x_1 + x_3 - 1))\} \quad (E.49)
 \end{aligned}$$

$$\begin{aligned}
 I_{ij}^{f9} &= \frac{-1\sqrt{a}}{6} \int_{2\sqrt{c}}^{1+c-4a} dx_3 \int_{x_1^-}^{x_1^+} dx_1 D_{ij}^{p_1 p_2} (4c + 2x_1 - x_3 - 2) \\
 &\quad (c^2 - (4a + x_3 - 2)c + (x_1 - 1)(x_1 + x_3 - 1)) \quad (E.50)
 \end{aligned}$$

$$\mathbf{N}_q = \begin{cases} \frac{\mathbf{N}_{13}}{\cos \beta_0}, & \text{for } q = d \\ \frac{\mathbf{N}_{14}}{\sin \beta_0}, & \text{for } q = u \end{cases}$$

Gaugino via \tilde{q}

$$\Gamma \left(\tilde{G} \rightarrow q\tilde{q} \rightarrow \Psi_\mu q\tilde{q} \right) = \frac{\left| \mathbf{N}_{11} Y_{\tilde{q}_L} \sin \Theta_W \pm_{q=d}^{q=u} \mathbf{N}_{12} \cos \Theta_W \right|^2}{32(2\pi)^3 M_p^2} \frac{6g_Z^2}{2} \frac{m_\chi^5}{m_{\frac{3}{2}}^2} I_{\tilde{q}_L \tilde{q}_L}^a \quad (\text{E.51a})$$

$$+ \frac{\left| \mathbf{N}_{11} Y_{\tilde{q}_R} \sin \Theta_W \right|^2}{32(2\pi)^3 M_p^2} \frac{6g_Z^2}{2} \frac{m_\chi^5}{m_{\frac{3}{2}}^2} I_{\tilde{q}_R \tilde{q}_R}^a \quad (\text{E.51b})$$

$$+ \frac{\left| \mathbf{N}_{11} Y_{\tilde{q}_R} \sin \Theta_W \right|^2}{32(2\pi)^3 M_p^2} \frac{3g_Z^2}{2} \frac{m_\chi^4}{m_{\frac{3}{2}}^2} 2I_{\tilde{q}_R \tilde{q}_R}^{f2} \quad (\text{E.51c})$$

$$+ \frac{\left| \mathbf{N}_{11} Y_{\tilde{q}_L} \sin \Theta_W \pm_{q=d}^{q=u} \mathbf{N}_{12} \cos \Theta_W \right|^2}{32(2\pi)^3 M_p^2} \frac{3g_Z^2}{2} \frac{m_\chi^4}{m_{\frac{3}{2}}^2} I_{\tilde{q}_L \tilde{q}_L}^{f8} \quad (\text{E.51d})$$

$$- \frac{\text{Re}[(\mathbf{N}_{11} Y_{\tilde{q}_L} \sin \Theta_W \pm_{q=d}^{q=u} \mathbf{N}_{12} \cos \Theta_W)(\pm_{q=d}^{q=u} \mathbf{N}_{11} Y_{\tilde{q}_R} \sin \Theta_W)^*]}{32(2\pi)^3 M_p^2} \times \frac{6g_Z^2}{2} \frac{m_\chi^4}{m_{\frac{3}{2}}^2} I_{\tilde{q}_L \tilde{q}_R}^d \quad (\text{E.51e})$$

$$+ \frac{\text{Re}[(\mathbf{N}_{11} Y_{\tilde{q}_L} \sin \Theta_W \pm_{q=d}^{q=u} \mathbf{N}_{12} \cos \Theta_W)(\pm_{q=d}^{q=u} \mathbf{N}_{11} Y_{\tilde{q}_R} \sin \Theta_W)^*]}{32(2\pi)^3 M_p^2} \times \frac{3g_Z^2}{2} \frac{m_\chi^5}{m_{\frac{3}{2}}^2} \{ I_{\tilde{q}_L \tilde{q}_R}^{f3} + I_{\tilde{q}_R \tilde{q}_L}^{f6} \} \quad (\text{E.51f})$$

The terms given by Eq. (E.51a), (E.51b) and Eq. (E.51f), whereas the summand $I_{\tilde{q}_L \tilde{q}_R}^{f3}$ in Eq. (E.51f) disappears, are leading in the limit $m_q \rightarrow 0$ (i.e. $a \rightarrow 0$). In the limit of very heavy squarks and negligible quark and gravitino masses Eq. (E.51a) becomes

$$- \frac{\left| \mathbf{N}_{11} Y_{\tilde{q}_L} \sin \Theta_W \pm_{q=d}^{q=u} \mathbf{N}_{12} \cos \Theta_W \right|^2}{32(2\pi)^3 M_p^2} \frac{g_Z^2}{20} \frac{m_\chi^9}{m_q^4 m_{\frac{3}{2}}^2}. \quad (\text{E.52})$$

Higgsino via \tilde{q}

$$\Gamma \left(\tilde{H} \rightarrow q\tilde{q} \rightarrow \Psi_\mu q\bar{q} \right) = \frac{|\mathbf{N}_q|^2}{32(2\pi)^3 M_p^2} \left(\frac{m_q}{m_Z} \right)^2 \frac{6g_Z^2}{2} \frac{m_\chi^5}{m_{\frac{3}{2}}^2} \{I_{\tilde{q}_L\tilde{q}_L}^a + I_{\tilde{q}_R\tilde{q}_R}^a\} \quad (\text{E.53a})$$

$$+ \frac{|\mathbf{N}_q|^2}{32(2\pi)^3 M_p^2} \left(\frac{m_q}{m_Z} \right)^2 \frac{6g_Z^2}{2} \frac{m_\chi^4}{m_{\frac{3}{2}}^2} I_{\tilde{q}_L\tilde{q}_R}^d \quad (\text{E.53b})$$

$$+ \frac{|\mathbf{N}_q|^2}{32(2\pi)^3 M_p^2} \left(\frac{m_q}{m_Z} \right)^2 \frac{3g_Z^2}{2} \frac{m_\chi^5}{m_{\frac{3}{2}}^2} \{I_{\tilde{q}_L\tilde{q}_R}^{f1} + I_{\tilde{q}_R\tilde{q}_L}^{f1}\} \quad (\text{E.53c})$$

$$+ \frac{|\mathbf{N}_q|^2}{32(2\pi)^3 M_p^2} \left(\frac{m_q}{m_Z} \right)^2 \frac{3g_Z^2}{2} \frac{m_\chi^4}{m_{\frac{3}{2}}^2} 2I_{\tilde{q}_L\tilde{q}_L}^{f2} \quad (\text{E.53d})$$

Apart from the obvious fact that all Higgsino contributions vanish in the limit $m_q \rightarrow 0$ (i.e. $a \rightarrow 0$), the terms given by Eq. (E.53a) and (E.53c) are leading in this limit.

Gauginos interferences between intermediate squark \tilde{q} and γ, Z

It is in the limit $a = \frac{m_q^2}{m_\chi^2} \rightarrow 0$. Then, all Higgsino-neutralino contributions disappear on trace level already, i.e. they are suppressed due to Yukawa coupling and in addition because their traces are all proportional to \sqrt{a} or higher powers of a . So they are small even compared to other processes with Yukawa coupling. Note that $a = 0 \neq c$ is sensible only as long as $c > a$. t is suppressed anyway. We consider also large gravitino masses $m_{3/2}$, so that proper care has to be taken in the limit $c = \frac{m_{3/2}^2}{m_\chi^2} \rightarrow 0$.

Definitions:

$$\begin{aligned} I1_{ij}(I, II) &= \frac{-1}{3} \int_{2\sqrt{c}}^{1+c} dx_3 \int_{x_1^-(a=0)}^{x_1^+(a=0)} dx_1 D_{ij}^{pp1}(a=0)(c-x_3+1) \\ &\quad \{-(x_1-1)^3 - 2c(x_1-1)^2 - c^2(x_1-1) \\ &\quad + 2\sqrt{c}(x_1+x_3-1)(x_1-1) + c^{5/2} - c^{3/2}(x_3-3)\} \quad (\text{E.54}) \end{aligned}$$

$$\begin{aligned}
 I2_{ij}(I, II) &= \frac{1}{3} \int_{2\sqrt{c}}^{1+c} dx_3 \int_{x_1^-(a=0)}^{x_1^+(a=0)} dx_1 D_{ij}^{pp2}(a=0)(c-x_3+1) \\
 &\quad \{(x_1+x_3-1)^3 - 2c(x_1+x_3-1)^2 + c^2(x_1+x_3-1) \\
 &\quad + 2\sqrt{c}(x_1-1)(x_1+x_3-1) + c^{5/2} - c^{3/2}(x_3-3)\} \quad (E.55)
 \end{aligned}$$

$$\begin{aligned}
 I3_{ij}(I, II) &= \frac{1}{3} \int_{2\sqrt{c}}^{1+c} dx_3 \int_{x_1^-(a=0)}^{x_1^+(a=0)} dx_1 D_{ij}^{pp1}(a=0)(c-x_3+1) \\
 &\quad \{c^{5/2} + (x_1+x_3-4)c^2 + 2(x_1-1)c^{3/2} \\
 &\quad - (x_1+x_3-1)(3x_1+x_3-5)c + (x_1-1)^2\sqrt{c} \\
 &\quad + (x_1-1)(x_1+x_3-1)^2\} \quad (E.56)
 \end{aligned}$$

$$\begin{aligned}
 I4_{ij}(I, II) &= \frac{-1}{3} \int_{2\sqrt{c}}^{1+c} dx_3 \int_{x_1^-(a=0)}^{x_1^+(a=0)} dx_1 D_{ij}^{pp2}(a=0)(c-x_3+1) \\
 &\quad \{(x_1+x_3-1)^3 - 2c(x_1+x_3-1)^2 + c^2(x_1+x_3-1) \\
 &\quad + 2\sqrt{c}(x_1-1)(x_1+x_3-1) + c^{5/2} - c^{3/2}(x_3-3)\} \quad (E.57)
 \end{aligned}$$

$$\begin{aligned}
 \Gamma \quad & (\chi \rightarrow \Psi_\mu(\gamma^*, Z^*/\tilde{q}^*) \rightarrow \Psi_\mu q\bar{q}) = \\
 & \frac{\text{Re}[(\mathbf{N}_{11} Y_{\tilde{q}_L} \sin \Theta_W \pm_{q=d}^{q=u} \mathbf{N}_{12} \cos \Theta_W)(\mathbf{N}_{11} \cos \Theta_W + \mathbf{N}_{12} \sin \Theta_W)^*]}{32(2\pi)^3 M_p^2} \\
 & Q(q) e 3g_Z \frac{m_\chi^5}{m_{\frac{3}{2}}^2} \{I1_{\gamma\tilde{q}_L}(I, II) + I2_{\gamma\tilde{q}_L}(I, II)\} \\
 + & \frac{\text{Re}[(\pm_{q=d}^{q=u} Y_{\tilde{q}_R} \mathbf{N}_{11} \sin \Theta_W)(\mathbf{N}_{11} \cos \Theta_W + \mathbf{N}_{12} \sin \Theta_W)^*]}{32(2\pi)^3 M_p^2} \\
 & Q(q) e 3g_Z \frac{m_\chi^5}{m_{\frac{3}{2}}^2} \{I3_{\gamma\tilde{q}_R}(I, II) + I4_{\gamma\tilde{q}_R}(I, II)\} \\
 + & \frac{\text{Re}[(\mathbf{N}_{11} Y_{\tilde{q}_L} \sin \Theta_W \pm_{q=d}^{q=u} \mathbf{N}_{12} \cos \Theta_W)(-\mathbf{N}_{11} \sin \Theta_W + \mathbf{N}_{12} \cos \Theta_W)^*]}{32(2\pi)^3 M_p^2} \\
 & 3g_Z k_L \frac{m_\chi^5}{m_{\frac{3}{2}}^2} \{I1_{Z\tilde{q}_L}(I, II) + I2_{Z\tilde{q}_L}(I, II)\} \\
 + & \frac{\text{Re}[(\pm_{q=d}^{q=u} Y_{\tilde{q}_R} \mathbf{N}_{11} \sin \Theta_W)(-\mathbf{N}_{11} \sin \Theta_W + \mathbf{N}_{12} \cos \Theta_W)^*]}{32(2\pi)^3 M_p^2} \\
 & 3g_Z \frac{m_\chi^5}{m_{\frac{3}{2}}^2} \{k_L I3_{Z\tilde{q}_R}(I, II) + k_R I4_{Z\tilde{q}_R}(I, II)\} \tag{E.58}
 \end{aligned}$$

Higgsino interferences between intermediate squark \tilde{q} and Z

Definitions:

$$\begin{aligned}
 I1_{ij}(II, IV) &= \frac{1}{12} \int_{2\sqrt{c}}^{1+c} dx_3 \int_{x_1^-(a=0)}^{x_1^+(a=0)} dx_1 D_{ij}^{pp1}(a=0) \\
 & \quad \{(2x_1 + x_3 - 5)c^{5/2} + 2c^2 \\
 & \quad - (x_1^2 + (4x_3 - 2)x_1 + (x_3 - 6)x_3 + 2)c^{3/2} \\
 & \quad + 2(x_1 - 1)(x_1 + x_3)c + (x_1 - 1)^2(-2x_1 - 3x_3 + 3)\sqrt{c} \\
 & \quad + 2(x_1 - 1)^2(x_1 + x_3 - 1)\} \tag{E.59}
 \end{aligned}$$

$$\begin{aligned}
 I2_{ij}(II, IV) &= \frac{-1}{12} \int_{2\sqrt{c}}^{1+c} dx_3 \int_{x_1^-(a=0)}^{x_1^+(a=0)} dx_1 D_{ij}^{pp2}(a=0) \\
 &\quad \{(2x_1 + x_3 + 1)c^{5/2} - 2c^2 \\
 &\quad + (x_1^2 - 2(x_3 + 1)x_1 - 2x_3^2 + 2) c^{3/2} \\
 &\quad - 2(x_1 - 2)(x_1 + x_3 - 1)c - (2x_1 - x_3 - 1)(x_1 + x_3 - 1)^2 \sqrt{c} \\
 &\quad + 2(x_1 - 1)(x_1 + x_3 - 1)^2\} \quad (E.60)
 \end{aligned}$$

Analytic results:

$$\begin{aligned}
 \Gamma(\chi \rightarrow v\Psi_\mu(Z^*/\tilde{q}^*) \rightarrow \Psi_\mu q\bar{q}) &= \\
 &\quad \frac{\text{Re}[(\mathbf{N}_{11} Y_{\tilde{q}L} \sin \Theta_W \pm_{q=d}^{q=u} \mathbf{N}_{12} \cos \Theta_W)(-\mathbf{N}_{13} \cos \beta_0 + \mathbf{N}_{14} \sin \beta_0)^*]}{32(2\pi)^3 M_p^2} \\
 &\quad 6m_Z g_Z k_L \frac{m_\chi^4}{m_{\frac{3}{2}}^2} \{I1_{Z\tilde{q}L}(II, IV) + I2_{Z\tilde{q}L}(II, IV)\} \\
 + \frac{\text{Re}[(\pm_{q=d}^{q=u} Y_{\tilde{q}R} \mathbf{N}_{11} \sin \Theta_W)(-\mathbf{N}_{13} \cos \beta_0 + \mathbf{N}_{14} \sin \beta_0)^*]}{32(2\pi)^3 M_p^2} \\
 &\quad 6m_Z g_Z \frac{m_\chi^4}{m_{\frac{3}{2}}^2} \{k_L I1_{Z\tilde{q}R}(II, IV) + k_R I2_{Z\tilde{q}R}(II, IV)\} \quad (E.61)
 \end{aligned}$$

Gaugino-Higgsino interferences

We found the interference between gaugino via γ , Z and Higgsino via h , H , A , Z to be analytically vanishing, i.e.

$$\begin{aligned}
 \Gamma(\tilde{G}/\tilde{H} \rightarrow \Psi_\mu(\gamma^*/h^*, H^*, A^*) \rightarrow \Psi_\mu q\bar{q}) &= 0 \\
 \Gamma(\tilde{G}/\tilde{H} \rightarrow \Psi_\mu(Z^*/h^*, H^*, A^*) \rightarrow \Psi_\mu q\bar{q}) &= 0 \\
 \Gamma(\tilde{G}/\tilde{H} \rightarrow \Psi_\mu v(Z^*/Z^*) \rightarrow \Psi_\mu q\bar{q}) &= 0. \quad (E.62)
 \end{aligned}$$

Gaugino-Higgsino interferences in the squark \tilde{q} channel

$$\begin{aligned} & \Gamma(\chi \rightarrow q\tilde{q} \rightarrow \Psi_\mu q\tilde{q}) = \\ & \Gamma(\tilde{G} \rightarrow q\tilde{q} \rightarrow \Psi_\mu q\tilde{q}) + \Gamma(\tilde{H} \rightarrow q\tilde{q} \rightarrow \Psi_\mu q\tilde{q}) \\ & + \frac{\text{Re}[(\mathbf{N}_{11} Y_{\tilde{q}_L} \sin \Theta_W \pm_{q=d}^{q=u} \mathbf{N}_{12} \cos \Theta_W)(\mathbf{N}_q)^*]}{32(2\pi)^3 M_p^2} \frac{m_q}{m_Z} \frac{6g_Z^2}{2} \frac{m_\chi^5}{m_{\frac{3}{2}}^2} I_{\tilde{q}_L \tilde{q}_R}^b \end{aligned} \quad (\text{E.63a})$$

$$- \frac{\text{Re}[(\pm_{q=d}^{q=u} Y_{\tilde{q}_R} \mathbf{N}_{11} \sin \Theta_W)(\mathbf{N}_q)^*]}{32(2\pi)^3 M_p^2} \frac{m_q}{m_Z} \frac{6g_Z^2}{2} \frac{m_\chi^5}{m_{\frac{3}{2}}^2} I_{\tilde{q}_R \tilde{q}_R}^b \quad (\text{E.63b})$$

$$+ \frac{\text{Re}[(\mathbf{N}_{11} Y_{\tilde{q}_L} \sin \Theta_W \pm_{q=d}^{q=u} \mathbf{N}_{12} \cos \Theta_W)(\mathbf{N}_q)^*]}{32(2\pi)^3 M_p^2} \frac{m_q}{m_Z} \frac{6g_Z^2}{2} \frac{m_\chi^4}{m_{\frac{3}{2}}^2} I_{\tilde{q}_L \tilde{q}_R}^c \quad (\text{E.63c})$$

$$- \frac{\text{Re}[(\pm_{q=d}^{q=u} \mathbf{N}_{11} Y_{\tilde{q}_R} \sin \Theta_W)(\mathbf{N}_q)^*]}{32(2\pi)^3 M_p^2} \frac{m_q}{m_Z} \frac{6g_Z^2}{2} \frac{m_\chi^4}{m_{\frac{3}{2}}^2} I_{\tilde{q}_L \tilde{q}_R}^c \quad (\text{E.63d})$$

$$+ \frac{\text{Re}[(\pm_{q=d}^{q=u} \mathbf{N}_{11} Y_{\tilde{q}_R} \sin \Theta_W)(\mathbf{N}_q)^*]}{32(2\pi)^3 M_p^2} \frac{m_q}{m_Z} \frac{3g_Z^2}{2} \frac{m_\chi^5}{m_{\frac{3}{2}}^2} I_{\tilde{q}_L \tilde{q}_R}^{f4} \quad (\text{E.63e})$$

$$+ \frac{\text{Re}[(\pm_{q=d}^{q=u} \mathbf{N}_{11} Y_{\tilde{q}_R} \sin \Theta_W)(\mathbf{N}_q)^*]}{32(2\pi)^3 M_p^2} \frac{m_q}{m_Z} \frac{3g_Z^2}{2} \frac{m_\chi^5}{m_{\frac{3}{2}}^2} 2I_{\tilde{q}_R \tilde{q}_L}^{f4} \quad (\text{E.63f})$$

$$- \frac{\text{Re}[(\mathbf{N}_{11} Y_{\tilde{q}_L} \sin \Theta_W \pm_{q=d}^{q=u} \mathbf{N}_{12} \cos \Theta_W)(\mathbf{N}_q)^*]}{32(2\pi)^3 M_p^2} \frac{m_q}{m_Z} \frac{3g_Z^2}{2} \frac{m_\chi^5}{m_{\frac{3}{2}}^2} I_{\tilde{q}_R \tilde{q}_L}^{f4} \quad (\text{E.63g})$$

$$+ \frac{\text{Re}[(\pm_{q=d}^{q=u} \mathbf{N}_{11} Y_{\tilde{q}_R} \sin \Theta_W)(\mathbf{N}_q)^*]}{32(2\pi)^3 M_p^2} \frac{m_q}{m_Z} \frac{3g_Z^2}{2} \frac{m_\chi^4}{m_{\frac{3}{2}}^2} I_{\tilde{q}_R \tilde{q}_R}^{f5} \quad (\text{E.63h})$$

$$+ \frac{\text{Re}[(\mathbf{N}_{11} Y_{\tilde{q}_L} \sin \Theta_W \pm_{q=d}^{q=u} \mathbf{N}_{12} \cos \Theta_W)(\mathbf{N}_q)^*]}{32(2\pi)^3 M_p^2} \frac{m_q}{m_Z} \frac{3g_Z^2}{2} \frac{m_\chi^4}{m_{\frac{3}{2}}^2} I_{\tilde{q}_L \tilde{q}_L}^{f7} \quad (\text{E.63i})$$

$$+ \frac{\text{Re}[(\mathbf{N}_{11} Y_{\tilde{q}_L} \sin \Theta_W \pm_{q=d}^{q=u} \mathbf{N}_{12} \cos \Theta_W)(\mathbf{N}_q)^*]}{32(2\pi)^3 M_p^2} \frac{m_q}{m_Z} \frac{3g_Z^2}{2} \frac{m_\chi^5}{m_{\frac{3}{2}}^2} I_{\tilde{q}_L \tilde{q}_R}^{f9} \quad (\text{E.63j})$$

In the limit applied to Eq. (E.51) none of the interference terms survives. Even compared to Eq. (E.53a) all these terms are small, since they go with $m_\chi^4 < m_\chi^5$.

Appendix F

Correction

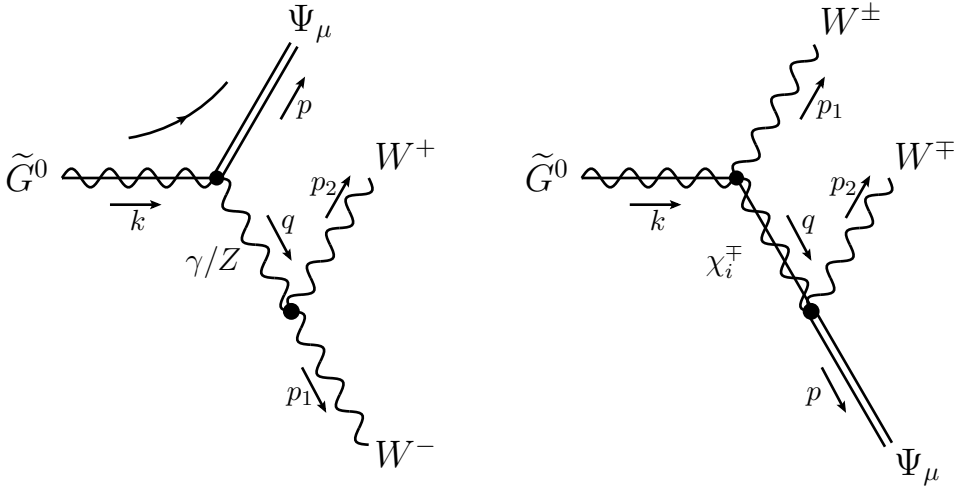


Figure F.1: Tree-level Feynman diagrams of the gaugino \tilde{G}^0 3-body decay via off-shell γ or Z into gravitino and a pair of W^+W^- , i.e. $\tilde{G} \rightarrow \Psi_\mu \gamma^*/Z^* \rightarrow \Psi_\mu W^+W^-$, and via off-shell charginos, i.e. $\tilde{G} \rightarrow W^\pm \chi_i^{\mp*} \rightarrow \Psi_\mu W^+W^-$, where the fermion flux follows the fermion number flux.

After the submission of the thesis we found, that in the decay into gravitino and a pair of W bosons are indeed no contributions of higher order. Concerning the wino 4-vertex of Figure 4.4 all contributions of higher order $\propto m_\chi^9$ or $\propto m_\chi^7$ cancel exactly with the decays via off-shell photon and Z boson and via off-shell charginos, that are drawn in Figure F.1. This cancellation is required by gauge invariance. For the leading order $\propto m_\chi^9$ this is also found in [58]. Thus the fast decay of the heavy wino NLSP via the wino 4-vertex does not exist!

Furthermore, we mentioned the decay channel $\tilde{H} \rightarrow \Psi_\mu Zh$ shown in Figure 4.6. In this case cancellation of the enhanced contribution $\propto m_\chi^7$ occurs with decays via off-shell

Z boson, off-shell A boson and off-shell neutralinos, that are drawn in Figure F.2. As already shown, this channel is negligible in the mass range under consideration, see the discussion below Eq. (4.30). So this observation does not change the results of Chapter 5 at all. In the formulas for Γ_{tot} and B_{had} of Chapter 4 the contributions of 4-vertices vanish.

In the course of these computations, that represent highly non-trivial checks, other minor mistakes have been found. These are corrected as well as a small number of typos. We added the note on the SPIRES reference and citation services.

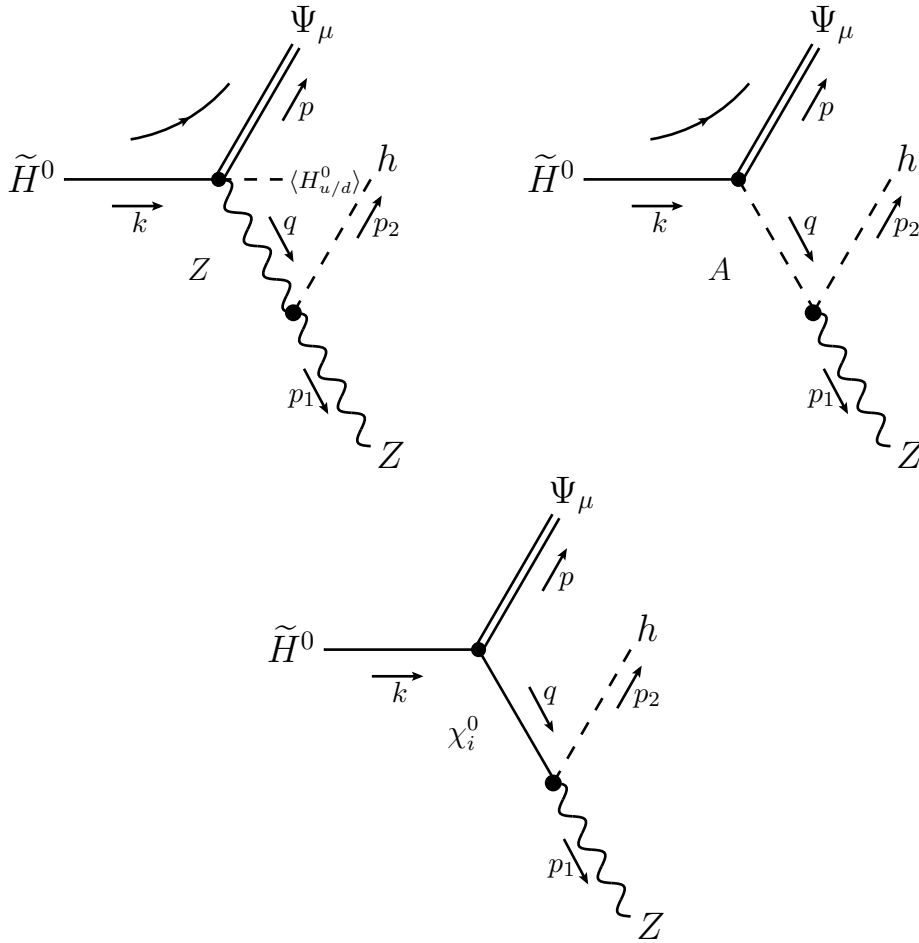


Figure F.2: Tree-level Feynman diagrams of the Higgsino \tilde{H}^0 3-body decay via off-shell Z and A into gravitino, h and Z boson and via off-shell neutralinos, where the fermion flux follows the fermion number flux.

Bibliography

- [1] WMAP Collaboration, E. Komatsu *et al.*, “Five-Year Wilkinson Microwave Anisotropy Probe (WMAP) Observations:Cosmological Interpretation,” *Astrophys. J. Suppl.* **180** (2009) 330–376, [arXiv:0803.0547 \[astro-ph\]](#).
- [2] B. C. Allanach *et al.*, “The Snowmass points and slopes: Benchmarks for SUSY searches,” *Eur. Phys. J.* **C25** (2002) 113–123, [arXiv:hep-ph/0202233](#).
- [3] F. D. Steffen, “Gravitino dark matter and cosmological constraints,” *JCAP* **0609** (2006) 001, [arXiv:hep-ph/0605306](#).
- [4] H. Pagels and J. R. Primack, “Supersymmetry, Cosmology and New TeV Physics,” *Phys. Rev. Lett.* **48** (1982) 223.
- [5] J. R. Ellis, J. E. Kim, and D. V. Nanopoulos, “Cosmological Gravitino Regeneration and Decay,” *Phys. Lett.* **B145** (1984) 181.
- [6] D. V. Nanopoulos, K. A. Olive, and M. Srednicki, “After Primordial Inflation,” *Phys. Lett.* **B127** (1983) 30.
- [7] J. R. Ellis, D. V. Nanopoulos, and S. Sarkar, “The Cosmology of Decaying Gravitinos,” *Nucl. Phys.* **B259** (1985) 175.
- [8] K. Kohri, T. Moroi, and A. Yotsuyanagi, “Big-bang nucleosynthesis with unstable gravitino and upper bound on the reheating temperature,” *Phys. Rev.* **D73** (2006) 123511, [arXiv:hep-ph/0507245](#).
- [9] M. Kawasaki, K. Kohri, and T. Moroi, “Big-bang nucleosynthesis and hadronic decay of long-lived massive particles,” *Phys. Rev.* **D71** (2005) 083502, [arXiv:astro-ph/0408426](#).
- [10] M. Kawasaki, K. Kohri, and T. Moroi, “Hadronic decay of late-decaying particles and big-bang nucleosynthesis,” *Phys. Lett.* **B625** (2005) 7–12, [arXiv:astro-ph/0402490](#).

-
- [11] K. Jedamzik, “Big bang nucleosynthesis constraints on hadronically and electromagnetically decaying relic neutral particles,” *Phys. Rev.* **D74** (2006) 103509, [arXiv:hep-ph/0604251](#).
- [12] K. Jedamzik, “Did something decay, evaporate, or annihilate during big bang nucleosynthesis?,” *Phys. Rev.* **D70** (2004) 063524, [arXiv:astro-ph/0402344](#).
- [13] J. Ellis, “Physics Beyond the Standard Model,” [arXiv:0902.0357 \[hep-ph\]](#).
- [14] J. Pradler and F. D. Steffen, “Thermal Gravitino Production and Collider Tests of Leptogenesis,” *Phys. Rev.* **D75** (2007) 023509, [arXiv:hep-ph/0608344](#).
- [15] M. Fukugita and T. Yanagida, “Baryogenesis Without Grand Unification,” *Phys. Lett.* **B174** (1986) 45.
- [16] W. Buchmuller, P. Di Bari, and M. Plumacher, “Leptogenesis for pedestrians,” *Ann. Phys.* **315** (2005) 305–351, [arXiv:hep-ph/0401240](#).
- [17] L. Roszkowski, R. Ruiz de Austri, and K.-Y. Choi, “Gravitino dark matter in the CMSSM and implications for leptogenesis and the LHC,” *JHEP* **08** (2005) 080, [arXiv:hep-ph/0408227](#).
- [18] J. L. Feng, S. Su, and F. Takayama, “Supergravity with a gravitino LSP,” *Phys. Rev.* **D70** (2004) 075019, [arXiv:hep-ph/0404231](#).
- [19] J. R. Ellis, K. A. Olive, Y. Santoso, and V. C. Spanos, “Gravitino dark matter in the CMSSM,” *Phys. Lett.* **B588** (2004) 7–16, [arXiv:hep-ph/0312262](#).
- [20] J. L. Feng, A. Rajaraman, and F. Takayama, “Probing gravitational interactions of elementary particles,” *Int. J. Mod. Phys.* **D13** (2004) 2355–2359, [arXiv:hep-th/0405248](#).
- [21] L. Covi, J. Hasenkamp, S. Pokorski, and J. Roberts, “Gravitino Dark Matter and general neutralino NLSP,”. in preparation.
- [22] **Particle Data Group** Collaboration, C. Amsler *et al.*, “Review of particle physics,” *Phys. Lett.* **B667** (2008) 1.
- [23] V. Mukhanov, “Physical foundations of cosmology,”. Cambridge, UK: Univ. Pr. (2005) 421 p.
- [24] G. Bertone, D. Hooper, and J. Silk, “Particle dark matter: Evidence, candidates and constraints,” *Phys. Rept.* **405** (2005) 279–390, [arXiv:hep-ph/0404175](#).

- [25] G. Jungman, M. Kamionkowski, and K. Griest, “Supersymmetric dark matter,” *Phys. Rept.* **267** (1996) 195–373, [arXiv:hep-ph/9506380](#).
- [26] S. M. Carroll, “Spacetime and geometry: An introduction to general relativity,” San Francisco, USA: Addison-Wesley (2004) 513 p.
- [27] S. Davidson and A. Ibarra, “A lower bound on the right-handed neutrino mass from leptogenesis,” *Phys. Lett.* **B535** (2002) 25–32, [arXiv:hep-ph/0202239](#).
- [28] G. Belanger, F. Boudjema, A. Pukhov, and A. Semenov, “micrOMEGAs: A program for calculating the relic density in the MSSM,” *Comput. Phys. Commun.* **149** (2002) 103–120, [arXiv:hep-ph/0112278](#).
- [29] W. Hu and J. Silk, “Thermalization and spectral distortions of the cosmic background radiation,” *Phys. Rev.* **D48** (1993) 485–502.
- [30] R. Lamon and R. Durrer, “Constraining gravitino dark matter with the cosmic microwave background,” *Phys. Rev.* **D73** (2006) 023507, [arXiv:hep-ph/0506229](#).
- [31] G. Sigl, K. Jedamzik, D. N. Schramm, and V. S. Berezinsky, “HELIUM PHOTODISINTEGRATION AND NUCLEOSYNTHESIS: IMPLICATIONS FOR TOPOLOGICAL DEFECTS, HIGH ENERGY COSMIC RAYS, AND MASSIVE BLACK HOLES,” *Phys. Rev.* **D52** (1995) 6682–6693, [arXiv:astro-ph/9503094](#).
- [32] S. P. Martin, “A Supersymmetry Primer,” [arXiv:hep-ph/9709356](#).
- [33] H. E. Haber and G. L. Kane, “The Search for Supersymmetry: Probing Physics Beyond the Standard Model,” *Phys. Rept.* **117** (1985) 75–263.
- [34] R. Barbier *et al.*, “R-parity violating supersymmetry,” *Phys. Rept.* **420** (2005) 1–202, [arXiv:hep-ph/0406039](#).
- [35] J. Pradler, “Electroweak Contributions to Thermal Gravitino Production,” [arXiv:0708.2786 \[hep-ph\]](#).
- [36] M. Greife, “Neutrino signals from gravitino dark matter with broken R- parity,” DESY-THESIS-2008-043.
- [37] M. Bolz, “Thermal production of gravitinos,” DESY-THESIS-2000-013.
- [38] S. R. Coleman and J. Mandula, “ALL POSSIBLE SYMMETRIES OF THE S MATRIX,” *Phys. Rev.* **159** (1967) 1251–1256.

-
- [39] R. Haag, J. T. Lopuszanski, and M. Sohnius, “All Possible Generators of Supersymmetries of the s Matrix,” *Nucl. Phys.* **B88** (1975) 257.
- [40] J. Wess and J. Bagger, “Supersymmetry and supergravity,” Princeton, USA: Univ. Pr. (1992) 259 p.
- [41] J. Rosiek, “Complete Set of Feynman Rules for the Minimal Supersymmetric Extension of the Standard Model,” *Phys. Rev.* **D41** (1990) 3464.
- [42] B. C. Allanach, “SOFTSUSY: A C++ program for calculating supersymmetric spectra,” *Comput. Phys. Commun.* **143** (2002) 305–331, [arXiv:hep-ph/0104145](#).
- [43] M. Fujii and T. Yanagida, “Natural gravitino dark matter and thermal leptogenesis in gauge-mediated supersymmetry-breaking models,” *Phys. Lett.* **B549** (2002) 273–283, [arXiv:hep-ph/0208191](#).
- [44] M. Fujii and T. Yanagida, “Baryogenesis and gravitino dark matter in gauge-mediated supersymmetry breaking models,” *Phys. Rev.* **D66** (2002) 123515, [arXiv:hep-ph/0207339](#).
- [45] N. Ghodbane and H.-U. Martyn, “Compilation of SUSY particle spectra from Snowmass 2001 benchmark models,” [arXiv:hep-ph/0201233](#).
- [46] S. Bailly, K. Jedamzik, and G. Moultaqa, “Gravitino Dark Matter and the Cosmic Lithium Abundances,” [arXiv:0812.0788 \[hep-ph\]](#).
- [47] C. Cheung, A. L. Fitzpatrick, and D. Shih, “(Extra)Ordinary Gauge Mediation,” *JHEP* **07** (2008) 054, [arXiv:0710.3585 \[hep-ph\]](#).
- [48] M. E. Peskin and D. V. Schroeder, “An Introduction to quantum field theory,” Reading, USA: Addison-Wesley (1995) 842 p.
- [49] M. Guchait, “Exact solution of the neutralino mass matrix,” *Z. Phys.* **C57** (1993) 157–164.
- [50] A. Denner, H. Eck, O. Hahn, and J. Kublbeck, “Feynman rules for fermion number violating interactions,” *Nucl. Phys.* **B387** (1992) 467–484.
- [51] R. Mertig, M. Bohm, and A. Denner, “FEYN CALC: Computer algebraic calculation of Feynman amplitudes,” *Comput. Phys. Commun.* **64** (1991) 345–359.
- [52] M. Bolz, A. Brandenburg, and W. Buchmuller, “Thermal Production of Gravitinos,” *Nucl. Phys.* **B606** (2001) 518–544, [arXiv:hep-ph/0012052](#).

- [53] S. Weinberg, “Cosmological Constraints on the Scale of Supersymmetry Breaking,” *Phys. Rev. Lett.* **48** (1982) 1303.
- [54] J. L. Feng, A. Rajaraman, and F. Takayama, “Superweakly-interacting massive particles,” *Phys. Rev. Lett.* **91** (2003) 011302, [arXiv:hep-ph/0302215](#).
- [55] T. Lee and G.-H. Wu, “Interactions of a single Goldstino,” *Phys. Lett.* **B447** (1999) 83–88, [arXiv:hep-ph/9805512](#).
- [56] C. C. Nishi, “Simple derivation of general Fierz-like identities,” *Am. J. Phys.* **73** (2005) 1160–1163, [arXiv:hep-ph/0412245](#).
- [57] J. F. Nieves and P. B. Pal, “Generalized Fierz identities,” *Am. J. Phys.* **72** (2004) 1100–1108, [arXiv:hep-ph/0306087](#).
- [58] A. Ferrantelli, “Gravitino production from electroweak gauge boson scattering,” *JHEP* **01** (2009) 070, [arXiv:0712.2171 \[hep-ph\]](#).

Acknowledgements

I would like to thank my supervisor Laura Covi for proposing this exciting topic in the area of particle cosmology that fits exactly my research interest. I am grateful that her wide knowledge and expertise helped me throughout the work on this thesis. Furthermore, I would like to thank Günter Sigl for acting as second examiner of this thesis, thereby giving me the opportunity to carry out this thesis at the DESY Theory Group.

I am thankful to Jonathan Roberts for a fruitful collaboration. Many thanks go to Michael Greife for profound discussions on the topic of gravitino dark matter and a lot of concrete help. In addition, I thank my office mate Vladimir Mitev for many discussions and an enjoyable time. Thereby, I thank also Jan Möller, Jan Hajer and all the other members of the DESY theory group for an enjoyable time.

Finally, I am thankful to my family for their support. Especially, I thank my brother Kevin for proof reading major parts of this work and last but not least I thank my friends for their consideration to my studies.



SPIRES reference and citation services

If you want to refer to this thesis and you use BibTeX, please, add the line

```
SLACcitation = "%%CITATION = DESY-THESIS-2009-016;%%"
```

to your code in the .bib-file. Otherwise the SPIRES reference and citation services do not work automatically in this case.